
# ISLAMIC UNIVERSITY OF TECHNOLOGY (IUT)

## BREAST TUMOR CLASSIFICATION USING RF DATA FROM SPECIFIC REGIONS OF ULTRASOUND IMAGES

**A Thesis Presented to the Academic Faculty**

By

**SABIQ MUHTADI (152430)**

**SHAIBAN AHMED (152441)**

A Dissertation

Submitted in Partial Fulfillment of the Requirements for the Degree of

**Bachelor of Science in Electrical and Electronic Engineering**

*Academic Year: 2018-19*

**Department of Electrical and Electronic Engineering**

**Islamic University of Technology (IUT)**

**A Subsidiary Organ of OIC**

**Gazipur, Dhaka, Bangladesh**

**November, 2019**

A dissertation on

# BREAST TUMOR CLASSIFICATION USING RF DATA FROM SPECIFIC REGIONS OF ULTRASOUND IMAGES

Approved by

_____

**Prof. Dr. Md. Ruhul Amin**

Head of the Department
Department of Electrical and Electronic Engineering (EEE)
Islamic University of Technology (IUT)
Gazipur-1704, Bangladesh

Supervised by

_____

**Dr Md. Taslim Reza**

Assistant Professor
Department of Electrical and Electronic Engineering (EEE)
Islamic University of Technology (IUT)
Gazipur-1704, Bangladesh

# Declaration of Authorship

This is to certify that the work presented in this thesis paper is the outcome of research carried out by the candidates under the supervision of Dr. Md. Taslim Reza, Assistant Professor, Department of Electrical and Electronic Engineering (EEE), Islamic University of Technology (IUT). It is also declared that neither this thesis paper nor any part thereof has been submitted anywhere else for the reward of any degree or any judgement.

## Authors


Sabiq Muhtadi

ID-152430

Shaiban Ahmed

ID - 152441

*Dedicated to*

*Our beloved parents, whose support made it all possible for us*

# TABLE OF CONTENTS

## Chapter 1
## Introduction



## Chapter 2
## Literature Review



## Chapter 3
## Methodology



## Chapter 4
## Results and Discussion

## Chapter 5
## Conclusion and Future Work

# LIST OF FIGURES

# LIST OF TABLES

# LIST OF ABBREVIATIONS

| | |
|---|---|
| **RF** | Radio Frequency |
| **PRF** | Pulse Repetition Frequency |
| **TGC** | Time Gain Compensation |
| **BI-RADS** | Breast Imaging Reporting and Data System |
| **ACR** | American College of Radiology |
| **QUS** | Quantitative Ultrasound |
| **BSC** | Backscatter Co-efficient |
| **ESD** | Effective Scatterer Diameter |
| **ROC** | Receiver Operating Characteristics |
| **ANN** | Artificial Neural Network |
| **KNN** | K Nearest Neighbors |
| **SVM** | Support Vector Machine |
| **SWT** | Stationary Wavelet Transform |
| **FFT** | Fast Fourier Transform |
| **DWT** | Discrete Wavelet Transform |
| **ROI** | Region-of-Interest |
| **CV** | Clearly Visible |
| **NCV** | Not-Clearly-Visible |

# ACKNOWLEDGEMENTS

Foremost, we would like to express our sincere gratitude and gratefulness to Allah Almighty, for without His graces and blessings, this study would not have been possible.

Acknowledging all who helped us to complete this work, we wish to compliment the significant role of the university and the department that has been very amiable to us during the entire period of our research.

We are indebted to our honorable supervisor, Dr. Md. Taslim Reza sir for his selfless support, his motivation, patience, enthusiasm and extensive knowledge of the relevant fields. His continuous guidance and detailed supervision kept us going even during the hardest of hours. We could not have imagined a better mentor for our thesis work.

We would like to relay our heartfelt gratitude to Dr, Sheikh Kaisar Alam sir, Senior Member, IEEE, Visiting Research Professor at the Centre for Computational Biomedicine Imaging and Modelling, Rutgers University, the State University of New Jersey, for providing us with the invaluable medical data set based on which our research was conducted.

Lastly, our warmest tribute to our parents, friends and families, whose moral support and well wishes benefitted us spiritually in achieving our goals.

# ABSTRACT

Diagnostic ultrasound imaging of the breast is characterized by its non-invasive, radiation free and convenient nature. Such qualities distinguish it from other imaging modalities of the breast, such as mammography and MRI, and has made it an increasingly popular choice for researchers, clinicians as well as patients. Conventional ultrasound imaging of the breast is mainly qualitative in nature, based on analyzing morphological features, and often have a lack of functional and quantitative information. Thus, although conventional ultrasound has a high sensitivity to breast lesions, it often lacks the specificity required to classify such lesions into their benign or malignant counterparts. In this regard, quantitative ultrasound techniques present a viable alternative, as it can provide specific quantitative variables by which to assess tissue features, and thus potentially increase the specificity as well as classification accuracy related to the procedure. This thesis presents a classification approach for benign and malignant tumors of the breast, utilizing parameters extracted from the power spectrum of ultrasound radio-frequency echo signals. Our work shows a clear separation between the two types of lesions with regards to the parameters. Furthermore, the parameters are able to classify lesions with an accuracy of 100% using Linear Support Vector Mechanism, and thus has the potential to assist in the diagnostic procedure associated with the detection of breast cancer.

# Chapter 1
# Introduction

## *1.1 Introduction*

Breast cancer represents a modern-day epidemic [1], one that affects millions of women around the world. It represents a significant health concern both at a global level and at a national level, and represents a cancer with one of the highest mortality rates. Detection of breast cancer at an early stage is crucial towards the treatment and survival of breast cancer patients. In this respect, Medical Imaging and Screening modalities of breast cancer are essential for their ability to detect the cancer and move towards treatment.

Several screening technologies are utilized by medical practitioners in the imaging process. Mammography represents the most commonly used screening procedure, and acts as the gold standard for the screening and detection of breast cancer. Magnetic Resonance Imaging (MRI) is utilized alongside mammography for the screening of patients who are at high risk of breast cancer. Ultrasound and Ultrasonography techniques have also become widely available and useful in adjunct to mammography in the clinical setting. Originally, ultrasonography was used primarily as an inexpensive procedure for differentiating between cystic breast masses from solid breast masses. However, supplemental screening of breast cancer with ultrasound is expanding, as ultrasonography has been found to yield valuable information about the nature and extent of solid masses and other breast lesions. Furthermore, mammography presents significant limitations in the screening of dense breasts, and this is where ultrasonography comes to the fore.

Although ultrasound imaging procedures are mainly qualitative in nature, images formed using ultrasound of the breast have been found to yield significant quantitative variables and information by which to assess the properties of the tissue. Such quantitative information has the ability to not only identify lesions that may be present in the breast, but also classify the type of lesion, whether it is benign or malignant. Several studies have utilized the quantitative information available from ultrasound imaging procedures of the breast in an attempt to differentiate between benign and malignant tumors. This study aims to utilize parameters extracted from the power spectrum of

ultrasound radio-frequency echo signals in an attempt to differentiate between benign and malignant breast tumors. Points are chosen on the boundary of lesions, where differences are known to exist between benign and malignant tumors. These points serve as a reference in selecting three different regions-of-interest from which to extract the required parameters, one inside the lesion, another outside the lesion and the remaining consisting of areas both inside and outside the lesion. The area of the regions-of-interest are also varied, with three different sizes of each region-of-interest considered. Finally, the power spectrum of each region-of-interest is computed, and the required parameters extracted to be utilized for classification.

## *1.2 Significance of this Research*

The significance of the issue of breast cancer cannot be understated. From the perspective of Bangladesh, in 2018 alone, breast cancer made up 19% (12,764) of new cancer cases amongst females, making it the highest incident form of cancer for women, as well as the 3rd most incident form of cancer for both sexes [2]. Furthermore, breast cancer was responsible for 6.3% (6,846) of all cancer related deaths, making it the 2nd most significant cancer in terms of mortality rates for women, and 4th most significant for both sexes [2]. In Bangladesh, the occurrence of breast cancer is estimated to be about 22.5 per 100000 females of all ages, and breast cancer has the highest prevalence of 19.3 per 100000 compared to any other cancer for Bangladeshi women aged 15-44 years [3]. The epidemic of breast cancer is not simply contained to specific parts of the world either. In 2018, there were an expected 2,088,849 new cases of breast cancer worldwide (11.6% of all cancer cases), as well as 626,679 deaths (6.6% of all cancer related deaths) [2]. In the United States, studies indicate breast cancer as the most-commonly detected cancer, as well as the second most lethal cancer (after lung cancer) for women [4]. One in every eight women are affected by breast cancer in the period spanning from birth till death [5]. There is expected to be 268,600 new cases of invasive breast cancer in America in 2019 alone, amongst which 41,760 deaths are expected [5].

In terms of diagnosis, mammography represents the standard screening modality for breast cancer, and has the ability to reduce breast cancer mortality by as much as 30% [6,7]. However, there are also drawbacks associated with this modality. The density of the breast is one of the main barriers towards diagnosis with mammography, and women with dense breast tissues are more likely to have cancers not visible on mammograms [8]. The sensitivity of mammography in the diagnosis of

breast cancer is inversely proportional to the density of the breast [9,10], with sensitivity figures as low as 30-48% in patients with dense breasts [10].

On the other hand, breast ultrasound represents a relatively inexpensive and readily available mode of diagnosis which can be used for interventional procedures, and boasts a good level of tolerance by women as well as the distinct advantage of not using ionizing radiation [11]. It has been reported to diagnose cancers at an earlier stage than mammography [12], and is also useful in adjunction to mammography, with the ability to detect over 40% more cancers than mammography or physical examination alone [13,14]. The first large study utilizing modern high-resolution breast ultrasound was conducted by Stavros et al. [15], using standardized diagnostic criteria for lesion differentiation. In 625 benign and 125 malignant lesions, ultrasound differentiated between the lesion types with a sensitivity of 98.4% and a negative predictive value of 99.5%. Hence the potential of ultrasound in not only screening of cancer, but also distinction between types of cancer is evident.

Conventional ultrasound imaging techniques make use of B-mode images, which are qualitative in nature, and classification using B-mode images often rely on anatomical features of the tumor, such as shape, borders, echogenicity. On the other hand, Quantitative Ultrasound techniques are designed to provide numerical data related to tissue features, thus having the potential to improve the specificity associated with biomedical imaging [16,17]. Quantitative Ultrasound techniques include spectral-based parameterization of ultrasound signals, flow estimation through Doppler, tissue elastography techniques, shear wave imaging and envelope statistics [16].

### *1.3 Objectives of this Research*

The main objectives behind conducting this study are as follows:

I. To analyze features extracted from the power spectrum of the boundary of ultrasound radio-frequency echo signals, based on the size of the region-of-interest, and the area selected for analysis

II. To analyze the ability of the extracted features in classifying between benign and malignant tumors, and hence

III. To analyze the potential of the upper-axial boundary of benign and malignant tumors in classification between tumor types.

## *1.4 Main Contributions*

Based on the research objectives mentioned above, this thesis provides the following main contributions:

I. Four parameters are proposed, which are extracted from the power spectrum of ultrasound radio-frequency echo signals, and utilized for classification purposes

II. Three different regions-of-interest are proposed, from which the parameters are extracted, to observe the variation of parameter values, and hence classification accuracy with variation in position of region-of-interest

III. Three different sizes of the region of interest are proposed, to study the effect of variation in parameter values, and hence classification, with a variation in size of region-of-interest.

## *1.5 Thesis Outline*

Subject to the research objectives and targeted contributions mentioned above, this thesis is outlined as follows:

Chapter 1 is anticipated to provide the background and motivation behind this study, including the significance of this research, the main contributions of this research, as well as the objectives it hopes to accomplish. The outline of the thesis is also presented at the end of this chapter.

Chapter 2 focuses on the review of literature related to quantitative ultrasound procedures, as well as the theoretical and research aspects of the relevant current works.

Chapter 3 presents the proposed algorithm utilized for this research, an in depth look at the procedures and techniques applied in an attempt to extract the parameters utilized to differentiate between benign and malignant tumors of the breast.

Chapter 4 concentrates on the simulation and classification results obtained from the study, It also analyses the effect of the various variables on the outcome of the study, that is, classification of benign and malignant tumors.

Chapter 5 summarizes and concludes the work with discussion about future research scopes in this area.

# Chapter 2

# Literature Review

## *2.1 Introduction to Ultrasound Imaging*

Ultrasound imaging utilizes high frequency sound waves to characterize and image tissue. Of all the imaging modalities, ultrasound is by far the least expensive, as well as the most portable, and can acquire images at a real time frame rate with few or no safety concerns [18]. Ultrasound is generated and detected through the use of small hand-held transducers.

The generation of images by ultrasound is based on the 'pulse-echo' principle [19,20,21,22]. This is based on deformation of piezoelectric crystals that are embedded in the transducer due to an electric pulse. This deformation produces a high frequency (>1,000,000 Hz) sound wave, which is referred to as an ultrasound wave. The ultrasound wave has the ability to propagate through tissue under the application of the transducer. The resulting wave is referred to as an 'acoustic compression wave', that propagates through tissue at a speed of approximately 1530 m/s. Each compression is proceeded by a decompression, as is the case with all sound waves, and the rate of these events is referred to as the 'frequency' of the wave. Diagnostic ultrasound imaging generally employs frequencies ranging between 2.5 and 10 Mhz. This is far beyond the audible capability of humans, and thus the resulting sound wave is termed 'ultrasound'.

The principal components of an ultrasound wave are as follows:

I. Wavelength ($\lambda$) – the spatial distance between two compressions, or decompressions

II. Frequency (f) – inversely proportional to the wavelength

III. Velocity of sound (c) – which is a constant for any given medium

These three wave characteristics have a relationship as follows:

$$c = f\lambda$$

Hence an increase in the frequency, or in other words a decrease in the wavelength, implies lower penetration due to a higher amount of viscous effects, which leads to greater attenuation [22].

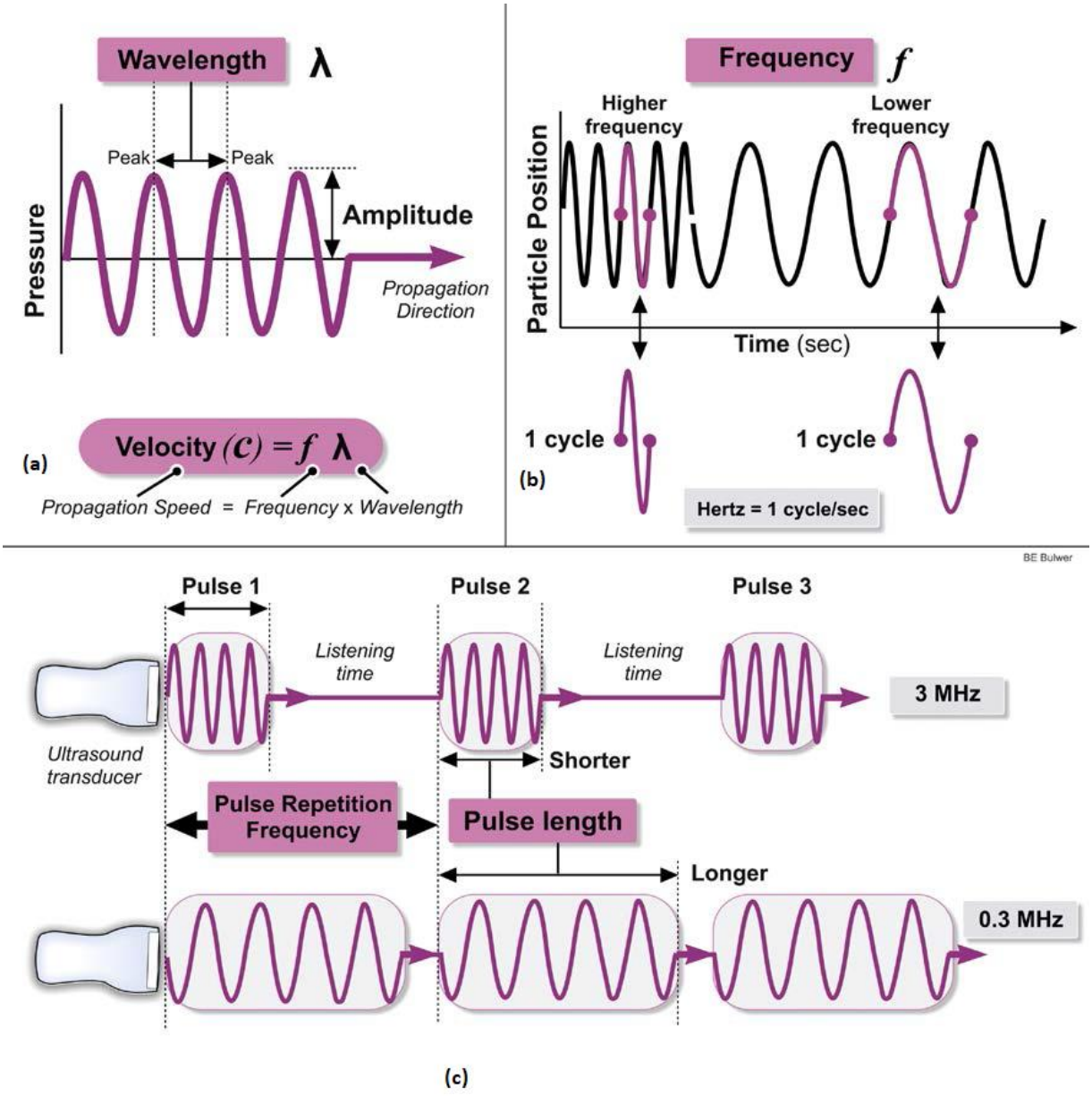


**Figure 2.1:** (a) and (b) are depictions of an ultrasound wave. The wave propagates through tissue at a specific wavelength, which is inversely proportional to the frequency, and a specific amplitude, which quantifies the amount of energy transported by the wave.

(c) Pulse length (duration) is determined primarily by the transducer frequency, to which it is inversely related. Higher frequency transducers can emit pulses of shorter length. These rate at which these pulses are emitted are referred to as the 'pulse repetition frequency'. Reprinted from "Physical principles of

ultrasound and generation of images" by Cikes M, D'hooge J and Solomon SD (2018), in *Essential Echocardiography*, 1st Edition, pp. 1- 15, Elsevier.

The progression of the acoustic wave through tissue will be disrupted by changes in tissue property, such as tissue density. This will lead to partial reflections of the ultrasound wave, also referred to as 'specular reflections', as well as scattering of the energy of the wave, referred to as backscatter.

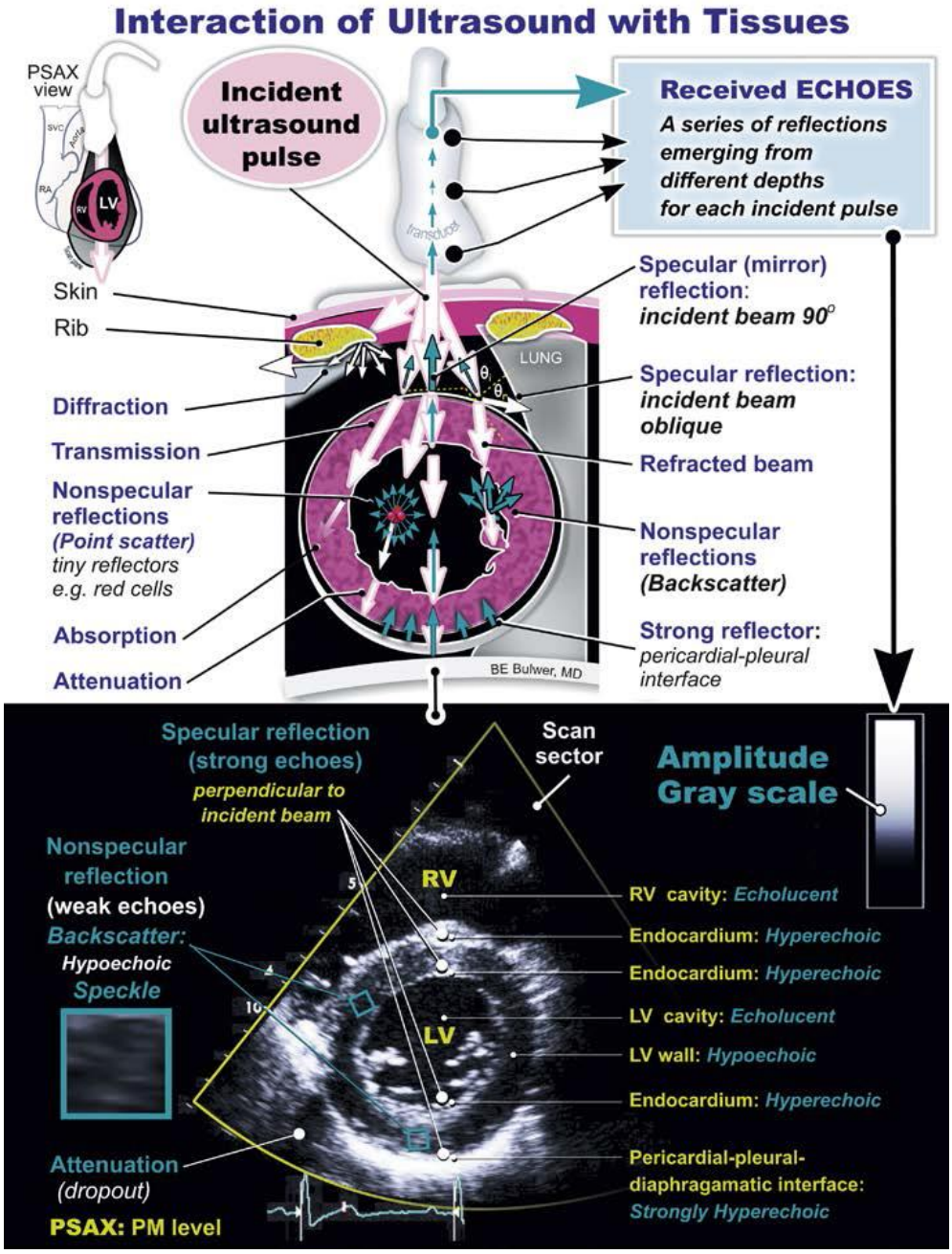

**Figure 2.2:** The interaction of the transmitted ultrasound wave with an acoustic interface. The interface causes a portion of the transmitted wave to be reflected, whilst another portion is transmitted through the tissue. The portion transmitted through the tissue may also be refracted, and may also later be reflected and return to the transducer as a 'specular reflection' or a 'backscatter reflection', thus carrying information through the amplitude of the signal. Reprinted from "Physical principles of ultrasound and generation of images" by Cikes M, D'hooge J and Solomon SD (2018), in *Essential Echocardiography*, 1st Edition, pp. 1- 15, Elsevier.

Specular reflections generally originate from interfaces of different types of tissue, whereas backscatter generally originates from within a tissue. In both cases, the reflections propagate back to the ultrasound transducer. This again leads to the deformation of the piezoelectric crystals embedded in the transducer, deforming the crystals, and thus generating an electrical signal. This signal is referred to as the radio-frequency (RF) signal, and is the raw, unprocessed data obtained from diagnostic ultrasound. The amplitude of this signal is proportional to the amount of deformation of the crystal, or, the amplitude of the reflected wave from the tissue under observation. In addition to defining the amplitude of the reflected signal, the depth of the reflecting structure may also be determined according to the interval between the emission and receiving of the pulse, as this is equivalent to the time required for the ultrasound wave to travel from the transducer during generation, through the tissue, and back to the transducer due to reflection. The data obtained from the amplitude and depth of reflection are used to form 'scan lines', and repetition of the previously mentioned procedures of image (scan line) acquisition as well as post processing is utilized for overall image construction. During acquisition of images, the ultrasound transducers emit waves in pulses consisting of a certain duration, which is referred to as the 'pulse length', and at a certain rate known as the 'pulse repetition frequency (PRF)'.

The data obtained from the scan lines can be visually represented as 'A-mode' or 'B-mode' images. A-mode represents the most fundamental modality of imaging RF signals, where A stands for the 'amplitude'. In this modality, images are formed based on the amplitude of the reflected ultrasound signal at certain distances from the transducer. However, visualization of A-mode images are relatively unattractive, and A-mode images are not generally utilized as an image display option.

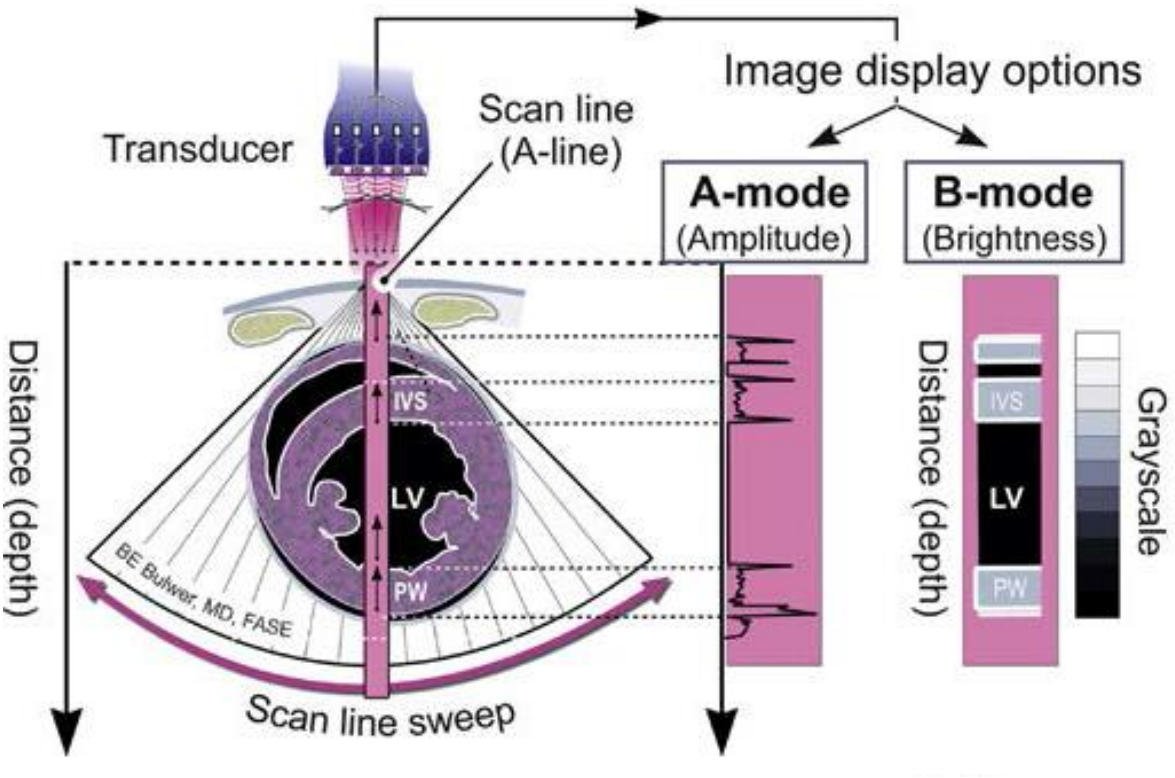


**Figure 2.3:** Generation and formation of ultrasound images. After an ultrasound pulse is emitted by the piezoelectric crystals embedded in the transducer (left), it transmits through tissue, is reflected from structures in the tissue, and propagates back towards the transducer. After processing of the received signals, they are displayed according to their amplitude and depth of reflection (right). A-mode images are formed using the amplitude spikes of the reflected signal. In B-mode images, the amplitude spikes are translated to grayscale, such that the least reflective tissues are visualized as anechoic or dark formations, and strong tissue reflectors are visualized as hyperechoic or bright spots. Reprinted from "Physical principles of ultrasound and generation of images" by Cikes M, D'hooge J and Solomon SD (2018), in *Essential Echocardiography*, 1st Edition, pp. 1- 15, Elsevier.

A-mode images are further processed to form B-mode images, where the B stands for 'brightness'. In B-mode images, the amplitude of the received signal is translated to grayscale. To achieve this, multiple points of the signal (i.e. pixels) are designated a number that represents a color on the grayscale, based on the local amplitude of the signal. In this way, the least reflective tissues, or tissues that conduct sound waves, are visualized as anechoic or dark spots, and strong tissue reflectors are visualized as hyperechoic or dark spots.

A limitation of ultrasound imaging comes from the fact that reflections from tissues farther away from the transducer have smaller amplitudes, due to attenuation effects. However, this effect may be compensated through the use of 'attenuation correction', which automatically amplifies signals propagating from deeper segments of the tissue. This process is referred to as 'automatic time gain compensation (TGC)'. In addition to automatic TGC, most systems contain TGC sliders, which enable the TGC to be modified during image acquisition.

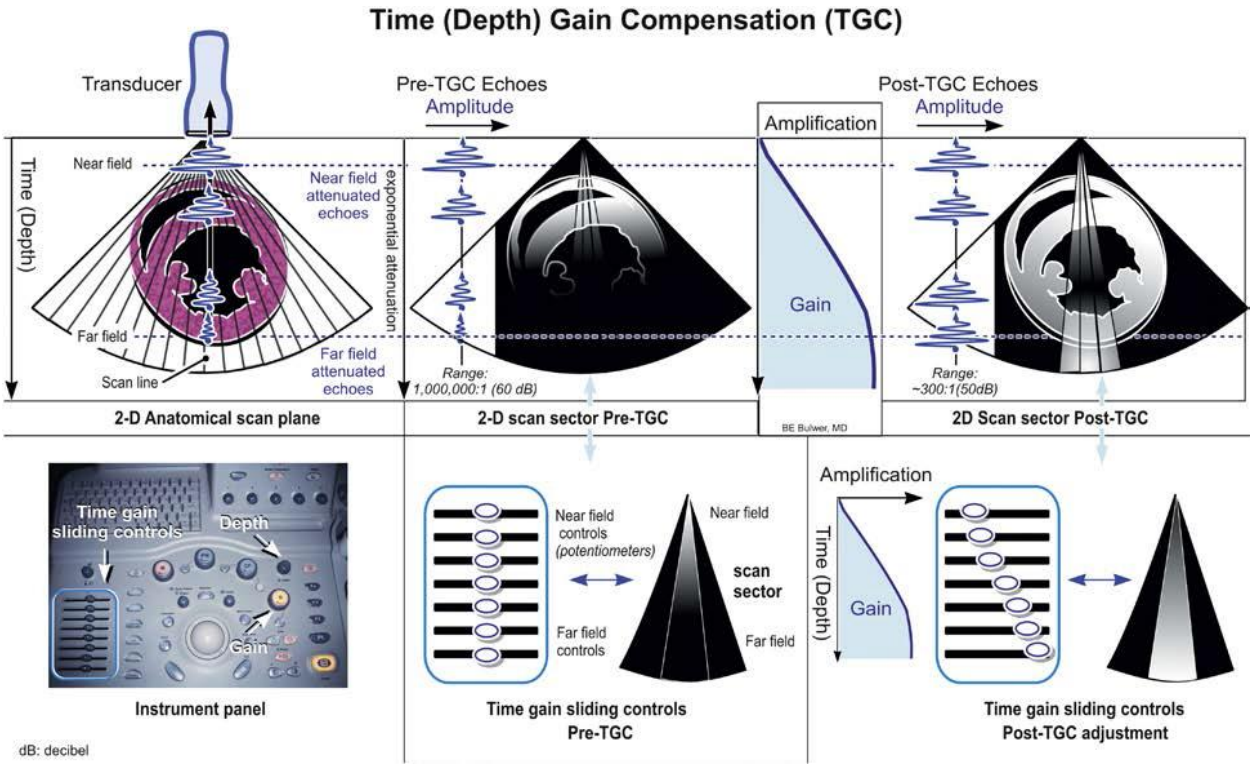


**Figure 2.4:** Attenuation correction. Reprinted from "Physical principles of ultrasound and generation of images" by Cikes M, D'hooge J and Solomon SD (2018), in *Essential Echocardiography*, 1st Edition, pp. 1- 15, Elsevier.

Resolution of an image may be defined as the shortest distance between two objects that is required to distinguish them as separate. Resolution in ultrasound images consists of wo major components: spatial resolution and temporal resolution. Furthermore, spatial resolution can be divided into axial resolution and lateral resolution, depending on the position of the object relative to the image line [19,20,21,22]. Temporal resolution, meanwhile, may be defined as the time between two corresponding

measurements, or the ability of a system to distinguish two temporal events as separate occurrences.

*Axial resolution* refers to the location of objects relative to the image line. The principle determinant of axial resolution is the pulse length. A shorter ultrasound pulse length translates to better axial resolution. Pulse length, meanwhile, is defined by the frequency of the transducer. A higher frequency transducer is able to provide shorter pulses, which yields better axial resolution.

*Lateral resolution* refers to spatial resolution perpendicular to the ultrasound beam. The principle determinant of lateral resolution is the width of the beam generated by the transducer.

*Elevational resolution* is referred to as the resolution perpendicular to the image line. It is somewhat similar to lateral resolution. The principle determinant of elevational resolution is the dimensions of the ultrasound beam in the elevational direction.

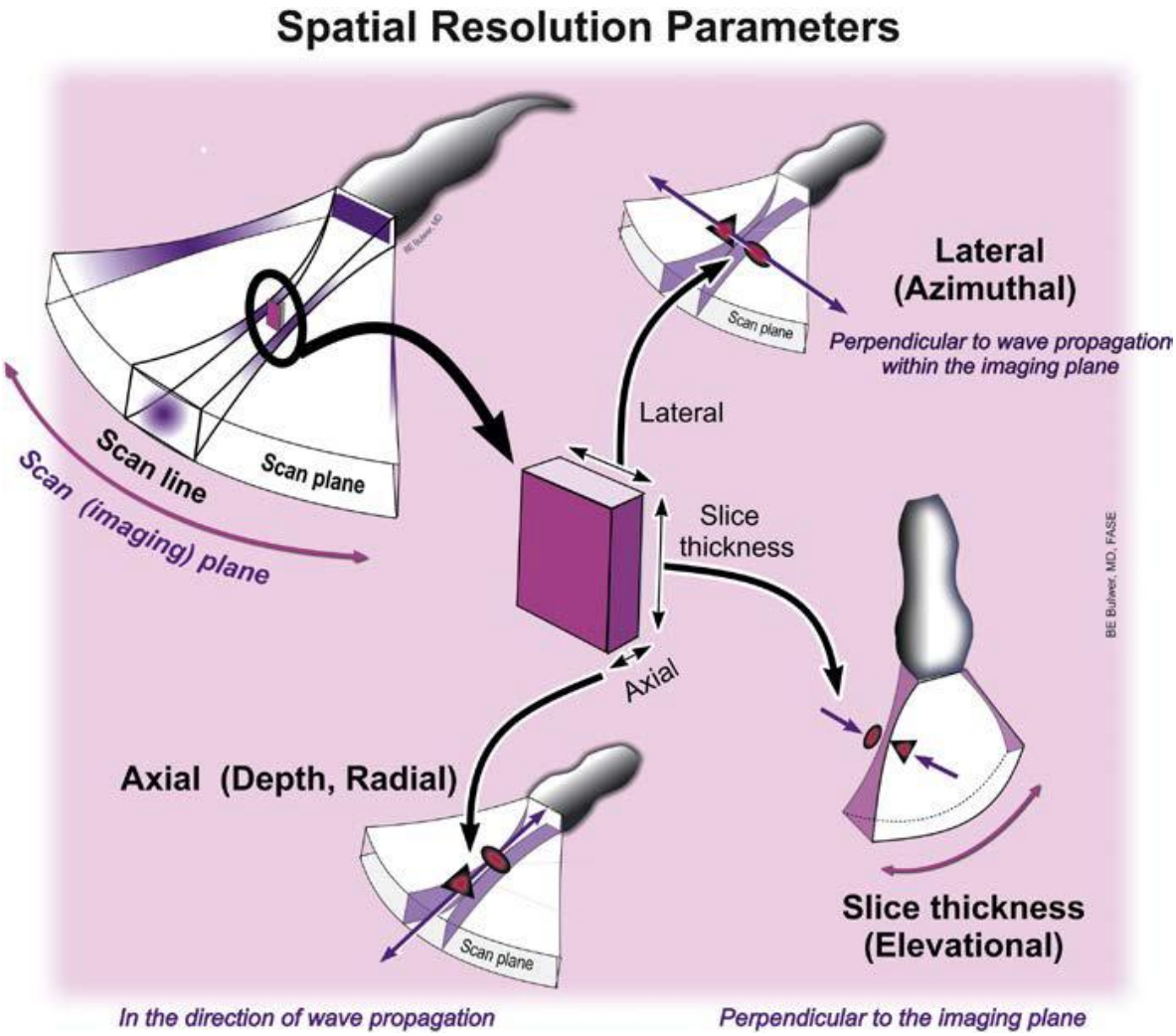


**Figure 2.5:** The components of spatial resolution. Lateral resolution refers to the spatial resolution perpendicular to the ultrasound beam, axial resolution refers to resolution along the image line, and elevation resolution refers to resolution perpendicular to the image line. Reprinted from "Physical principles of ultrasound and generation of images" by Cikes M, D'hooge J and Solomon SD (2018), in *Essential Echocardiography*, 1st Edition, pp. 1- 15, Elsevier.

## *2.2 Relevant Research*

Improvements to the quality of biomedical imaging has resulted in increased sensitivity to potentially harmful tissue features such as cancer, and application of such imaging techniques have resulted in an increase in the number of tumors detected, without the distinction of whether they are benign or malignant. This has resulted in an 'overdiagnosis' problem, which may be accompanied by 'overtreatment' [23,24].

As discussed in the introduction, conventional ultrasound imaging procedures utilize anatomical features of the tumor, such as shape, borders, echogenicity from B-mode data, and is inherently qualitative in nature. Most breast cancers, including more than 90% of invasive ductile carcinomas [25], are visible in conventional ultrasound images. Recent studies have shown that a combination of selected features in B-mode images of 'mammographically visible' tumors can be effective in classifying breast tumors into benign and malignant cases [15,26,27,28,29]. In this case, the Breast Imaging Reporting and Data System (BI-RADS) developed by the American College of Radiology (ACR) provides a glossary of features describing the ultrasound appearance of breast tumors [25,30]. The BI-RADS outlines six different types of possible findings, ranging from Category 0, which states that the assessment is incomplete, and additional imaging evaluation is necessary to classify the required tumor, up to Category 5, which suggests that the tumor is highly suggestive of malignancy, and appropriate measures should be taken.

In spite of the advantages offered by BI-RADS, the classification system depends upon qualitative features of the tumor, which may be subjective, and successful application using BI-RADS characteristics is dependent to a large degree upon the skills and knowledge of the clinician. QUS techniques seek to make the breast tumor evaluation process quantitative, reproducible and relatively operator dependent. Quantitative ultrasound techniques have received significant attention in recent years, and a comprehensive list of methods are available. We analyze three different aspects of QUS that have been able to distinguish between benign and malignant breast tumors with a high level of accuracy:

I. Classification using physical properties of tissue,

II. Classification using parameters developed from the spectrum of ultrasound echoes, and

III. Classification using statistical analysis of the envelope of backscattered ultrasound.

Analysis of physical properties of tissue, which includes backscatter co-efficient (BSC) and attenuation co-efficient, was first proposed by D'Astous and Foster [31]. In a later study, Nam et al. [32] attempted to differentiate between tumor types using the attenuation co-efficient and BSC

parameters, and reported attenuation co-efficients that were 20% higher for carcinoma than for fibroadenoma. They also found that most carcinomas exhibited lower values for frequency-average BSC than fibroadenomas, and that fibroadenomas had greater variability in Effective Scatterer Diameter (ESD) [32].

One of the first to utilize the spectrum of ultrasound echoes was Lizzi et al. [33, 34], who developed parameters from the spectrum of ultrasound echoes, which includes the spectral slope, spectral intercept and midband fit, and demonstrated the correlation of these parameters with tissue microstructure [33]. In a later study, Alam et al. [35] proposed a set of quantitative descriptors aimed at identifying cancerous breast lesions, which utilized acoustic features extracted from the parameters proposed by Lizzi et al., as well as morphometric properties related to the shape of the lesion. They reported a receiver-operating-characteristics (ROC) area of 0.947±0.045 for the 130 "biopsy-proven patients" that they considered for the study. Spectral features were also utilized by Kabir et al. [36], who attempted to classify benign and malignant breast tumors through features extracted from B-mode images after applying Contourlet Transform. The extracted features from their study yielded accuracies of 95% with Artificial Neural Network (ANN), 92.5% with K-Nearest Neighbors (KNN) and 90% with Support Vector Machine (SVM) classification approaches. It is not only in the avenue of breast cancer classification where spectral characteristics have yielded a high degree of success, but also for other forms of cancer, such as prostate cancer. Layek et al. [37] attempted to classify sonoelastography images of prostate cancer using Fourier and Wavelet based transformations. Their work yielded maximum classification rates of 97%, 94% and 96% were obtained using Stationary Wavelet Transform (SWT), Fast Fourier Transform (FFT) and Discrete Wavelet Transform (DWT) respectively

Statistical analysis of the envelope of backscattered ultrasound involves modelling the envelope using well known statistical distributions. Two such statistical distributions that have become significant for breast cancer are the Nakagami distribution and the homodyned K distribution. The Nakagami distribution presents a simple, generalized model, and was proposed as a model for ultrasonic backscatter by Shankar [38], and was later used for classification of breast masses by Shankar et al. [39], achieving ROC areas of 0.85±0.06 and 0.838±0.065 for the two parameters respectively. The homodyned K model for ultrasound echoes was initially proposed by Dutt and

Greenleaf [40], and later modified by Hruska [41], and Hruska and Oelze [42]. The homodyned K parameter along with BI-RADS classifiers was later applied by Trop et al. [43], who demonstrated their ability to reduce the number of biopsies performed on breast cancer patients by 25%, whilst maintaining 100% sensitivity.

The success of parameters extracted from the spectrum of ultrasound echoes in their ability to classify benign and malignant lesions of the breast is evident, suggesting that spectral characteristics and features of benign and malignant tumors have a high potential and ability to distinguish between these types of tumors. This thesis thus utilizes spectral characteristics of ultrasound RF echoes, more specifically the power spectrum of RF echoes, in an attempt to distinguish between tumor types.

# Chapter 3

# Methodology

## *3.1 Introduction*

This study utilizes four parameters extracted from the power spectrum of ultrasound radio-frequency (RF) echo signals: The peak power, the frequency corresponding to the peak power, termed the peak frequency, half-power bandwidth, and the area under the power spectrum curve within the half-power bandwidth, termed the half power energy. The procedure begins with selection of RF data of patients with tumors that can be clearly distinguished. The boundary of each lesion was traced by knowledgeable non-clinicians. Based on this trace of the tumor, points are manually demarcated on the tumor boundary, and these points are used as a reference to define the regions-of-interest (ROI) that will be analyzed in this study.

This study analyses three different ROI for each point demarcated on the boundary, one outside the lesion, one inside the lesion and the last consisting of areas both inside and outside the lesion, to study the effect of variation in classification accuracy based on the position of the ROI analysed. This study also analyses ROI of three varying sizes, to determine the effect of ROI size on parameter values, and hence classification capability. Next, the power spectrum of each ROI is obtained, and the parameters extracted, which are used for classification between tumor types through Linear Support Vector Mechanism (SVM). Figure 3.1 depicts a flowchart of the algorithm followed in this study.

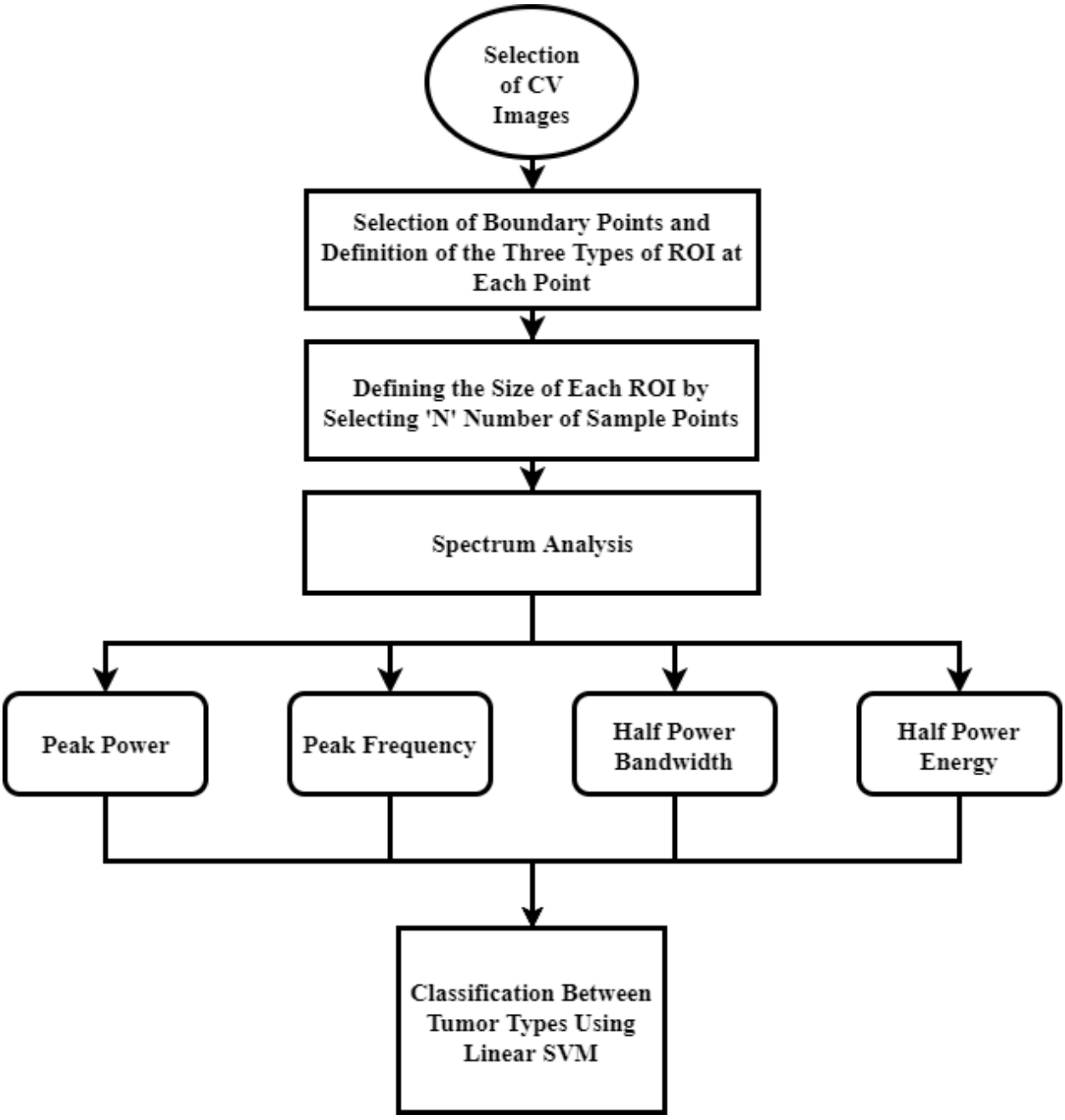


**Figure 3.1:** Algorithm Flowchart

## *3.2 Data Acquisition*

The data-set utilized for this study is from ATL's PMA study (IRB approved) undertaken in 1994 [35]. The data-set consists of RF data and analysis results for 135 patients, from which biopsy classified 100 to have benign masses, and 35 to have malignant masses. The data was acquired at three clinical sites (Thomas Jefferson University, University of Cincinnati and Yale University). The masses were imaged using a Philips Ultrasound (Bothell, WA) UM-9 HDI scanner with an L10-5 (7.5 MHz) linear-array transducer. RF echo-signal data was digitally acquired by interfacing a Spectrasonics Inc. (King of Prussia, PA) acquisition module with the scanner. The L10-5 transducer was used at a default power level and a single transmit focal length, selected by the operator. The RF data were sampled at 20 MHz with an effective dynamic range of 14 bits.

From the data-set, 17 benign and 11 malignant cases were selected for this study. The selection criteria were the visibility of the lesion boundary, and whether it could be distinguished clearly from the surrounding tissue. Visibility of the lesion boundary is crucial for this study as we manually demarcate points on the tumor boundary. Figure 3.2 depicts two cases where the lesion is clearly visible (CV) and not-clearly visible (NCV), for both benign and malignant lesions. Here CV represents the presence of features such as distinct visibility of the lesion boundary compared to the background, proper contrast and reduced noise levels, which leads to proper identification and demarcation of the lesion boundary points. On the other hand, NCV images lack the aforementioned features.

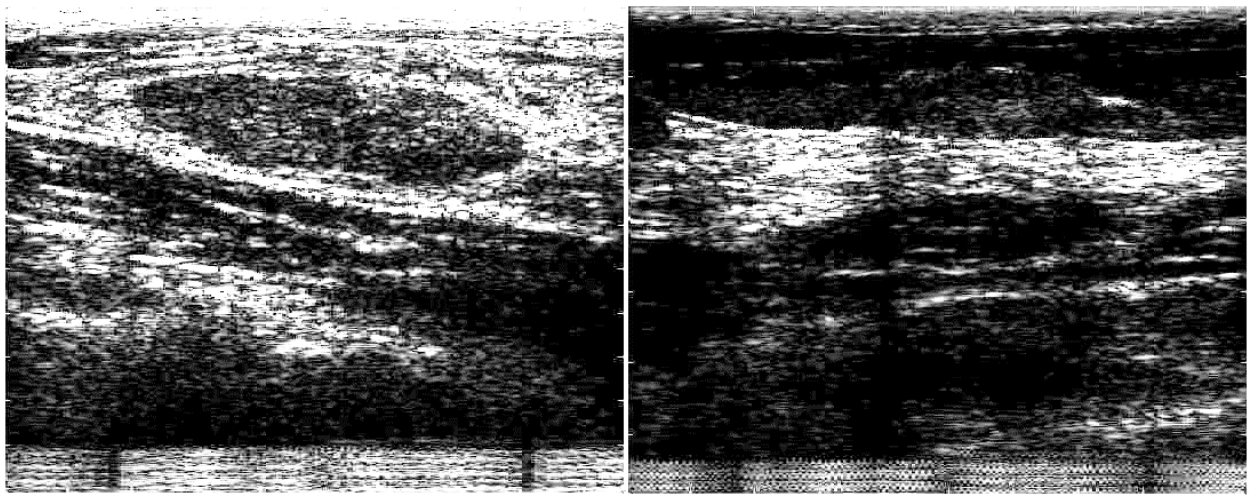

(a)

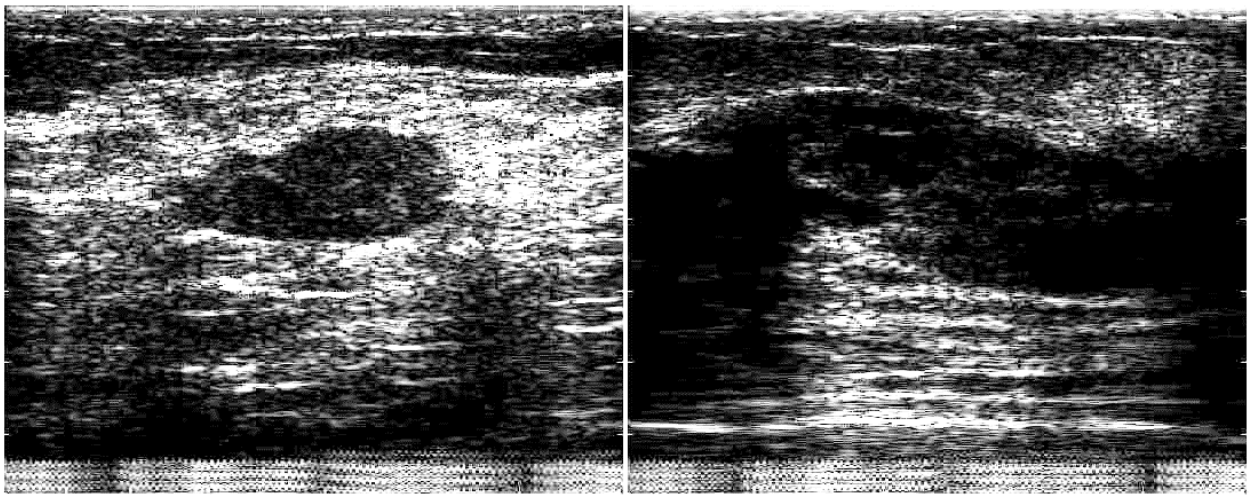

(b)

**Figure 3.2:** (a) CV Benign (left), NCV Benign (right)
(b) CV Malignant (left), NCV Malignant (right)

## *3.3 Manual Selection of Boundary Points and Definition of the Three Types of ROI*

For our analysis, the regions-of-interest (ROI) will be centered about points manually selected on the upper-axial boundary of each malignant or benign tumor. The points thus selected are termed 'boundary points.' The upper-axial boundary is considered because it is present at a lower depth than the lower-axial boundary, making it less susceptible to attenuation and diffraction effects. Points on the tumor boundary are of interest due to the morphological differences that are present between the boundaries of benign and malignant lesions [44]. As mentioned previously, traces of

each lesion were utilized for clear identification of the boundary, and correct placement of the points. The traces were created by knowledgeable non-clinicians, and the tumor-tracing program was written in Visual Basic TM (Microsoft Corporation, Redmond, WA). The boundary selection procedure is displayed in Figure 3.3. In an ideal semi-automated/automated procedure, the entire upper-axial boundary may be selected. For the time being, we will empirically consider 10 points on the upper axial boundary to observe the effect.

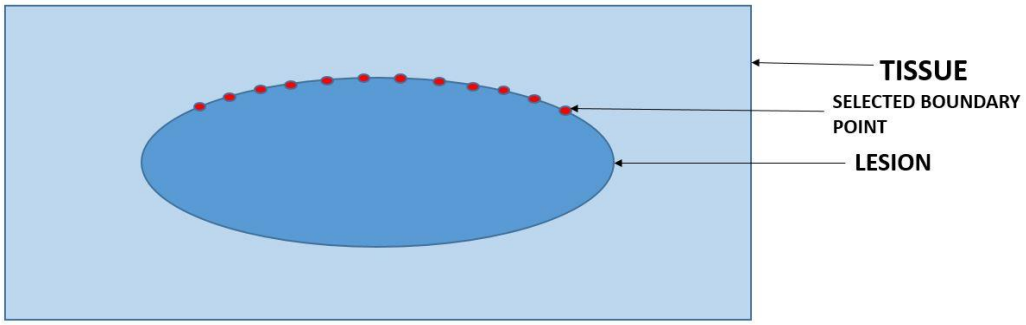


(a)

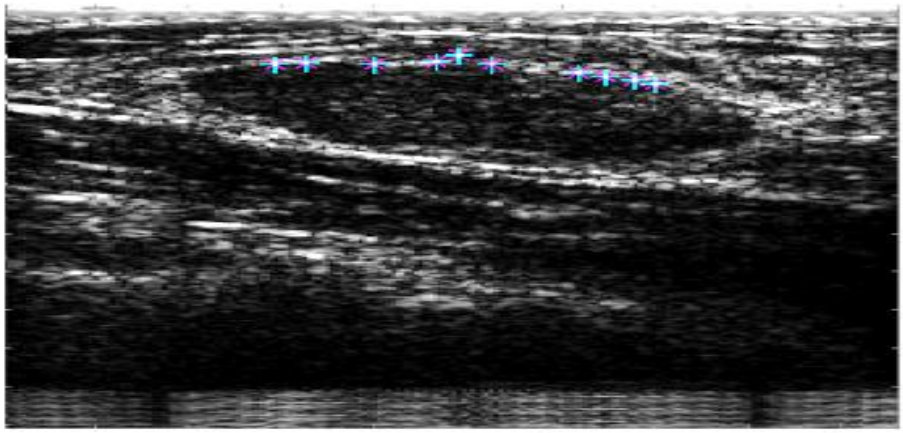

(b)

**Figure 3.3:** (a) Animated representation of the manual selection of points on tumor boundary
(b) Practical selection of the boundary points

This study considers three overlapping ROI, which are situated axially along the A-lines for each point selected on the lesion boundary. The overlapping nature of the ROI will allow for analysis of the changes in frequency domain parameters along the entire region of the upper boundary.

These ROI consist of a region above the boundary point, termed the upper region, a region below the boundary point, termed the lower region and a region consisting of areas both below and above the boundary point, termed the central region. Three different ROI were considered as they have the potential to provide greater avenues of distinction between benign and malignant masses, due to the different characteristics that may be present for both tumor types in each of the three regions.

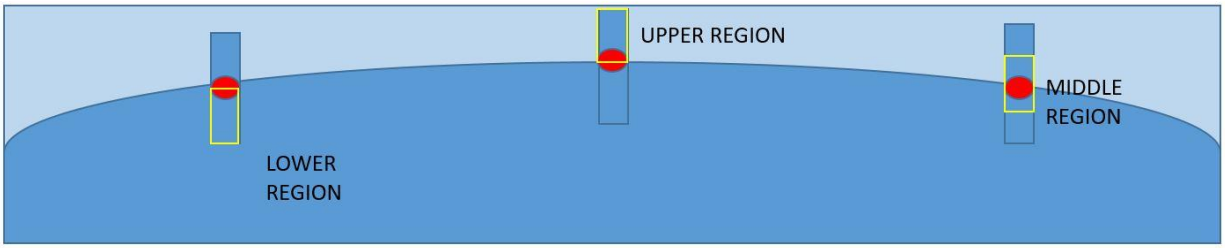


**Figure 3.4:** Representation of ROI at tumor boundary

The upper region will begin at the selected boundary point, and continue upwards for a specific number of samples in the RF image, thus containing area just outside the lesion boundary. The lower region will begin at the selected boundary point and continue downwards for the same number of samples, thus containing area inside the lesion boundary. The central region will be an overlap of upper and lower regions, with the selected boundary point present at the center. Figure 3.4 depicts these 3 ROI as they are present on the tumor boundary, whilst Figure 3.5 provides an in-depth look at the three ROI present at each boundary point.

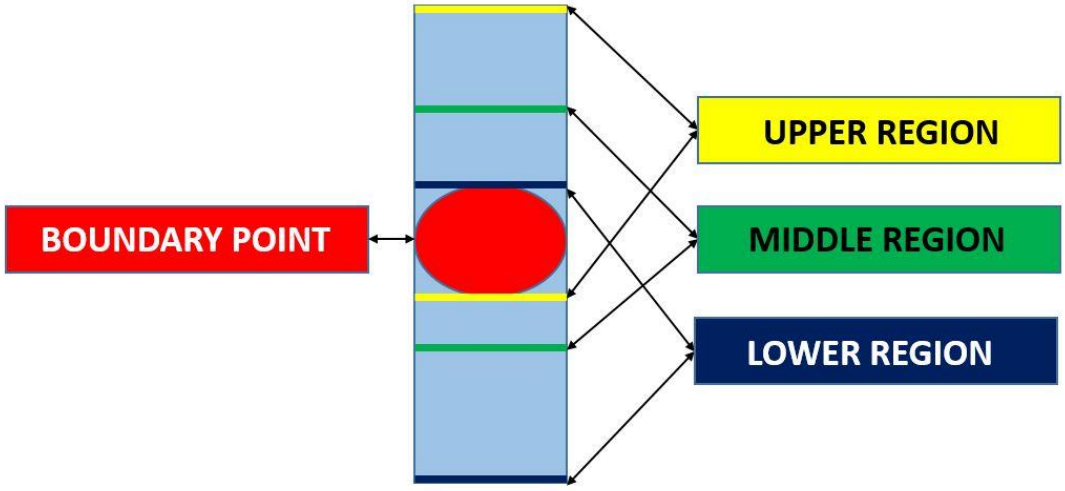


**Figure 3.5:** ROI at each boundary point

### *3.4 Defining the Size of Each ROI by Selecting 'N' Number of Sample Points*

Each ROI consists of a certain number of points along the A-lines of the patient RF data that we analyze, and we define this as the number of samples. The number of samples considered for analysis within each ROI again presents another avenue of discussion. As some of the tumors are located very close to the surface, choosing a large number of samples could mean inclusion of features such as blood vessels or skin into the upper region, which is undesirable for analysis purposes. Furthermore, a smaller number of samples may create a region that is too small to be adequately analyzed, and hence provide parameter values that are ineligible for classification purposes.

To overcome the uncertainty associated with choosing the appropriate number of samples in each ROI, we have chosen to analyze 3 different number of samples in this study: 30 samples, 50 samples and 70 samples. On the one hand, an ROI consisting of 30 samples should provide an adequate area to analyze and obtain suitable parameter values. On the other hand, an ROI consisting of 70 samples wouldn't include blood vessels or skin, and is thus again suitable for classification purposes. An ROI consisting of 50 samples provides an intermediate between the other two samples sizes, and the three varying sizes will allow for the analysis of classification accuracy against number of samples.

## *3.5 Feature Extraction*

All processing software were written in MATLAB$^{TM}$ (The Mathworks, Inc., Natick, MA). The first step involved obtaining the frequency response of the RF data for each tumor. Next, the power spectrum was obtained from the magnitude response, according to the formula for normalized power:

$$Power = \frac{(Magnitude)^2}{Length}$$

The parameters used for analysis were extracted from the power spectrum of each RF data. A description of the parameters is provided below:

i. **Peak power:** maximum value of power present in the power spectrum of each RF data.
ii. **Peak frequency:** the frequency corresponding to the peak power.
iii. **Half-power bandwidth:** interval between frequencies in the power spectrum where the power has dropped to 3dB value, or a factor of $1/\sqrt{2}$ of the peak value.
iv. **Half-power energy:** The area under the power spectrum curve within the Half-power Bandwidth.

A visual representation of each parameter in a power spectrum curve is provided in Figure 3.6.

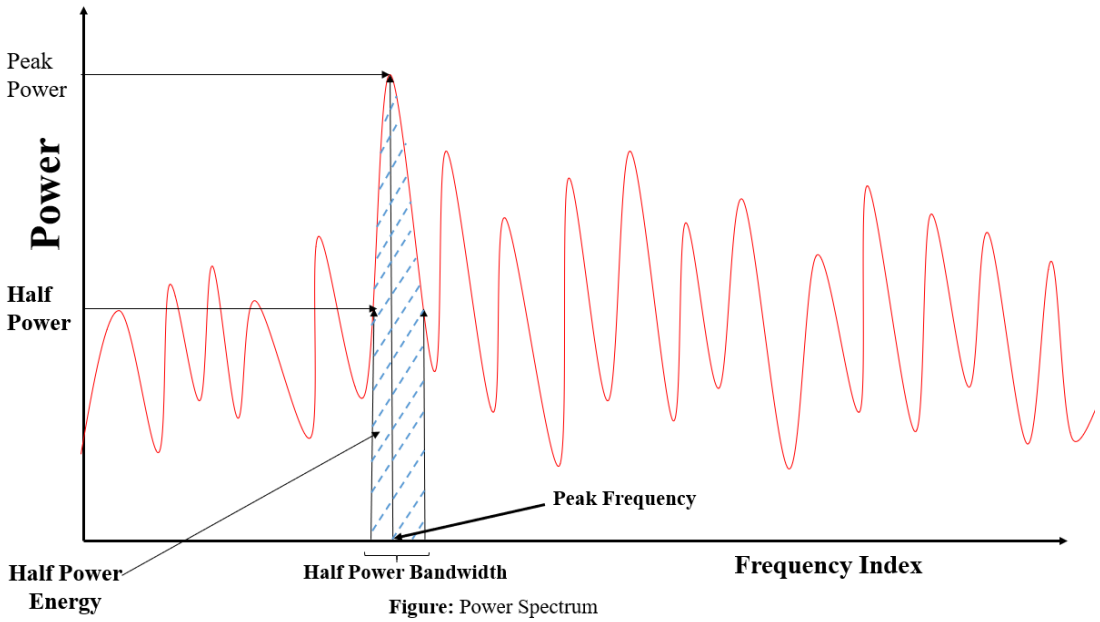


**Figure 3.6:** Peak power, peak frequency, half-power bandwidth and half-power energy in a power spectrum curve

## *3.6 Classification*

We utilize Linear SVM algorithm for classification. Each patient data consisted of 10 points, with each point used to define 3 ROI's. Furthermore, ROI's of three varying sizes are considered. For a certain number of sample points, i.e. 30 samples, 50 samples or 70 samples, the parameters obtained at the 10 selected points were averaged to acquire a single value for each of the upper, lower and central regions respectively. Hence, for a certain number of samples, each tumor yielded 3 unique values for each of the 4 parameters, one for the upper region, one for the lower region and one for the central region, and these values were used to classify the tumors. This process of obtaining parameter values for Linear SVM classification is described by the flowchart in Figure 3.7.

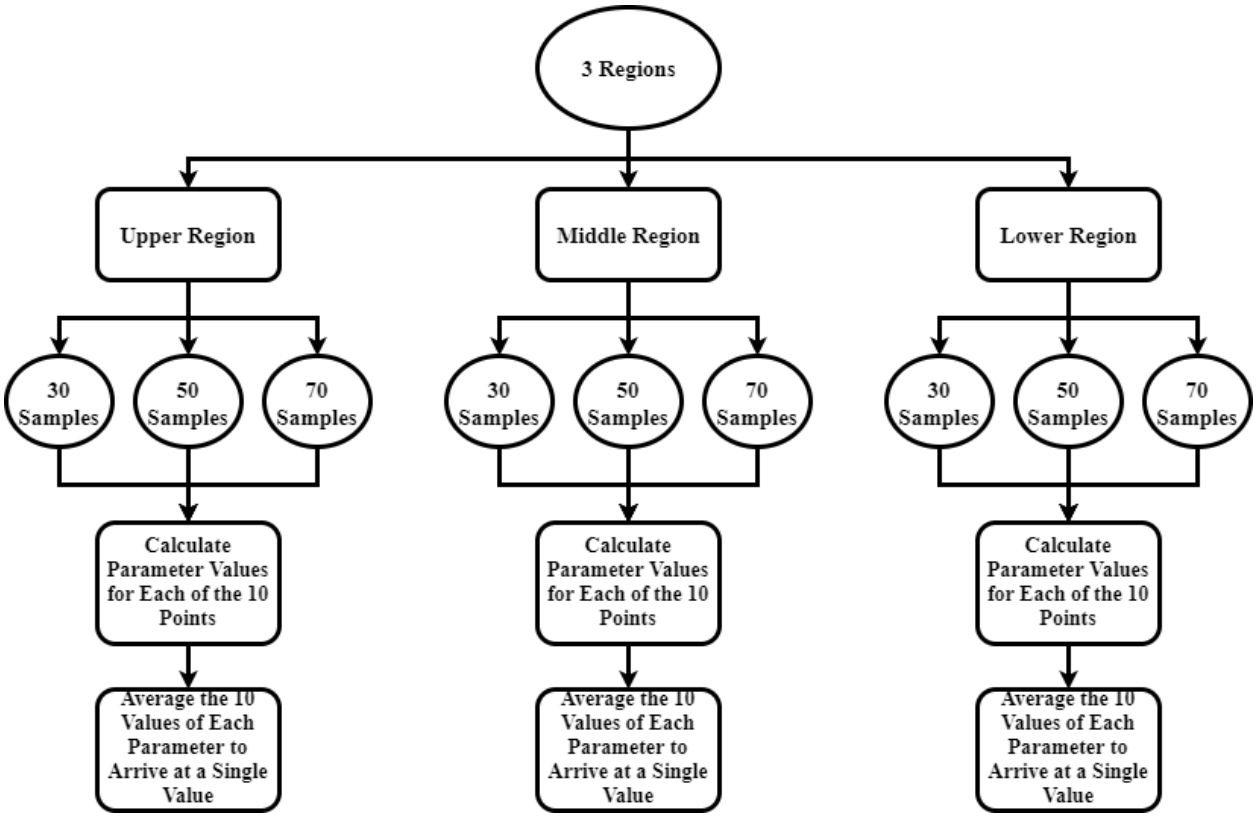


**Figure 3.7:** Process of obtaining values for classification using Linear SVM

## *3.7 Conclusion*

After the required parameters were extracted from each ROI, and the average values for each ROI were obtained, classification was performed using these average values. The classification procedure was conducted in two phases, where multiple combinations were tried, and a successive elimination based on highest classification accuracy of these combinations yielded the two best parameters, and the region from which these two parameters were attained.

# Chapter 4

# Results and Discussion

## *4.1 Introduction*

Data was analyzed for a total of 28 patients, amongst which there were 11 cancerous, and 17 non-cancerous tumor types. Classification was performed for three different sizes of ROI, i.e. 30 samples, 50 samples and 70 samples, individually, all taken axially along the corresponding A-lines.

## *4.2 Classification Procedure*

The classification process for each ROI size consisted of two phases:

I. **Phase 1:** Phase one consisted of two steps:

(i) **Step 1:** Classification was done using individual parameter values from all three regions, i.e. for each individual parameter, e.g. peak frequency, classification was carried out using the value of peak frequency in the lower region, the upper region and the middle region. After this was done for all 4 parameters, the two parameters providing the highest classification accuracy were selected for the next phase.

(ii) **Step 2:** Classification was done using all four parameter values in a specific region, i.e., for each region, e.g. the lower region, the values of all four parameters in that region were utilized for classification. Following this, the two regions providing the highest classification accuracy were selected for the next phase.

II. **Phase 2:** Phase two of the classification procedure took place as follows:

(i) Classification was conducted using the values of the two highest performing parameters from all three regions

(ii) Classification was conducted using the values of the two highest performing parameters from one of the highest performing regions

(iii) Classification was conducted using the values of the two highest performing parameters from the other selected region

This process is outlined in the flowchart in Figure 4.1.

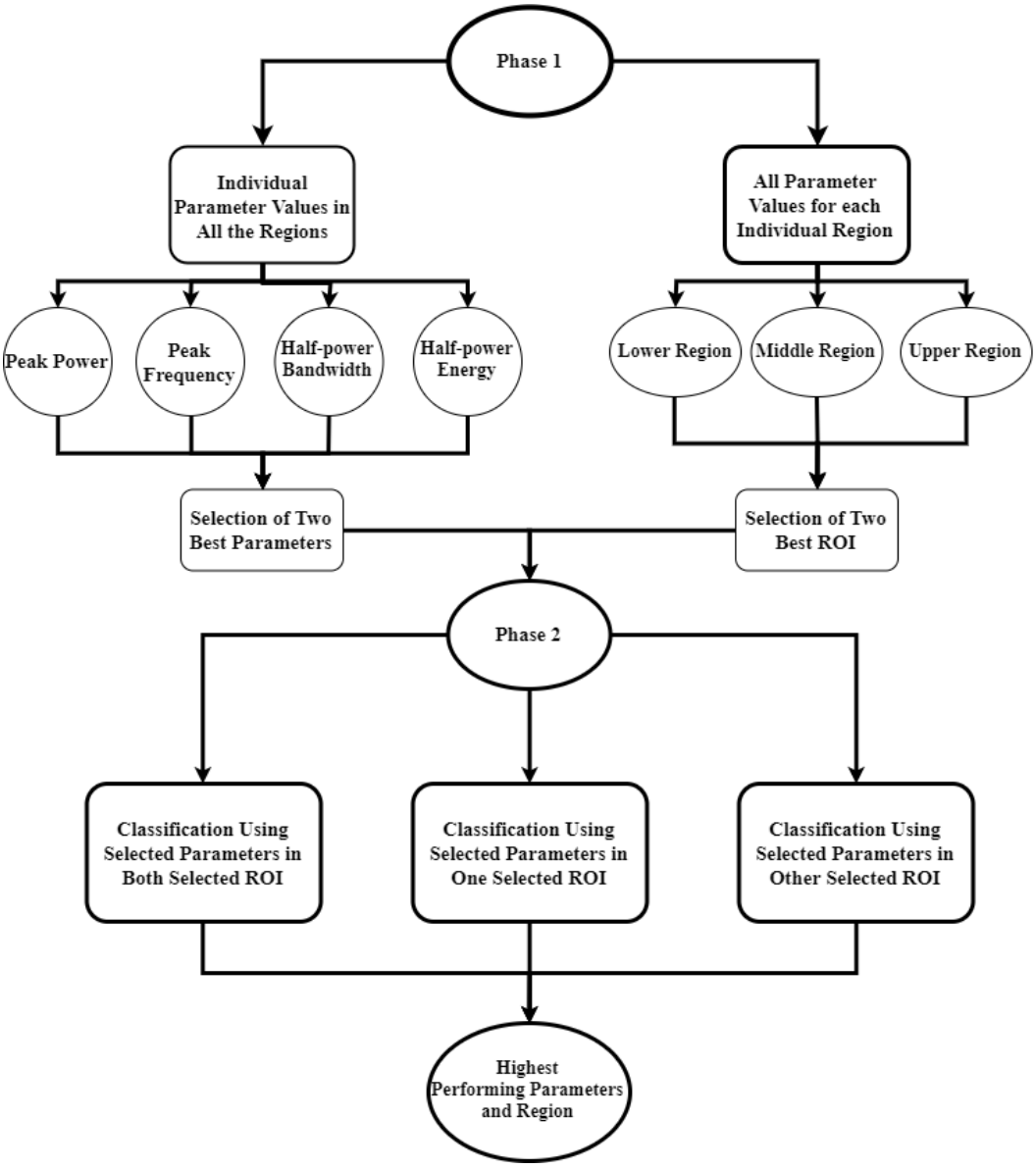


**Figure 4.1:** Classification procedure

## *4.3 Results for ROI Size of 30 Samples*

**Phase 1, Step 1: Classification using individual parameter values**

**Peak power:** The peak power from all three regions provided a classification accuracy of 85.7%.

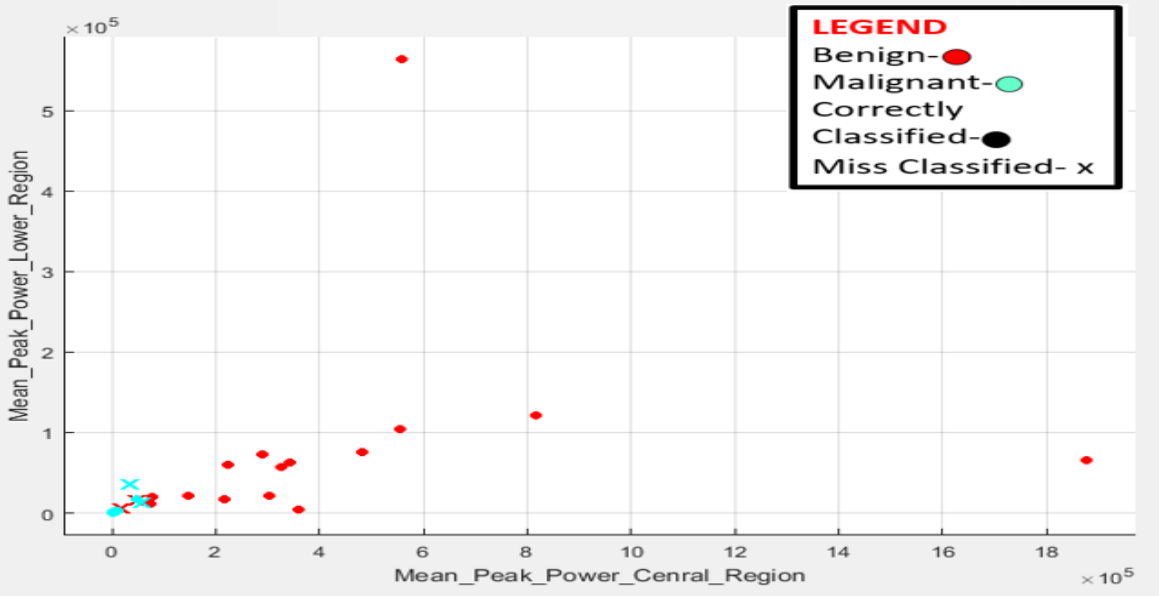


(a)

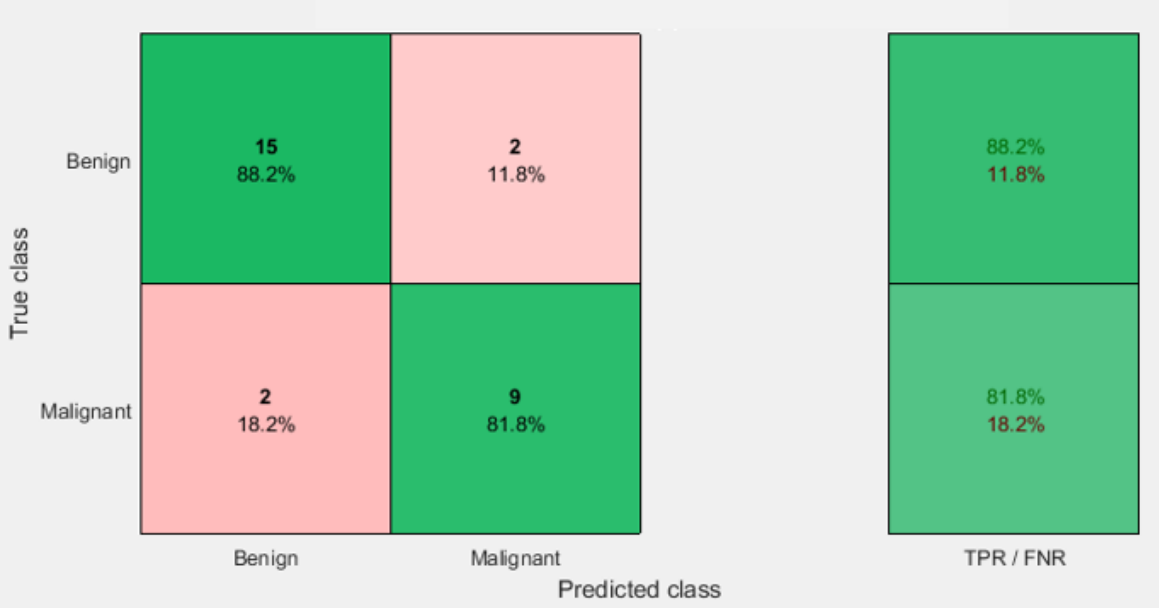


(b)

**Figure 4.2:** (a) Scatter Plot and (b) Confusion Matrix for classification using peak power values from all three regions (30 samples)

**Peak Frequency:** The peak frequency from all three regions provided a classification accuracy of 57.1%.

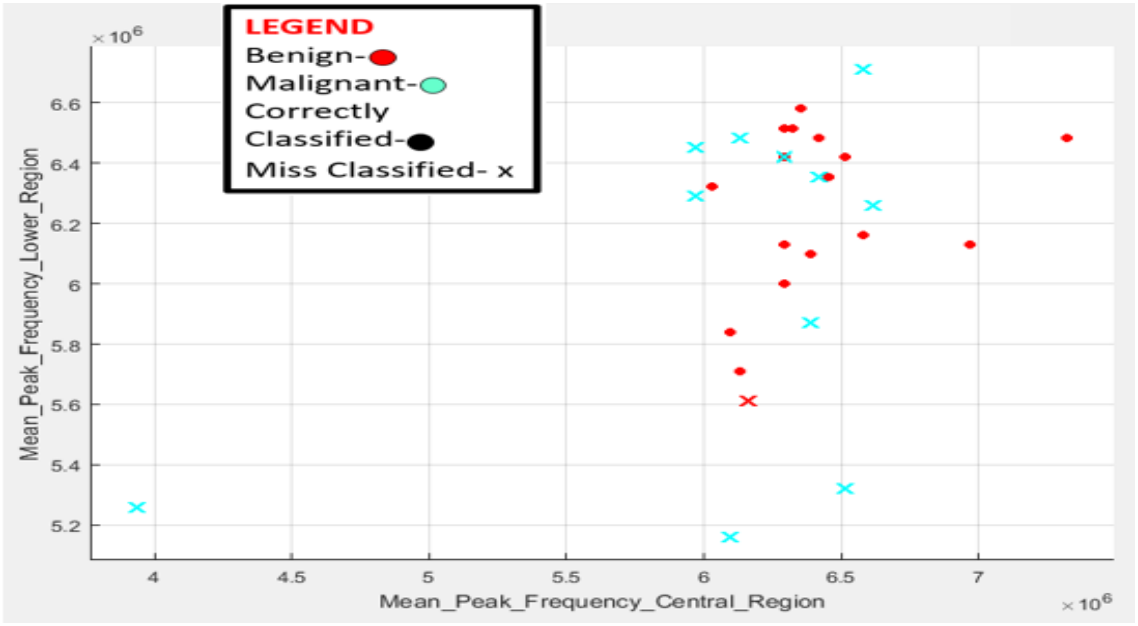


(a)

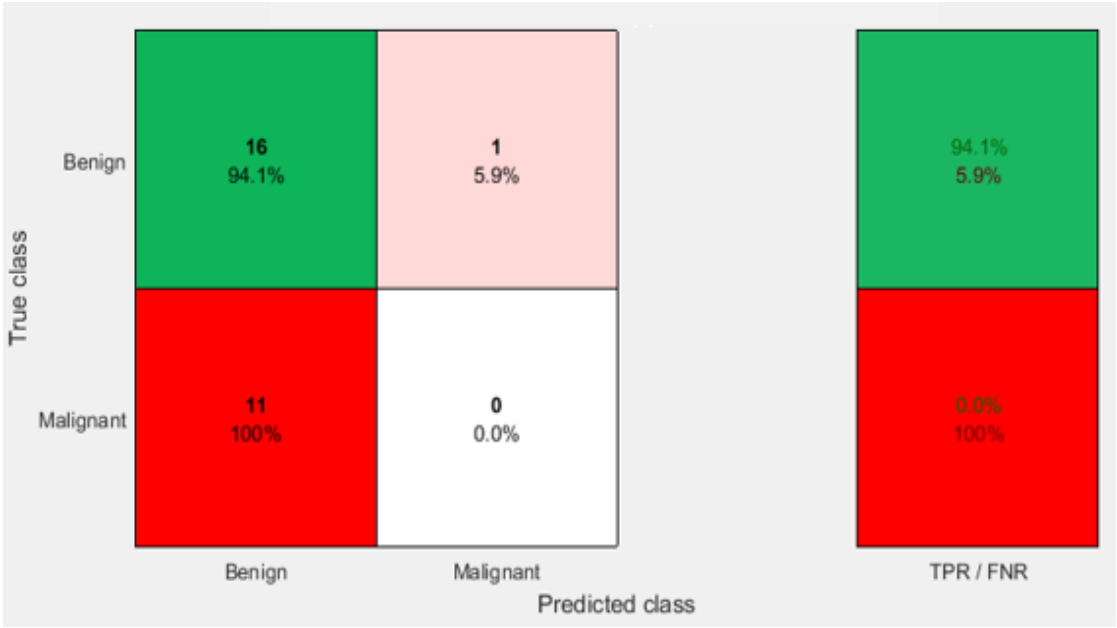


(b)

**Figure 4.3:** (a) Scatter Plot and (b) Confusion Matrix for classification using peak frequency values from all three regions (30 samples)

**Half-power bandwidth:** The half-power bandwidth from all three regions provided a classification accuracy of 75.0%.

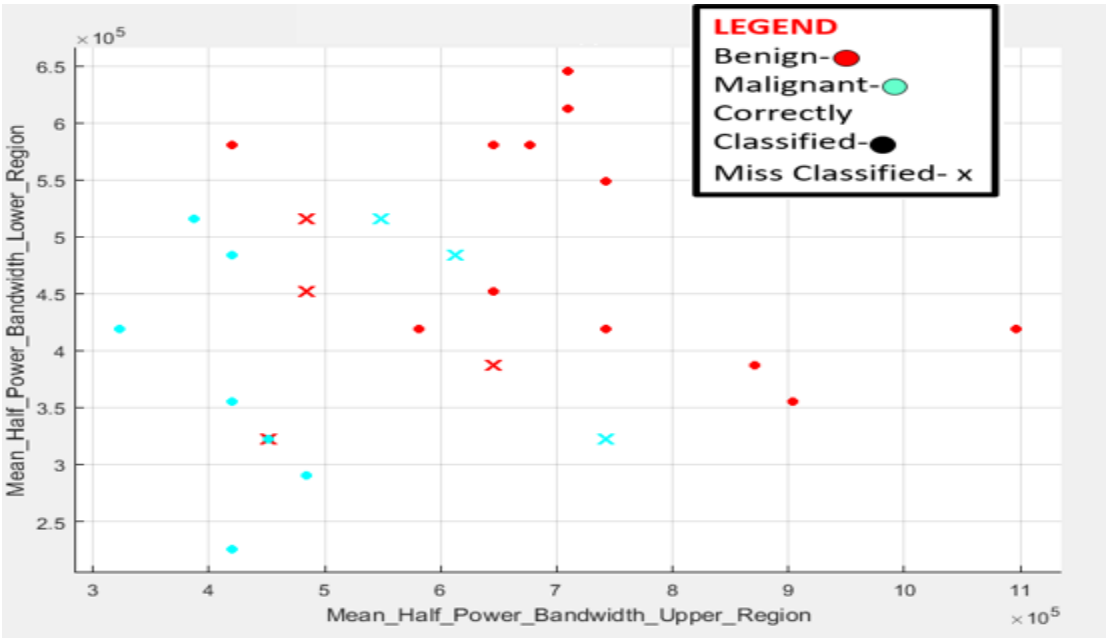


(a)

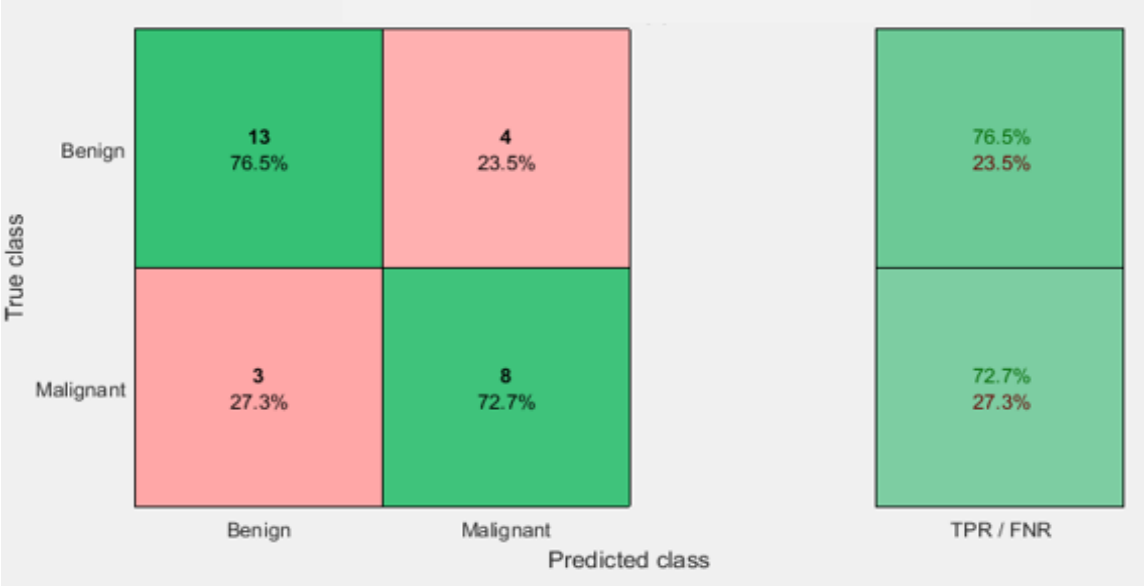


(b)

**Figure 4.4:** (a) Scatter Plot and (b) Confusion Matrix for classification using half-power bandwidth values from all three regions (30 samples)

**Half-power energy:** The half-power energy from all three regions provided a classification accuracy of 82.1%.

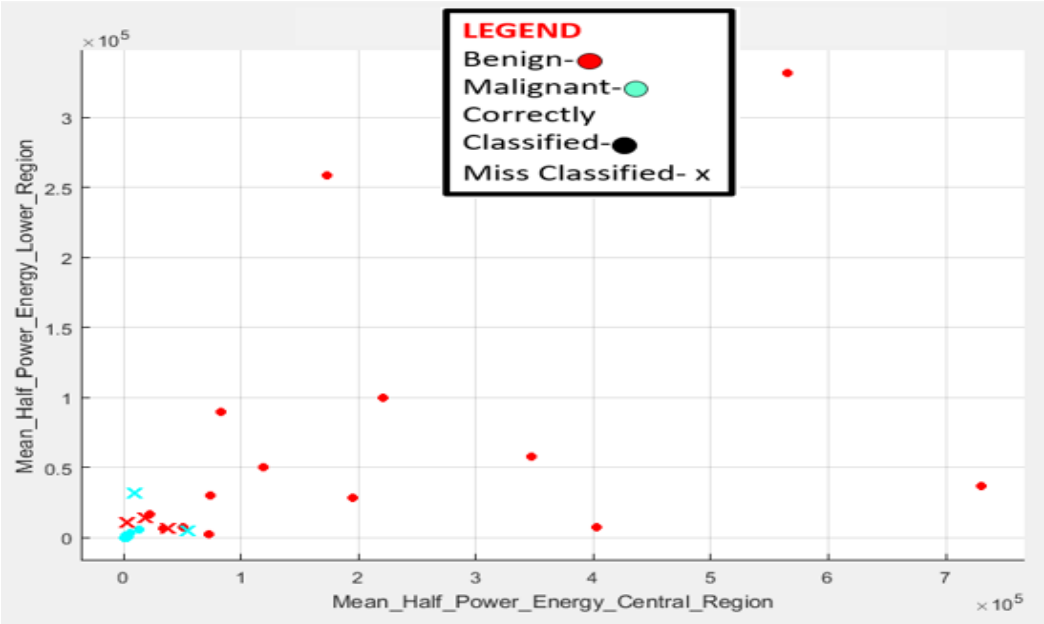


(a)

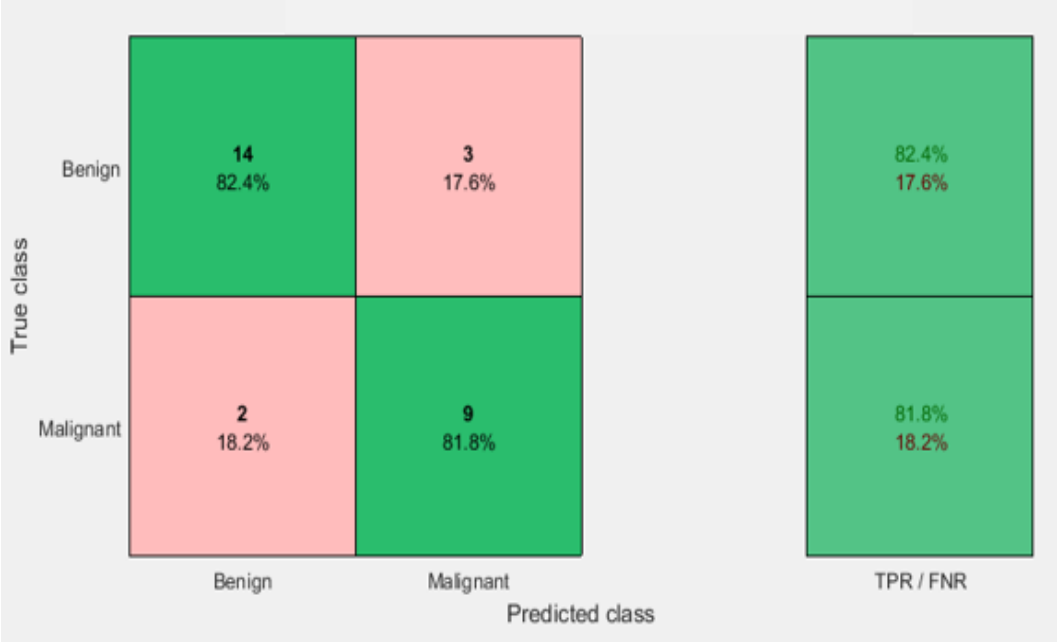


(b)

**Figure 4.5:** (a) Scatter Plot and (b) Confusion Matrix for classification using half-power energy values from all three regions (30 samples)

**Phase 1, Step 2: Classification using all parameter values in each ROI**

**Classification using all values in Lower Region:** The parameter values in the lower region provided a classification accuracy of 75%.

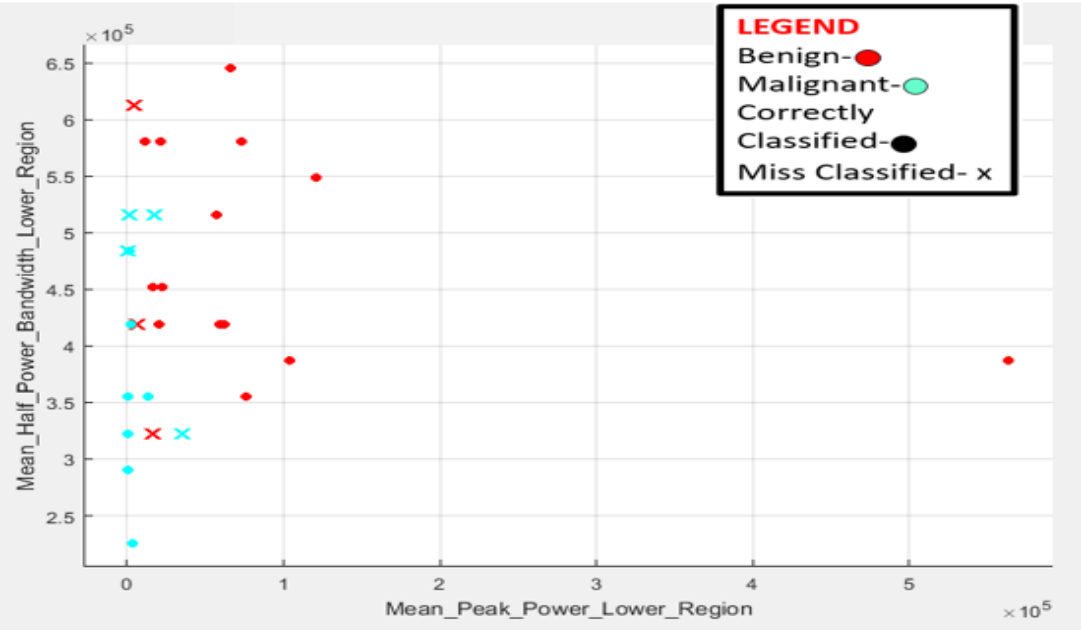


(a)

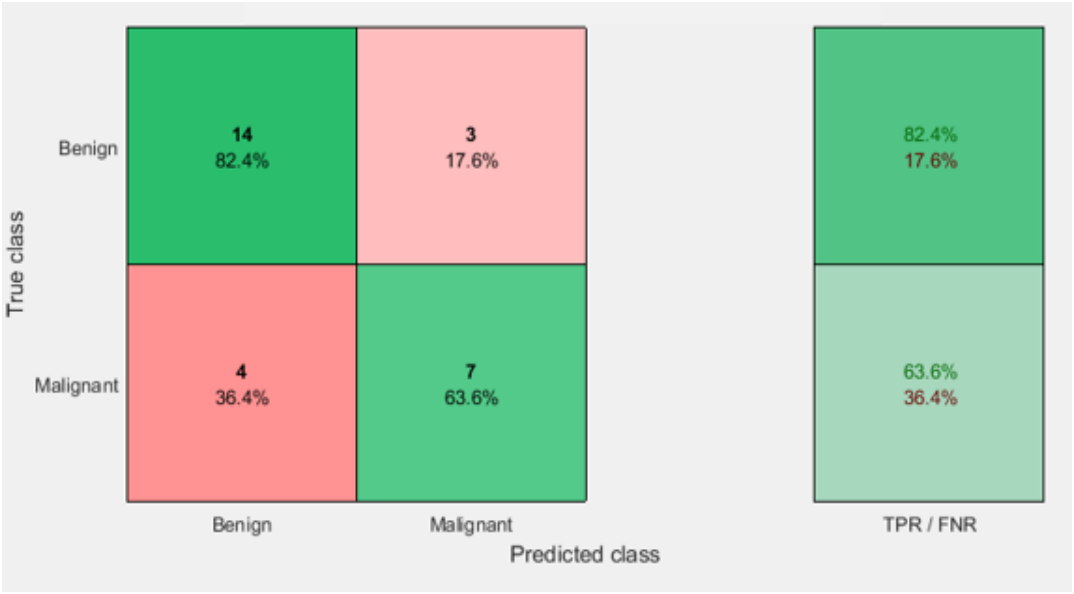


(b)

**Figure 4.6:** (a) Scatter Plot and (b) Confusion Matrix for classification using all parameter values in lower region (30 samples)

**Classification using all values in Central Region:** The parameter values in the lower region provided a classification accuracy of 89.3%.

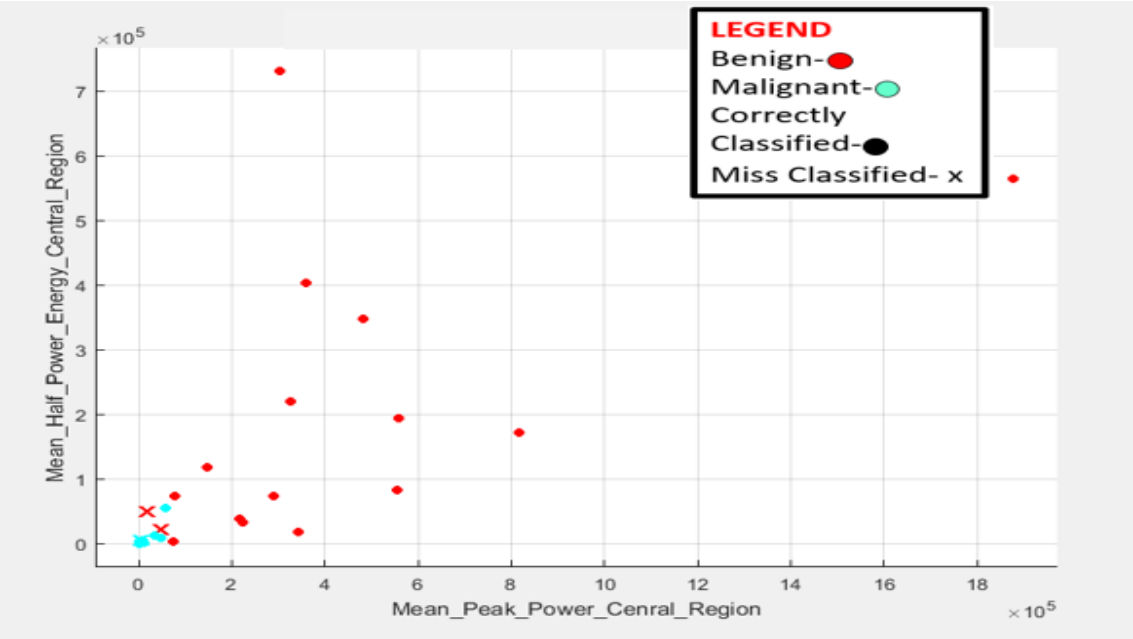


(a)

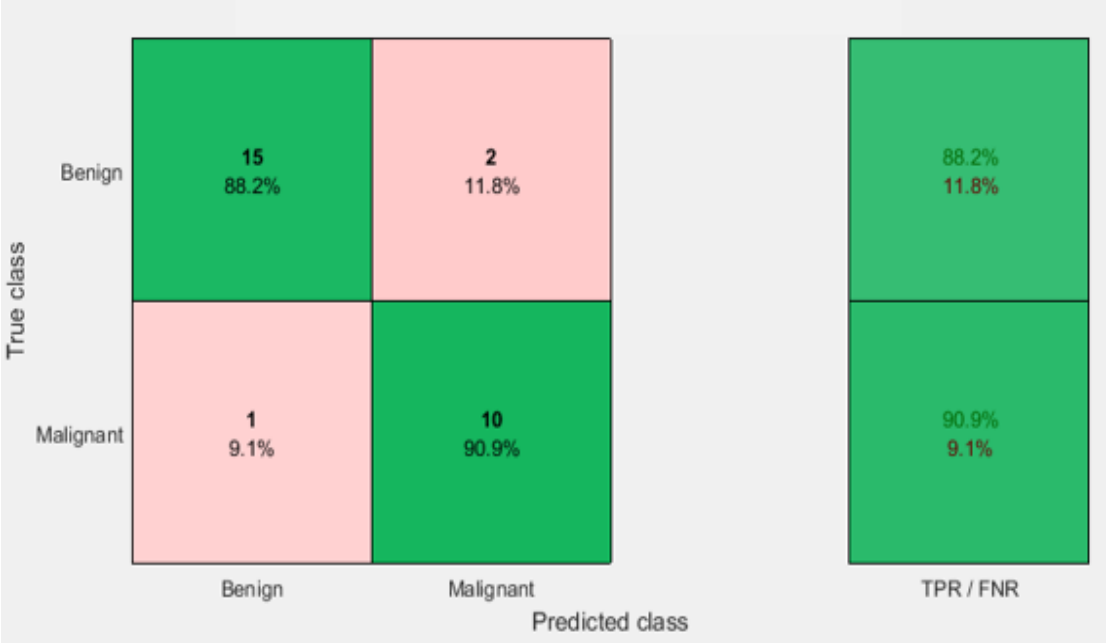


(b)

**Figure 4.7:** (a) Scatter Plot and (b) Confusion Matrix for classification using all parameter values in central region (30 samples)

**Classification using all values in Upper Region:** The parameter values in the lower region provided a classification accuracy of 85.7%.

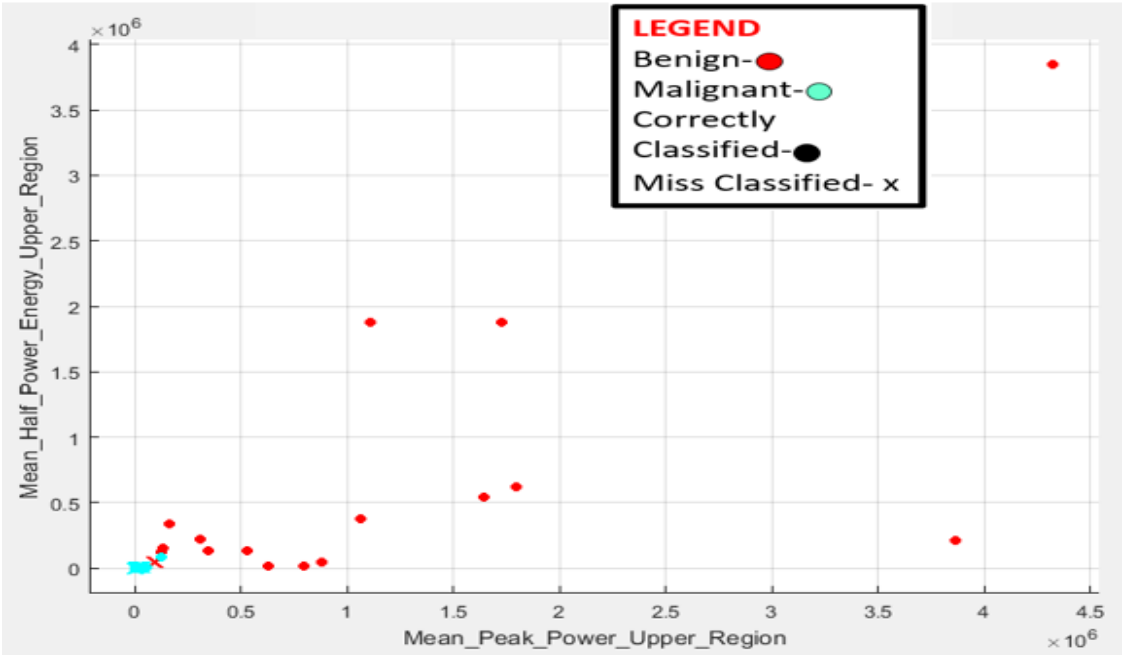


(a)


(b)

**Figure 4.8:** (a) Scatter Plot and (b) Confusion Matrix for classification using all parameter values in upper region (30 samples)

| Parameters | Percentage of Accuracy |
|---|---|
| **Peak Power** | 85.7% |
| **Peak Frequency** | 57.1% |
| **Half-power Bandwidth** | 75% |
| **Half-power Energy** | 82.1% |

(a)

| Regions | Percentage of Accuracy |
|---|---|
| **Upper Region** | 85.7% |
| **Central Region** | 89.3% |
| **Lower Region** | 75% |

(b)

**Table 4.1:** Phase one classification accuracies (30 samples)

Hence, for 30 samples, the two parameters providing the highest classification accuracy are:

(i) Peak power

(ii) Half-power energy

The two ROI providing the highest classification accuracy are:

(i) Upper region

(ii) Central region

**Phase 2: Classification using highest performing parameters and regions**

**Classification using peak power and half-power energy values from all three regions:** This process yielded an accuracy of 85.7%.

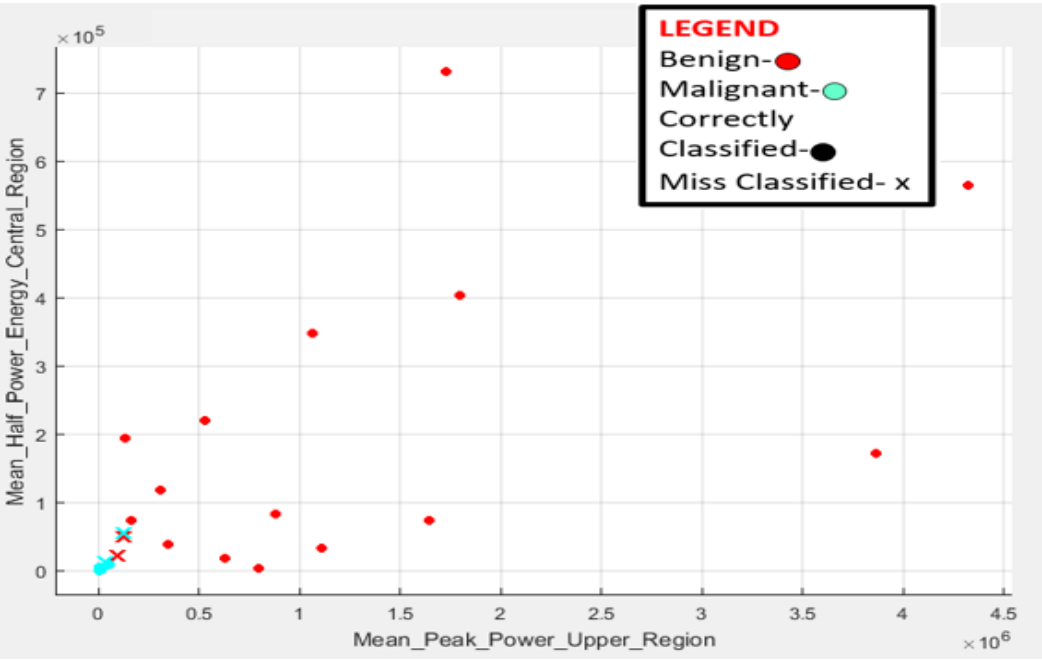


(a)

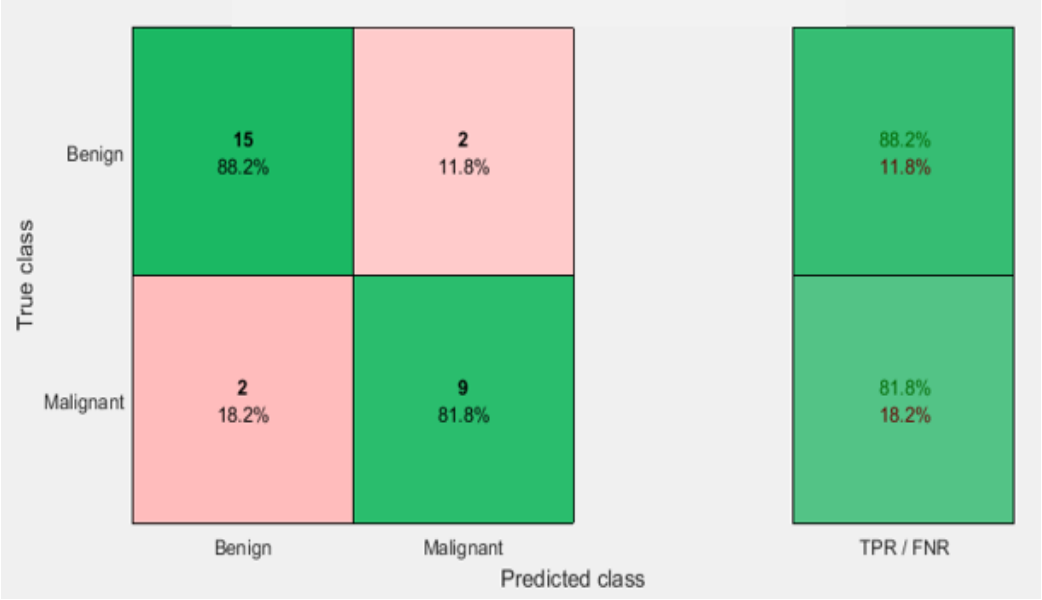


(b)

**Figure 4.9:** (a) Scatter Plot and (b) Confusion Matrix for classification using all peak power and half-power energy values in all three regions (30 samples)

**Classification using peak power and half-power energy values from central region:** This process yielded an accuracy of 85.7%.

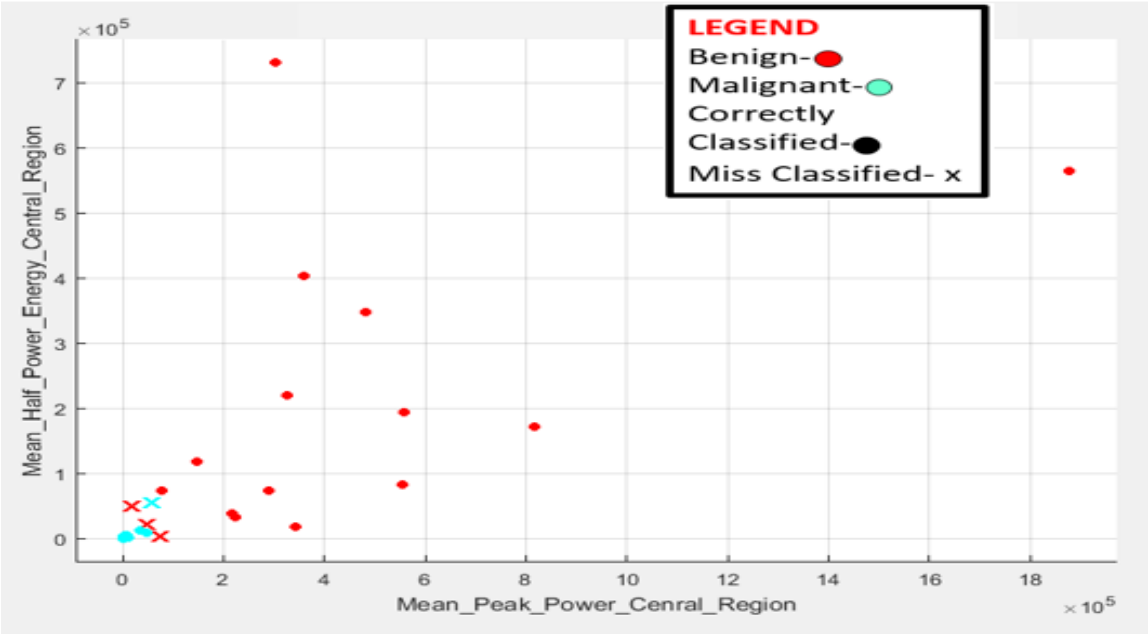


(a)


(b)

**Figure 4.10:** (a) Scatter Plot and (b) Confusion Matrix for classification using all peak power and half-power energy values in central region (30 samples)

**Classification using peak power and half-power energy values from upper region:** This process yielded an accuracy of 92.9%.

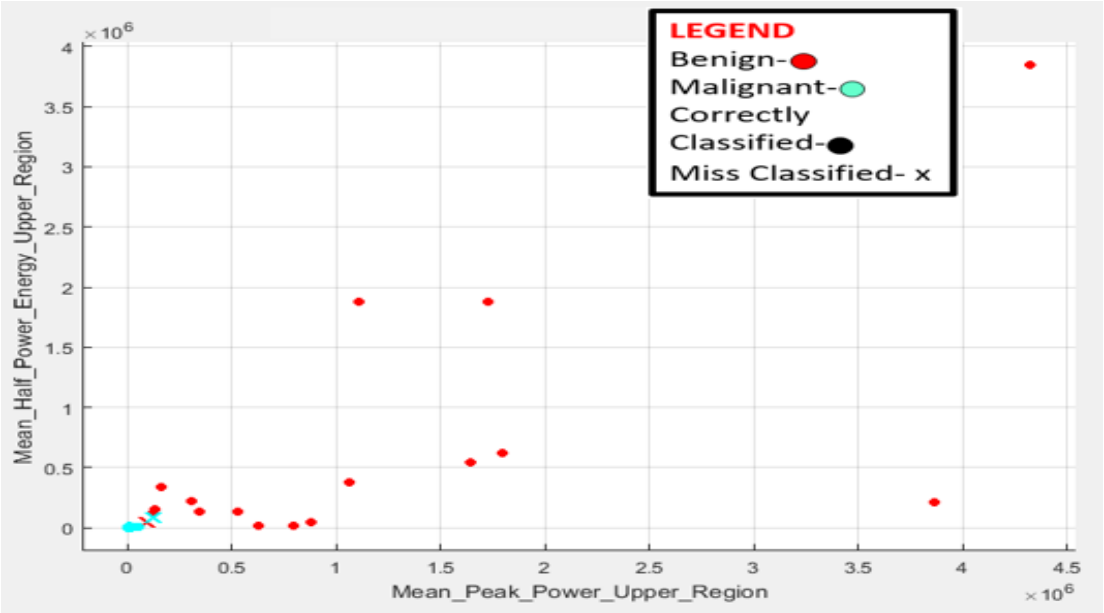


(a)

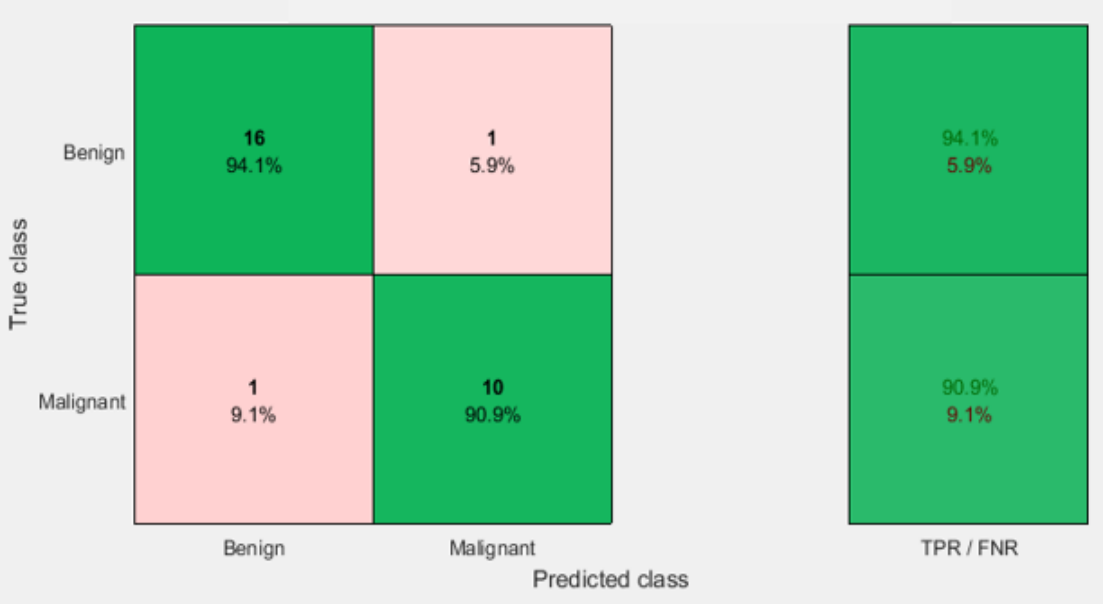


(b)

**Figure 4.11:** (a) Scatter Plot and (b) Confusion Matrix for classification using all peak power and half-power energy values in upper region (30 samples)

## *4.4 Results for ROI Size of 50 Samples*

**Phase 1, Step 1: Classification using individual parameter values**

**Peak power:** The peak power from all three regions provided a classification accuracy of 92.9%.

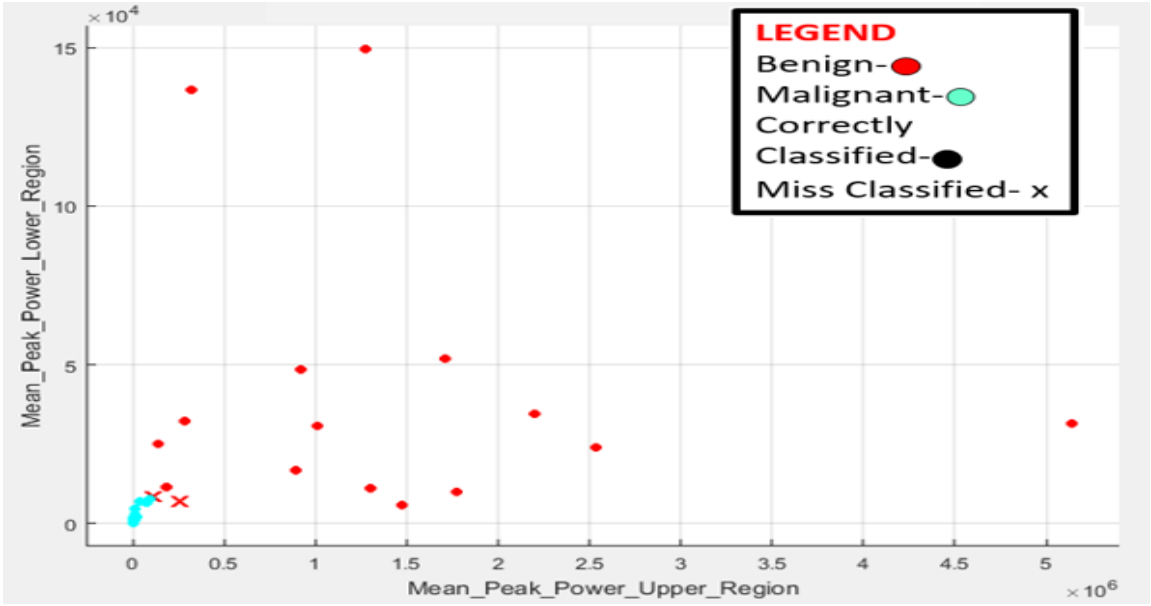


(a)

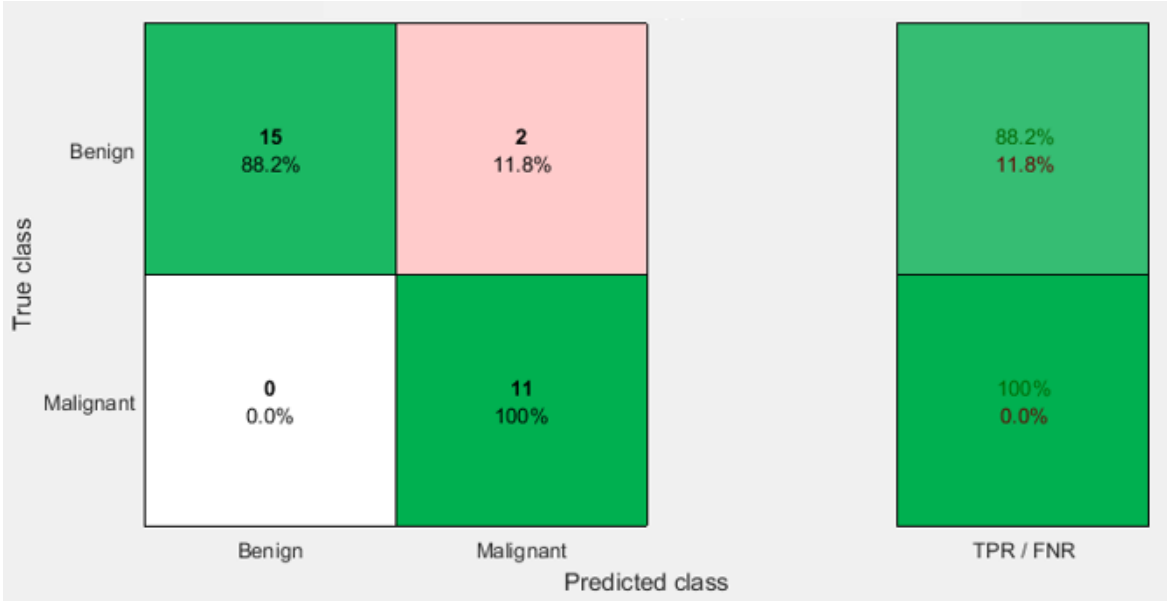


(b)

**Figure 4.12:** (a) Scatter Plot and (b) Confusion Matrix for classification using peak power values from all three regions (50 samples)

**Peak Frequency:** The peak frequency from all three regions provided a classification accuracy of 67.9%.

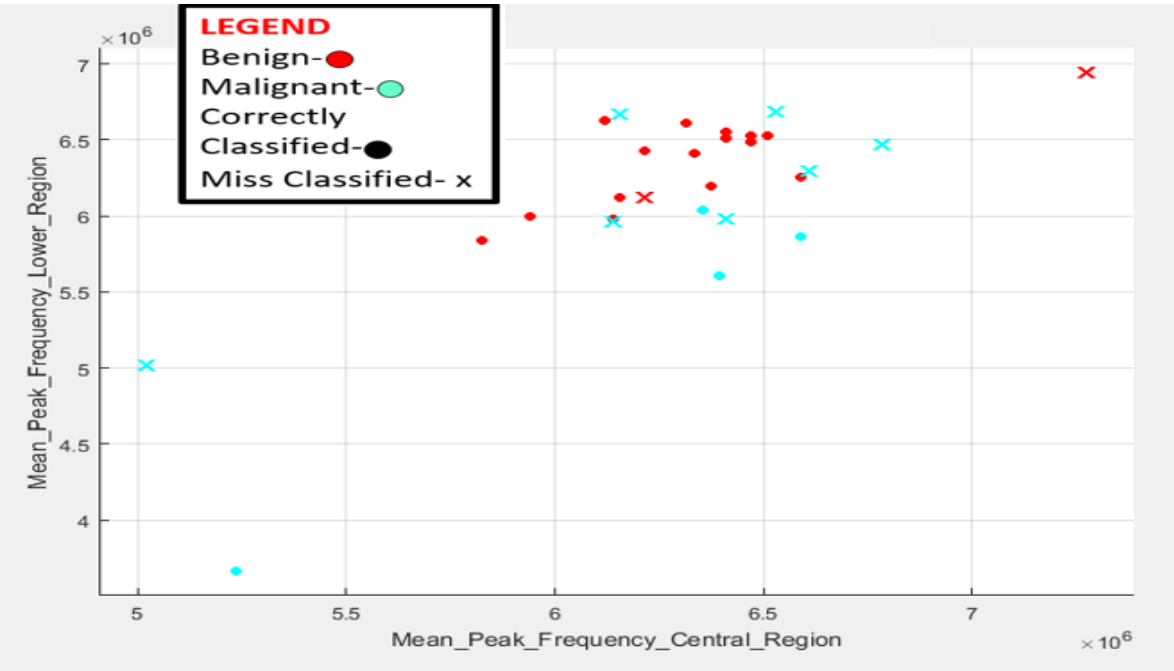


(a)

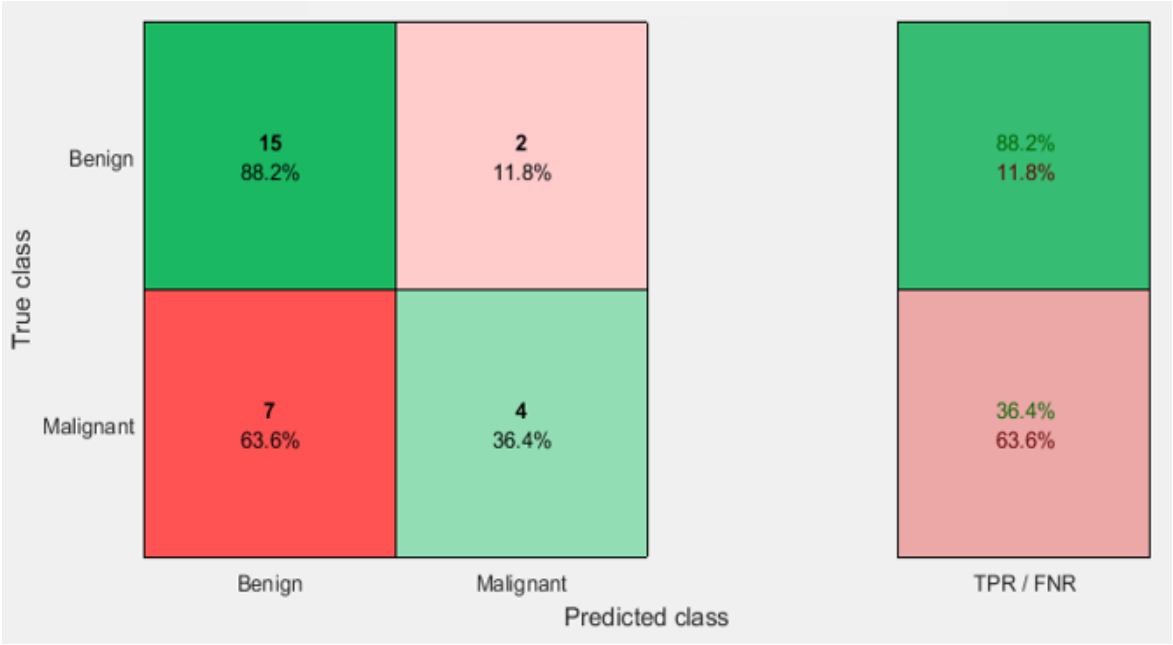


(b)

**Figure 4.13:** (a) Scatter Plot and (b) Confusion Matrix for classification using peak frequency values from all three regions (50 samples)

**Half-power bandwidth:** The half-power bandwidth from all three regions provided a classification accuracy of 78.6%.

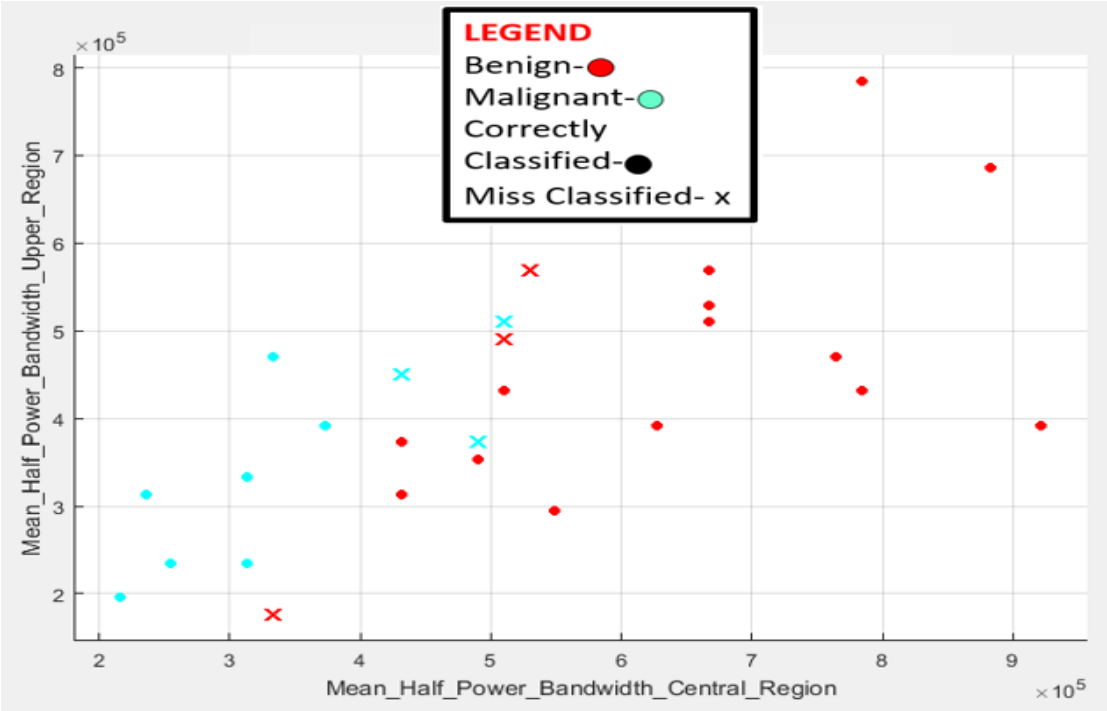


(a)


(b)

**Figure 4.14:** (a) Scatter Plot and (b) Confusion Matrix for classification using half-power bandwidth values from all three regions (50 samples)

**Half-power energy:** The half-power energy from all three regions provided a classification accuracy of 85.7%.

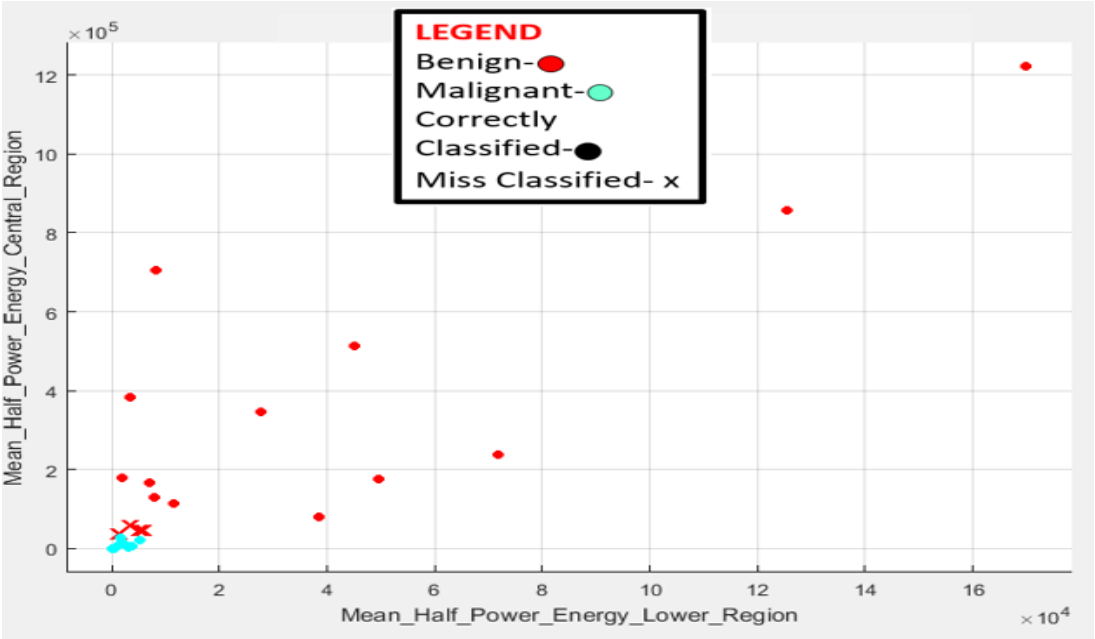


(a)

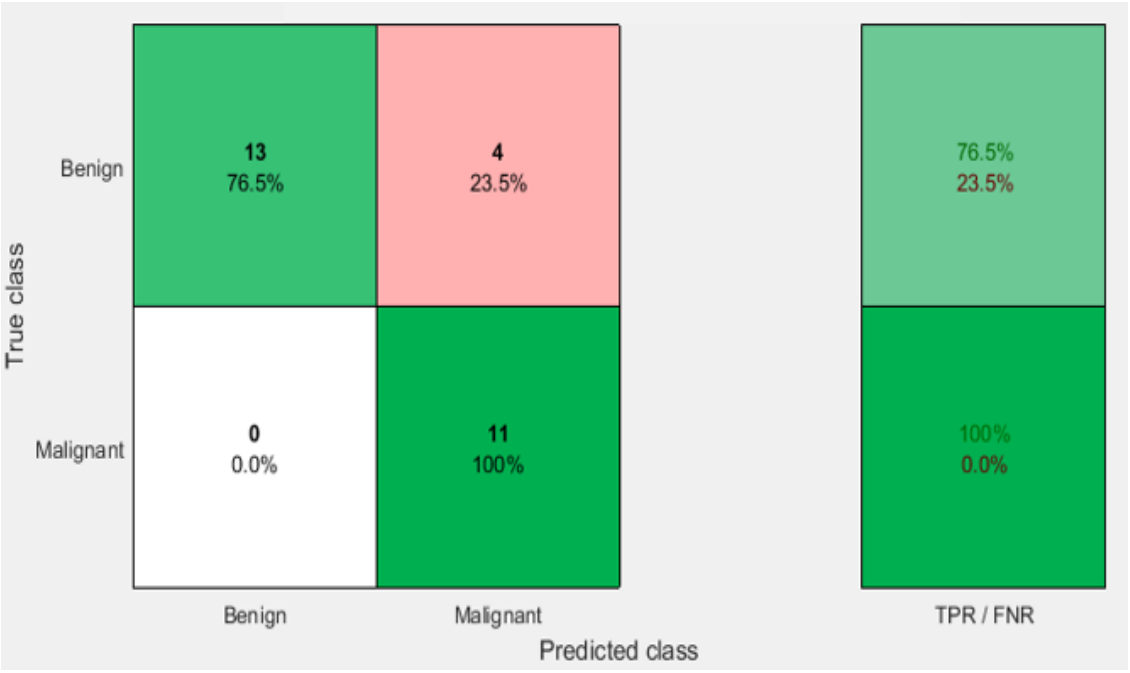


(b)

**Figure 4.15:** (a) Scatter Plot and (b) Confusion Matrix for classification using half-power energy values from all three regions (50 samples)

**Phase 1, Step 2: Classification using all parameter values in each ROI**

**Classification using all values in Lower Region:** The parameter values in the lower region provided a classification accuracy of 78.6%.

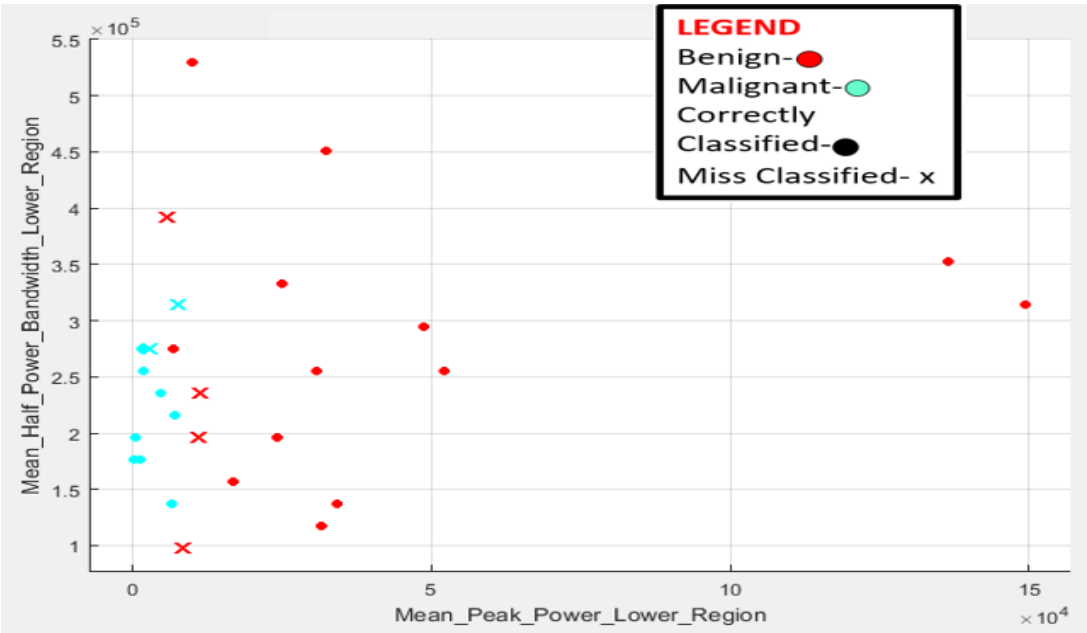


(a)

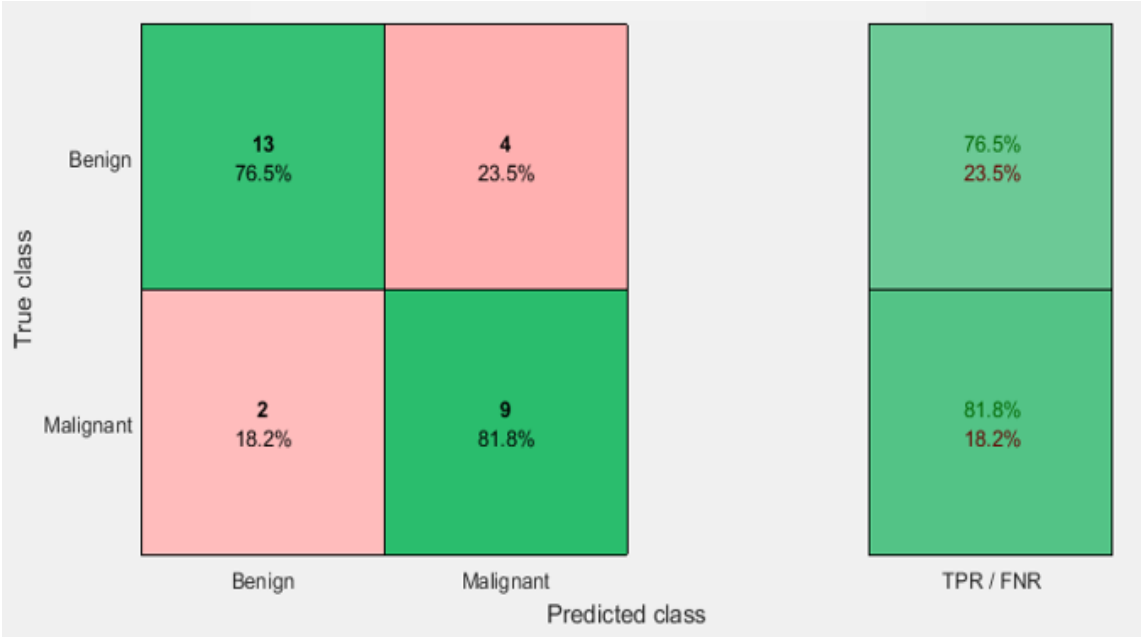


(b)

**Figure 4.16:** (a) Scatter Plot and (b) Confusion Matrix for classification using all parameter values in lower region (50 samples)

**Classification using all values in Central Region:** The parameter values in the lower region provided a classification accuracy of 85.7%.

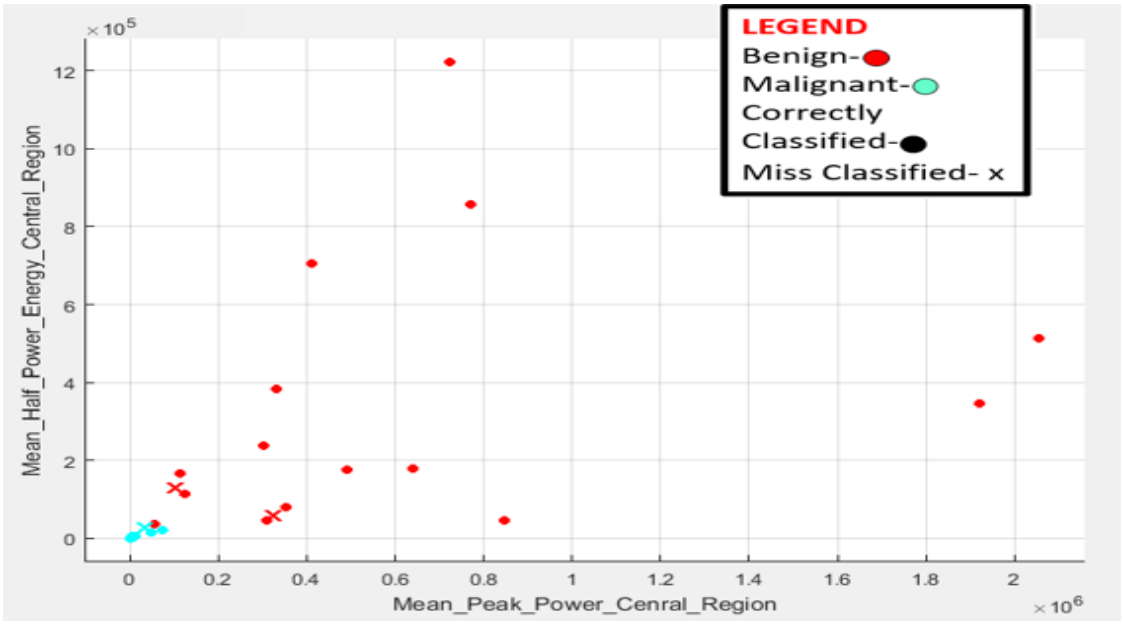


(a)

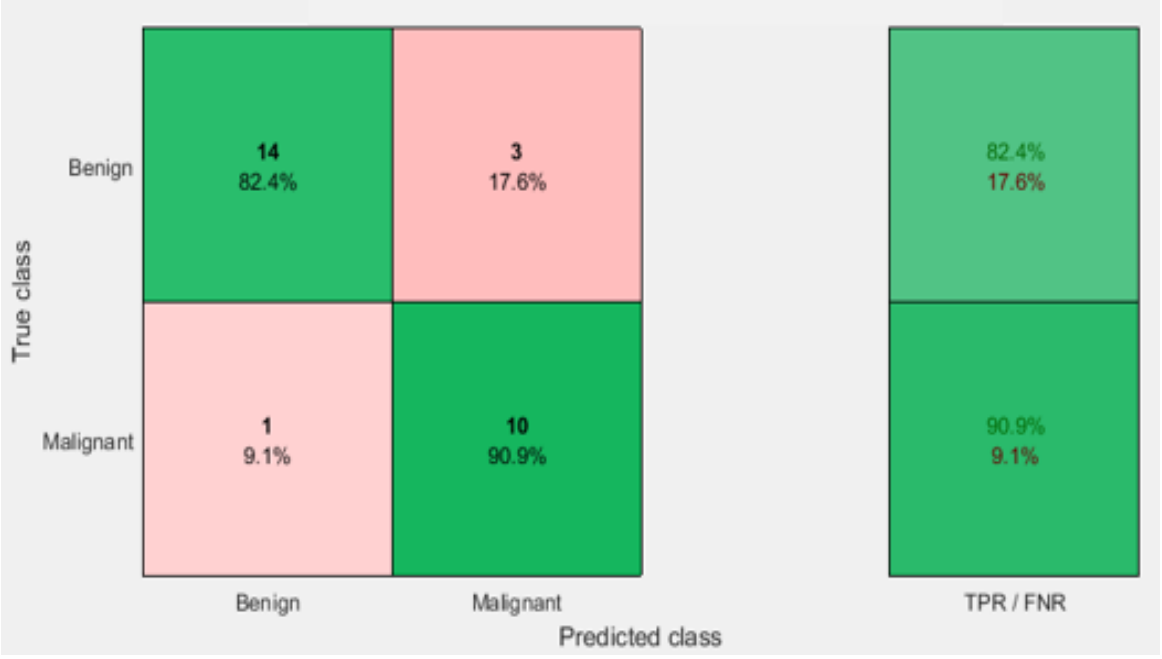


(b)

**Figure 4.17:** (a) Scatter Plot and (b) Confusion Matrix for classification using all parameter values in central region (50 samples)

**Classification using all values in Upper Region:** The parameter values in the lower region provided a classification accuracy of 89.3%.

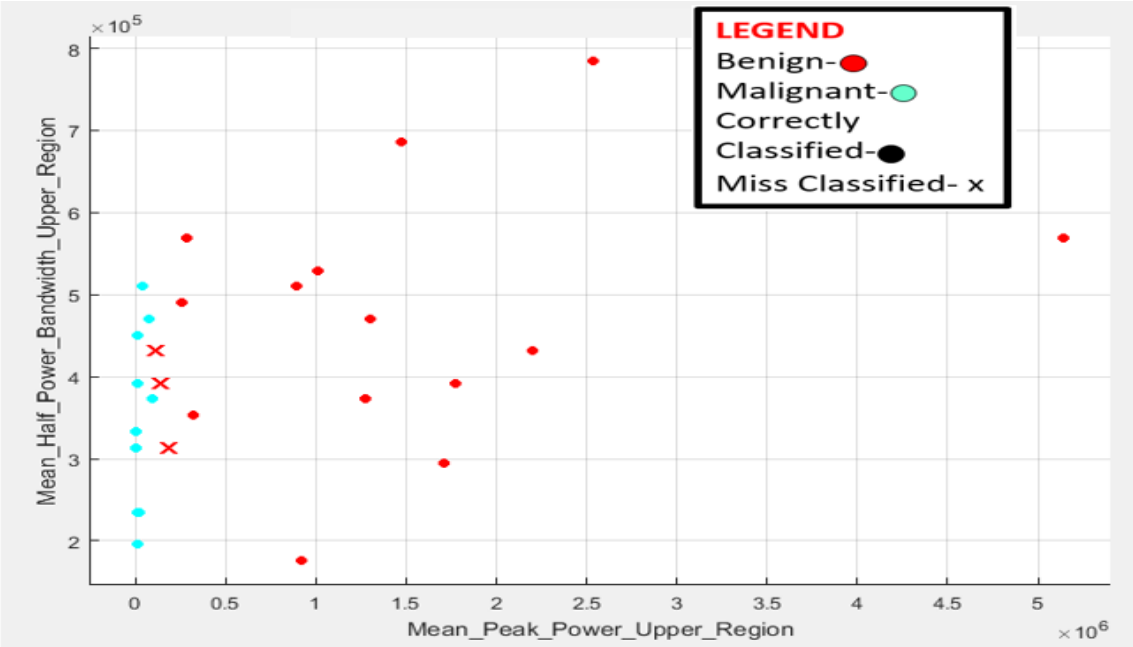


(a)

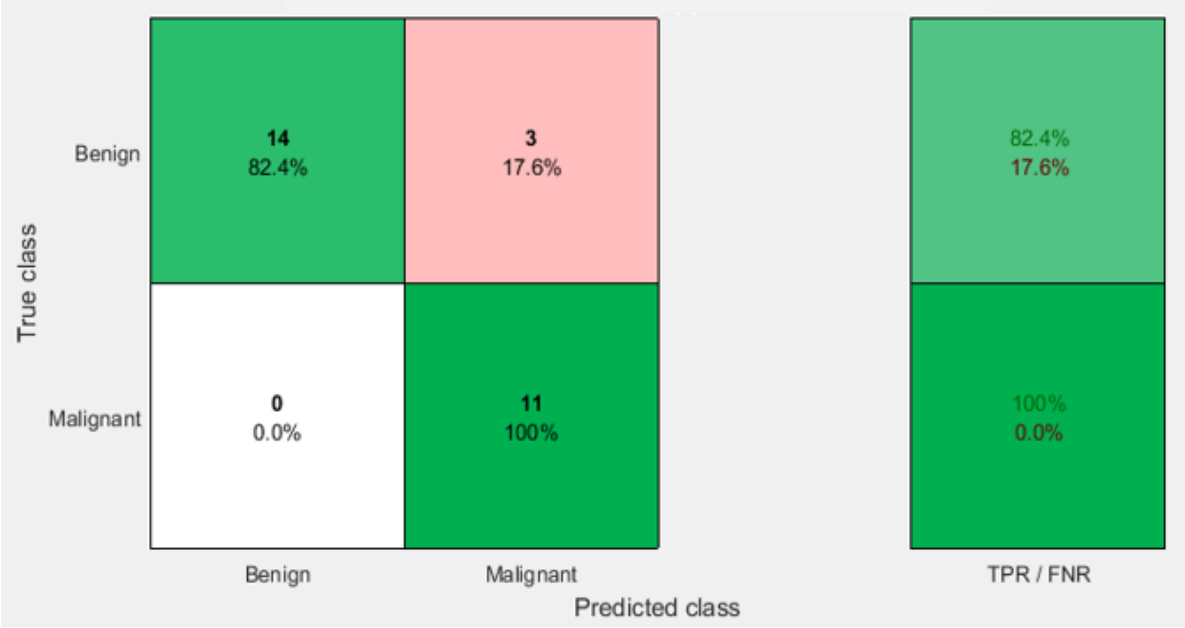


(b)

**Figure 4.18:** (a) Scatter Plot and (b) Confusion Matrix for classification using all parameter values in upper region (50 samples)

| Parameters | Percentage of Accuracy |
|---|---|
| **Peak Power** | 92.9% |
| **Peak Frequency** | 67.9% |
| **Half-power Bandwidth** | 78.6% |
| **Half-power Energy** | 85.7% |

(a)

| Regions | Percentage of Accuracy |
|---|---|
| **Upper Region** | 89.3% |
| **Central Region** | 85.7% |
| **Lower Region** | 78.6% |

(b)

**Table 4.2:** Phase one classification accuracies (50 samples)

Hence, for 30 samples, the two parameters providing the highest classification accuracy are:

(iii) Peak power

(iv) Half-power energy

The two ROI providing the highest classification accuracy are:

(iii) Upper region

(iv) Central region

**Phase 2: Classification using highest performing parameters and regions**

**Classification using peak power and half-power energy values from all three regions:** This process yielded an accuracy of 96.4%.

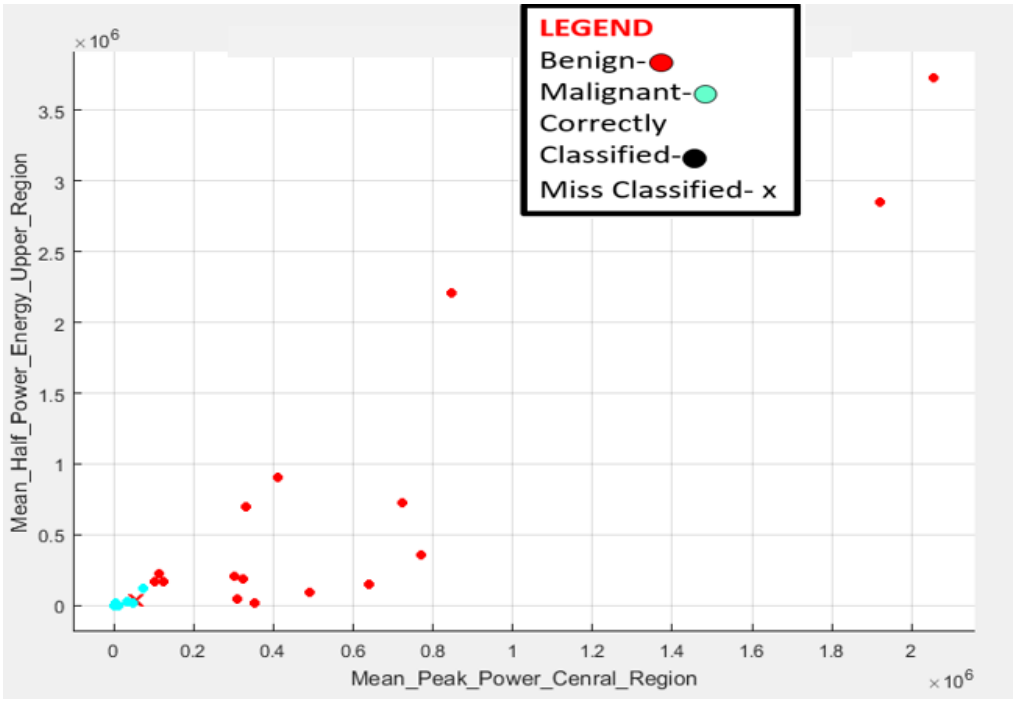


(a)

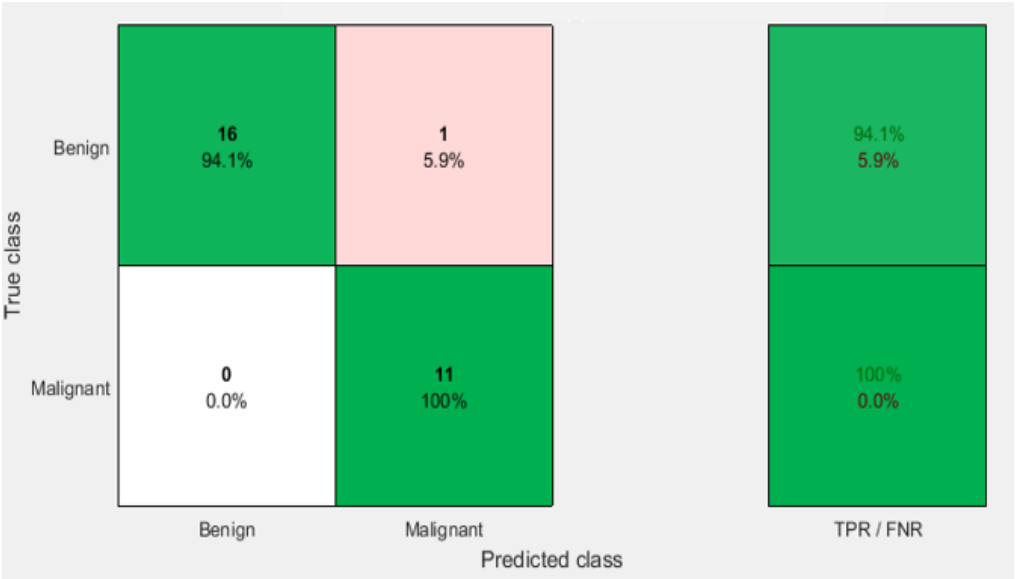


(b)

**Figure 4.19:** (a) Scatter Plot and (b) Confusion Matrix for classification using all peak power and half-power energy values in all three regions (50 samples)

**Classification using peak power and half-power energy values from central region:** This process yielded an accuracy of 96.4%.

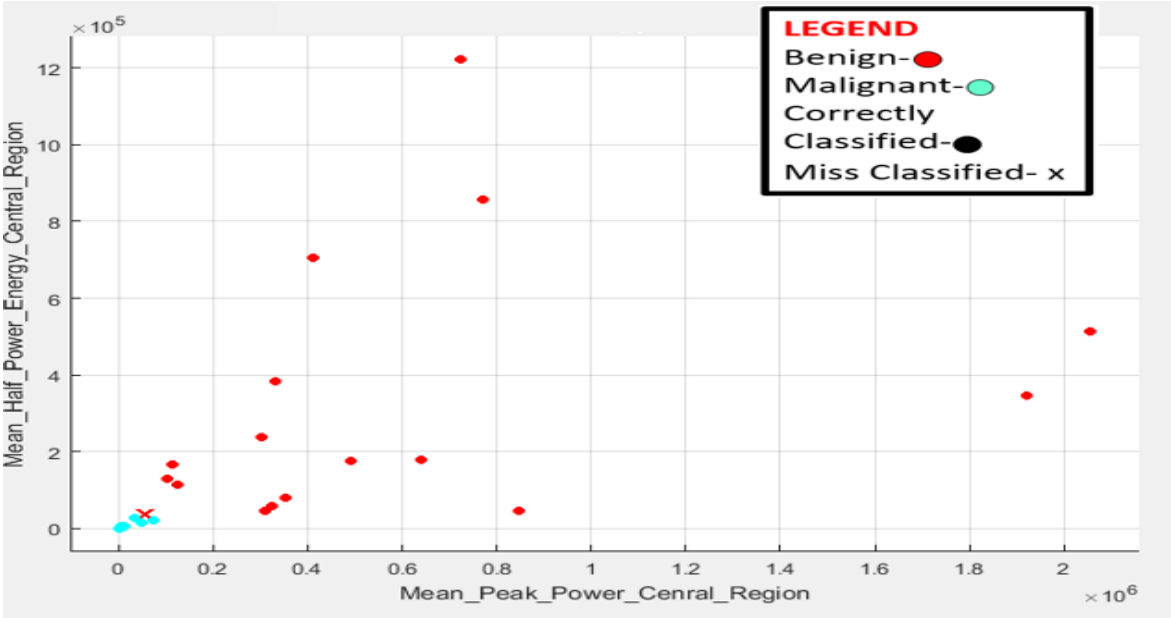


(a)

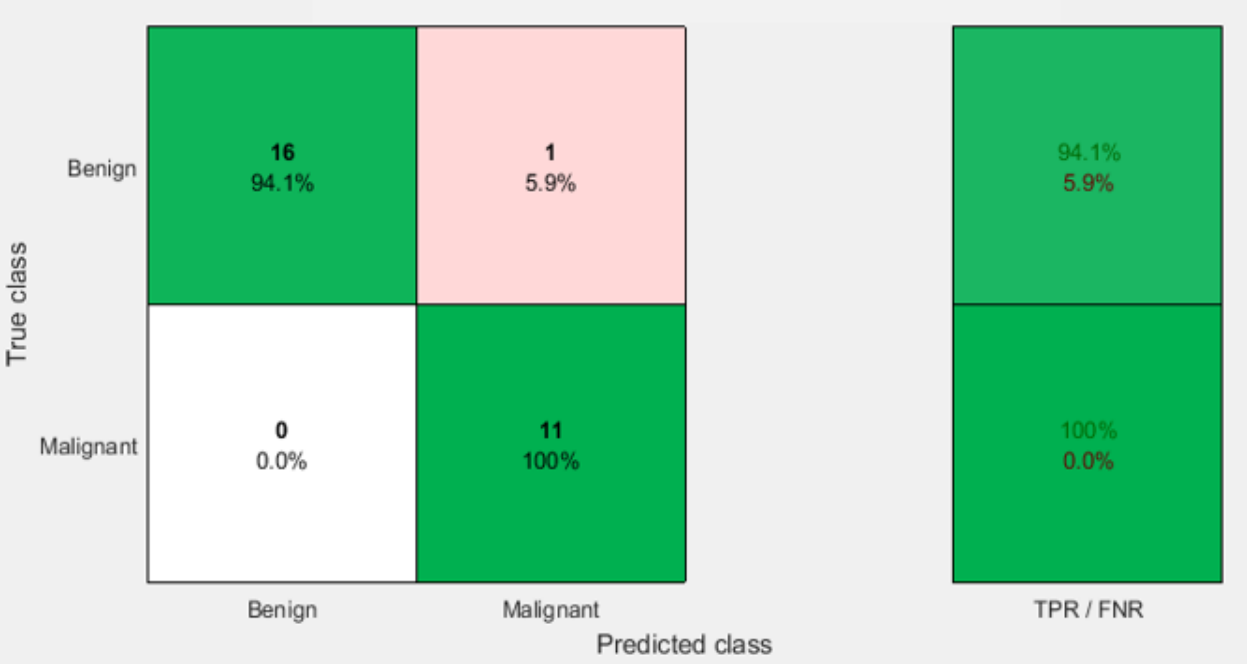


(b)

**Figure 4.20:** (a) Scatter Plot and (b) Confusion Matrix for classification using all peak power and half-power energy values in central region (50 samples)

**Classification using peak power and half-power energy values from upper region:** This process yielded an accuracy of 92.9%.

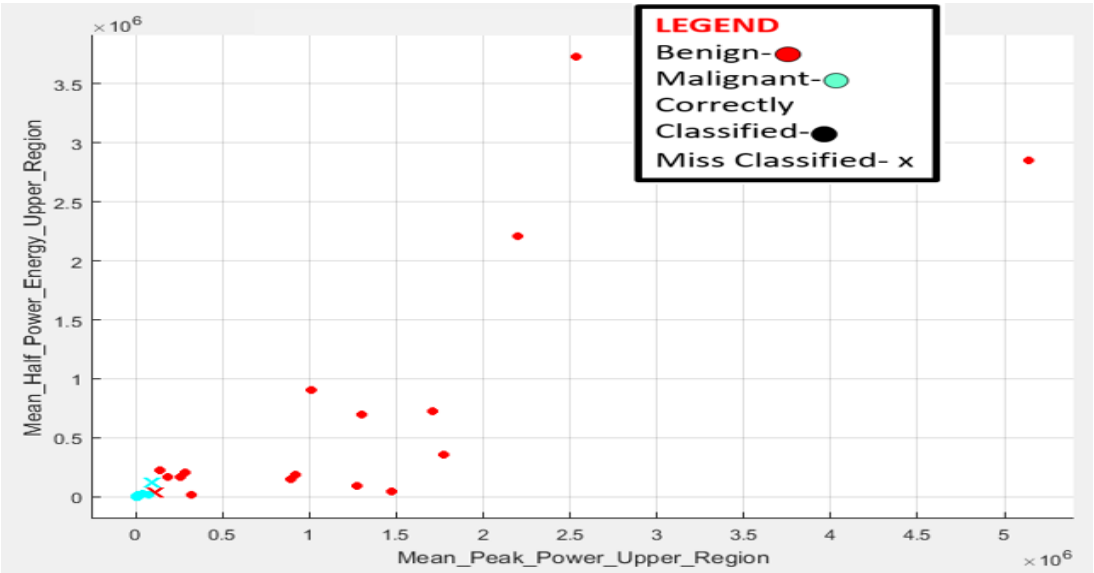


(a)

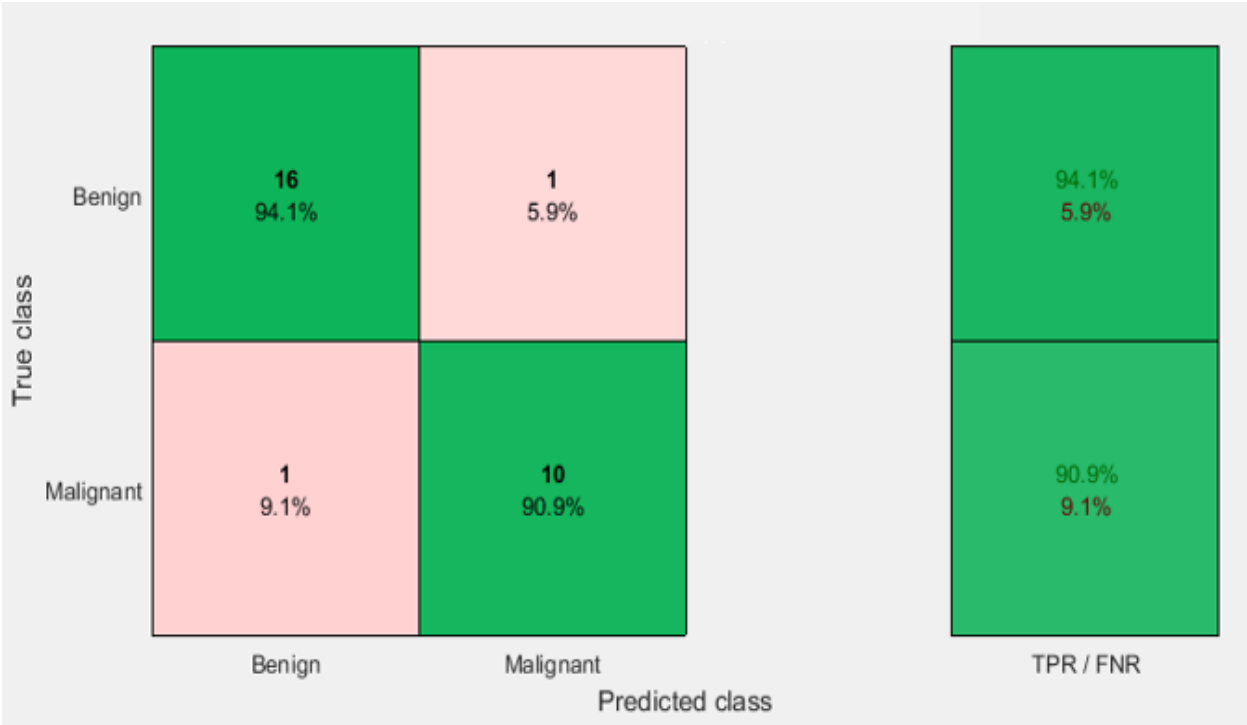


(b)

**Figure 4.21:** (a) Scatter Plot and (b) Confusion Matrix for classification using all peak power and half-power energy values in upper region (50 samples)

## *4.5 Results for ROI Size of 70 Samples*

**Phase 1, Step 1: Classification using individual parameter values**

**Peak power:** The peak power from all three regions provided a classification accuracy of 92.9%.

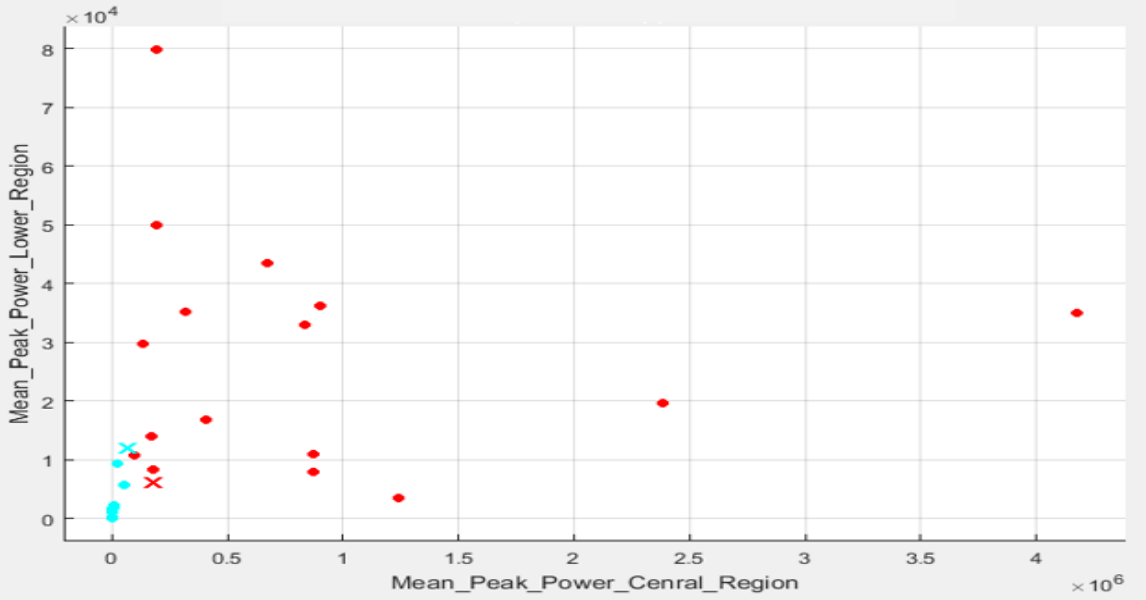


(a)

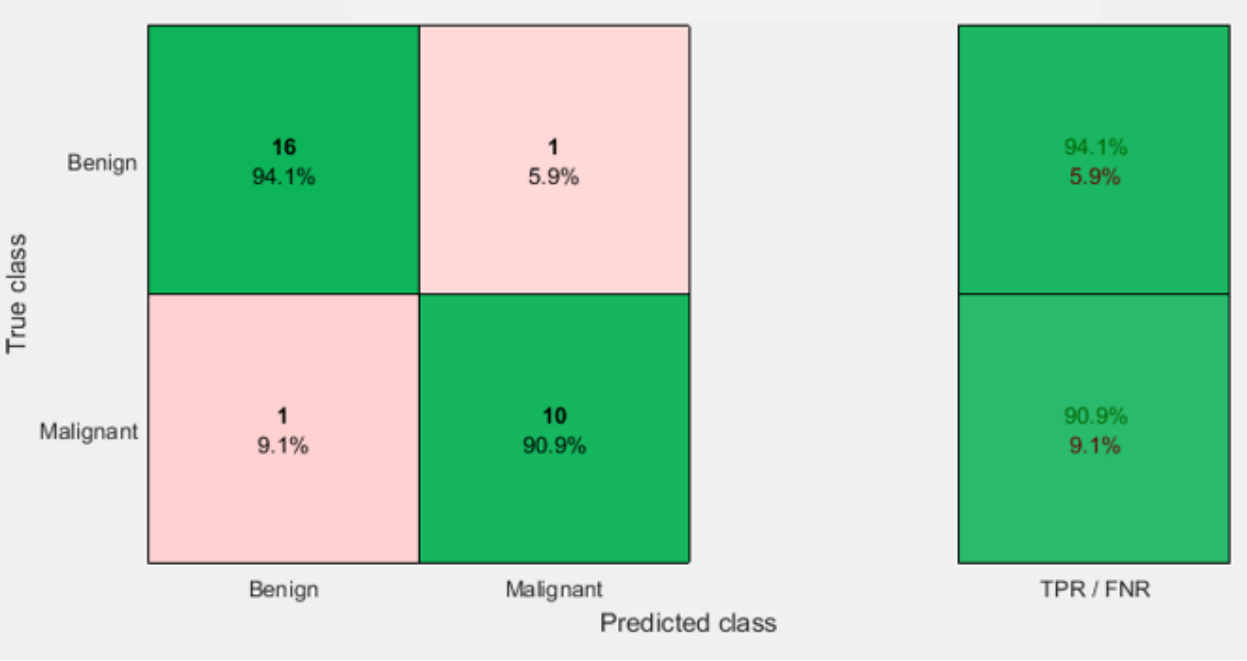


(b)

**Figure 4.22:** (a) Scatter Plot and (b) Confusion Matrix for classification using peak power values from all three regions (70 samples)

**Peak Frequency:** The peak frequency from all three regions provided a classification accuracy of 64.3%.

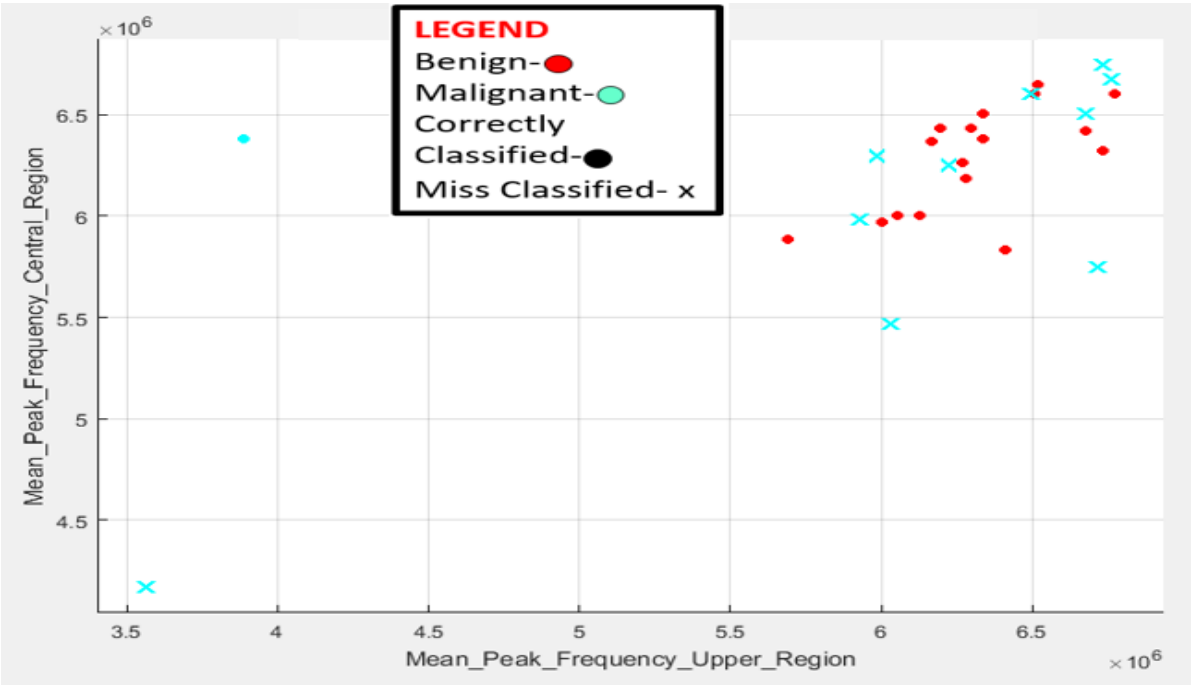


(a)

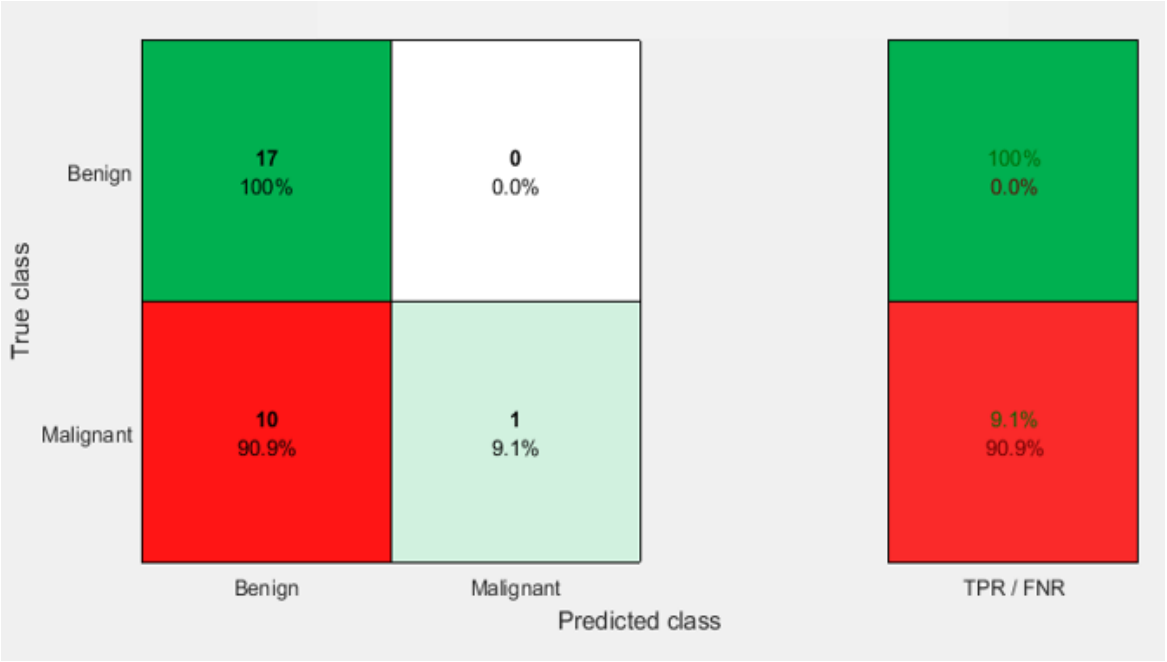


(b)

**Figure 4.23:** (a) Scatter Plot and (b) Confusion Matrix for classification using peak frequency values from all three regions (70 samples)

**Half-power bandwidth:** The half-power bandwidth from all three regions provided a classification accuracy of 67.9%.

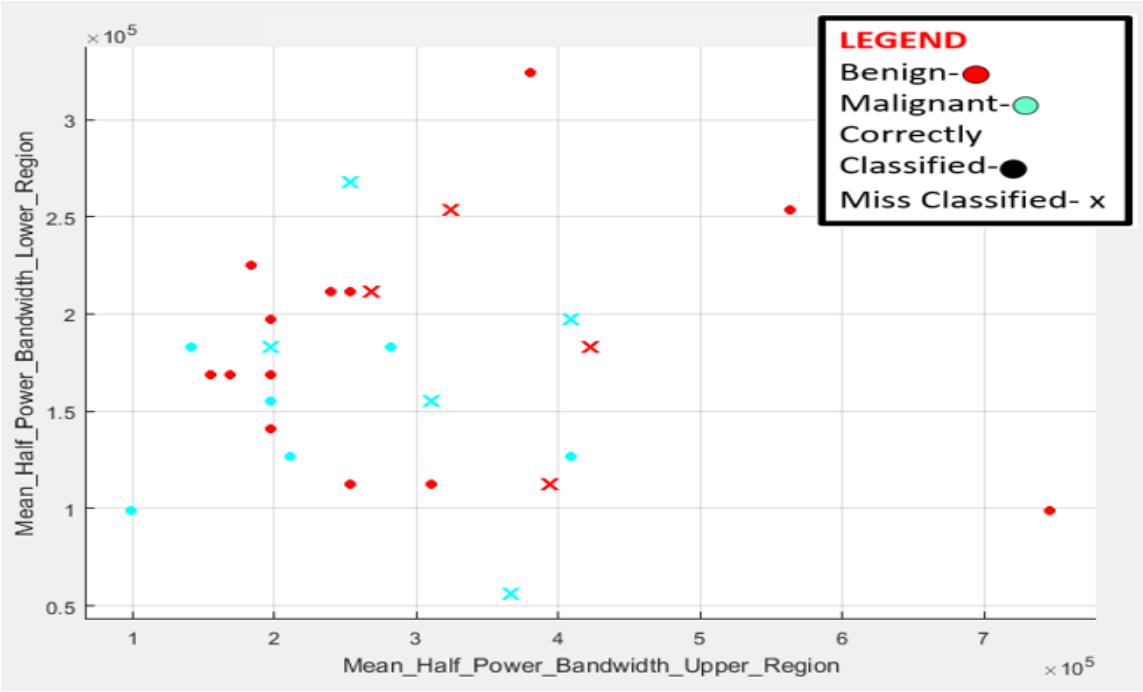


(a)

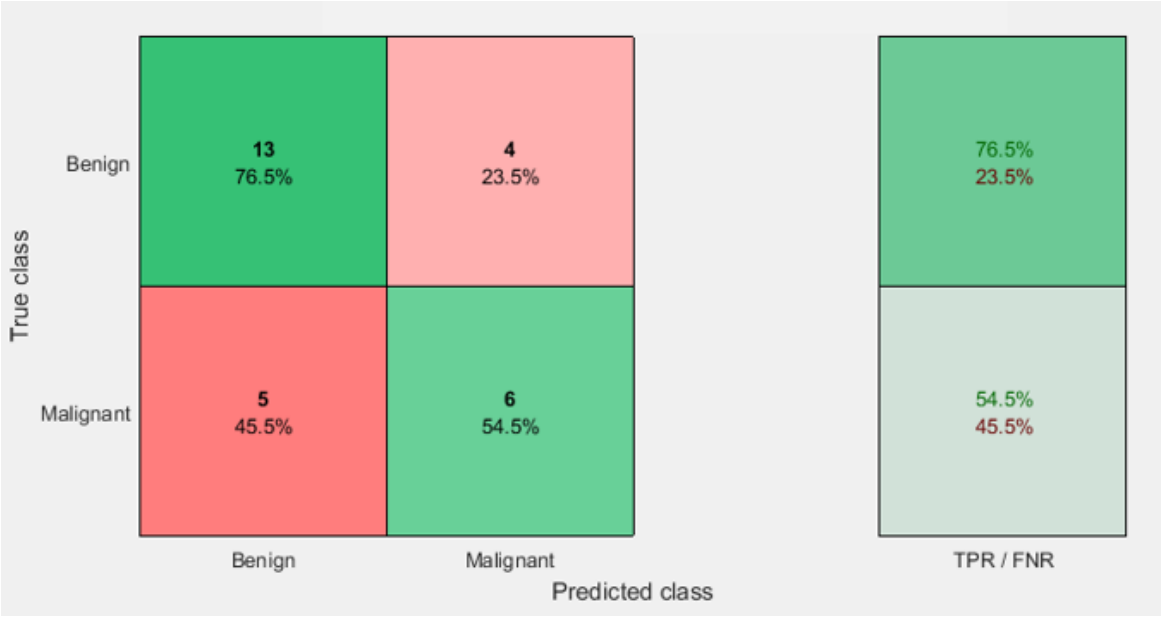


(b)

**Figure 4.24:** (a) Scatter Plot and (b) Confusion Matrix for classification using half-power bandwidth values from all three regions (70 samples)

**Half-power energy:** The half-power energy from all three regions provided a classification accuracy of 96.4%.

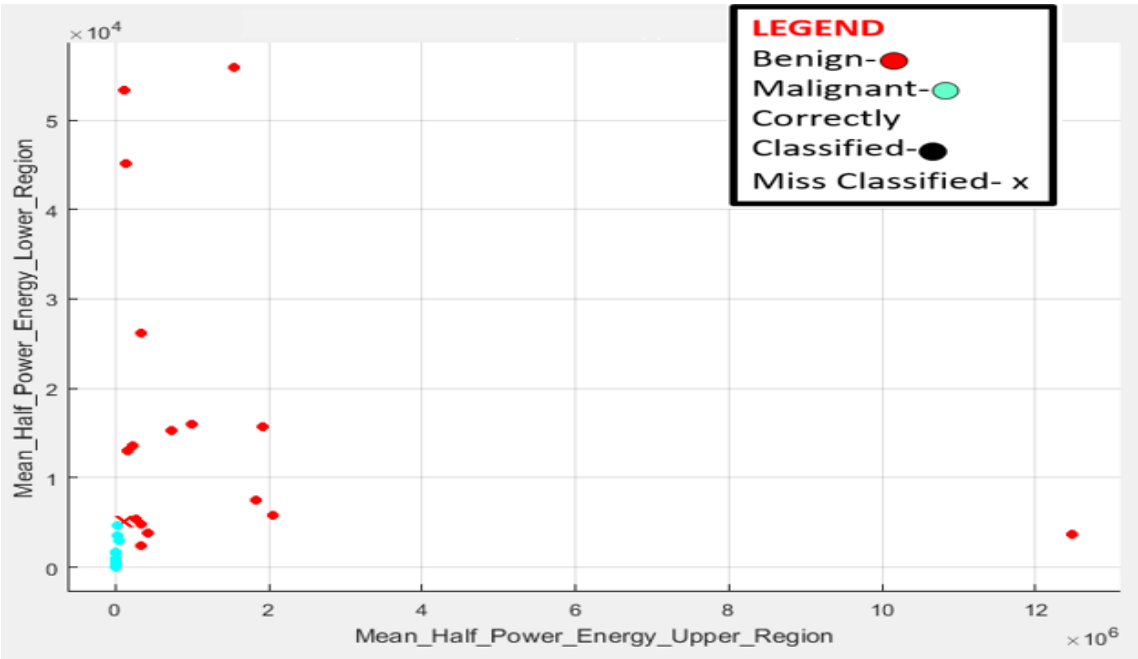


(a)

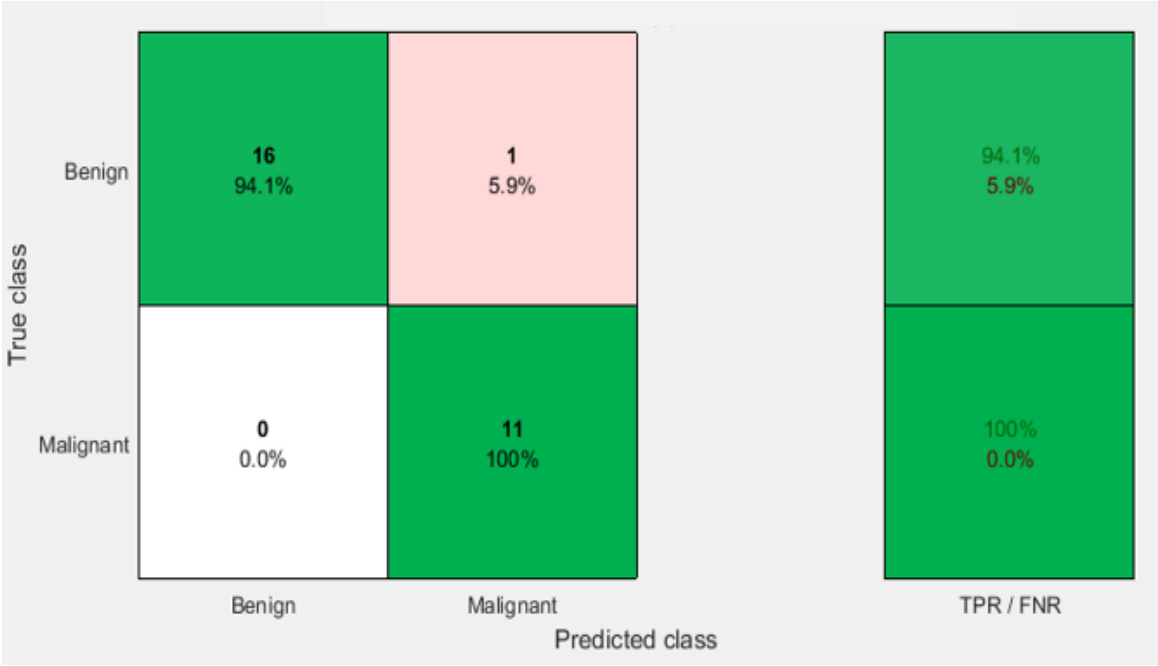


(b)

**Figure 4.25:** (a) Scatter Plot and (b) Confusion Matrix for classification using half-power energy values from all three regions (70 samples)

**Phase 1, Step 2: Classification using all parameter values in each ROI**

**Classification using all values in Lower Region:** The parameter values in the lower region provided a classification accuracy of 71.4%.

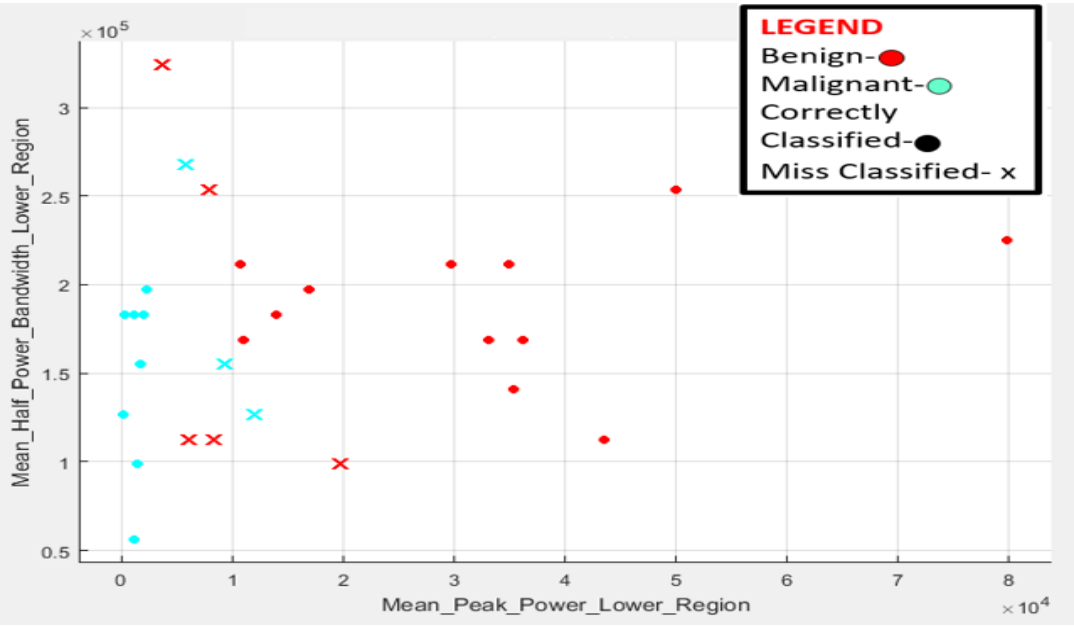


(a)


(b)

**Figure 4.26:** (a) Scatter Plot and (b) Confusion Matrix for classification using all parameter values in lower region (70 samples)

**Classification using all values in Central Region:** The parameter values in the lower region provided a classification accuracy of 85.7%.

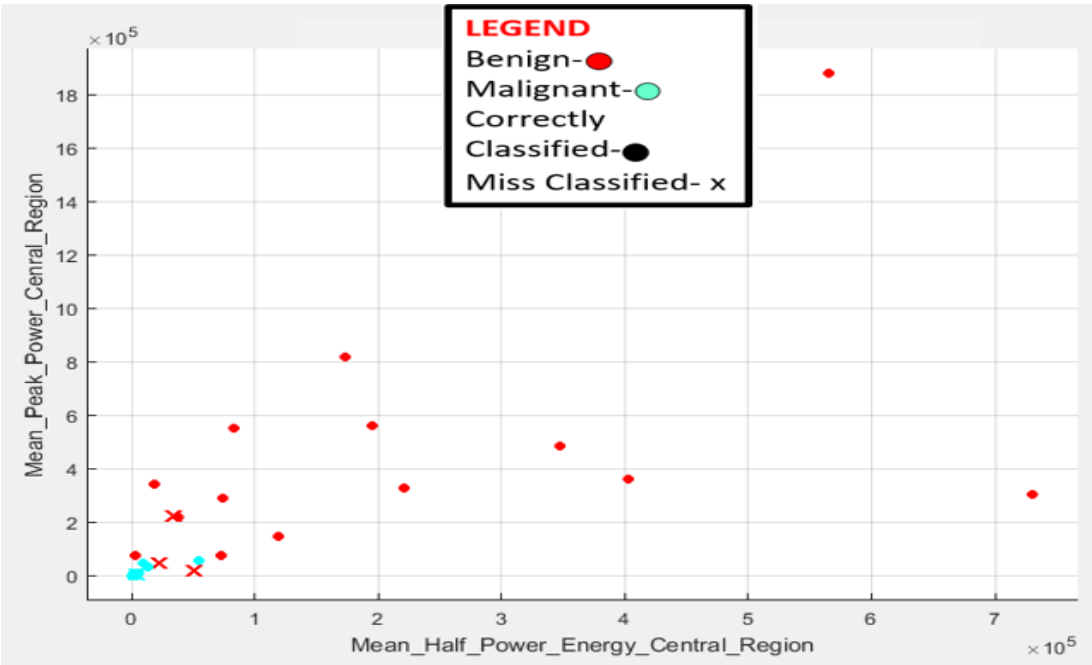


(a)

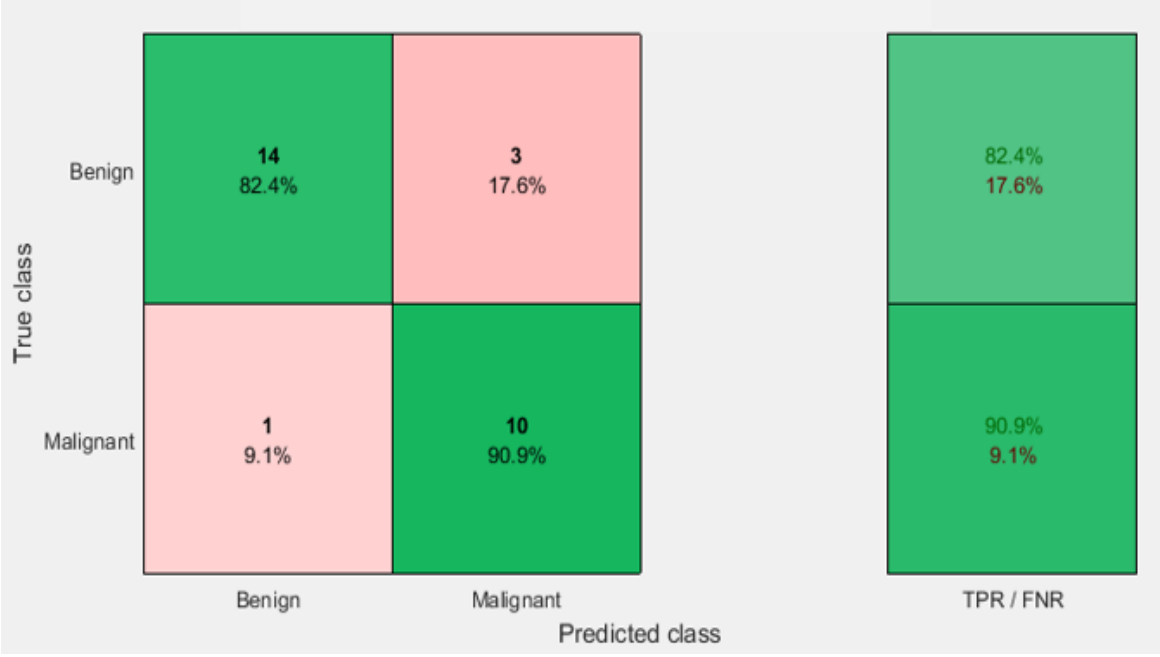


(b)

**Figure 4.27:** (a) Scatter Plot and (b) Confusion Matrix for classification using all parameter values in central region (70 samples)

**Classification using all values in Upper Region:** The parameter values in the lower region provided a classification accuracy of 82.1%.

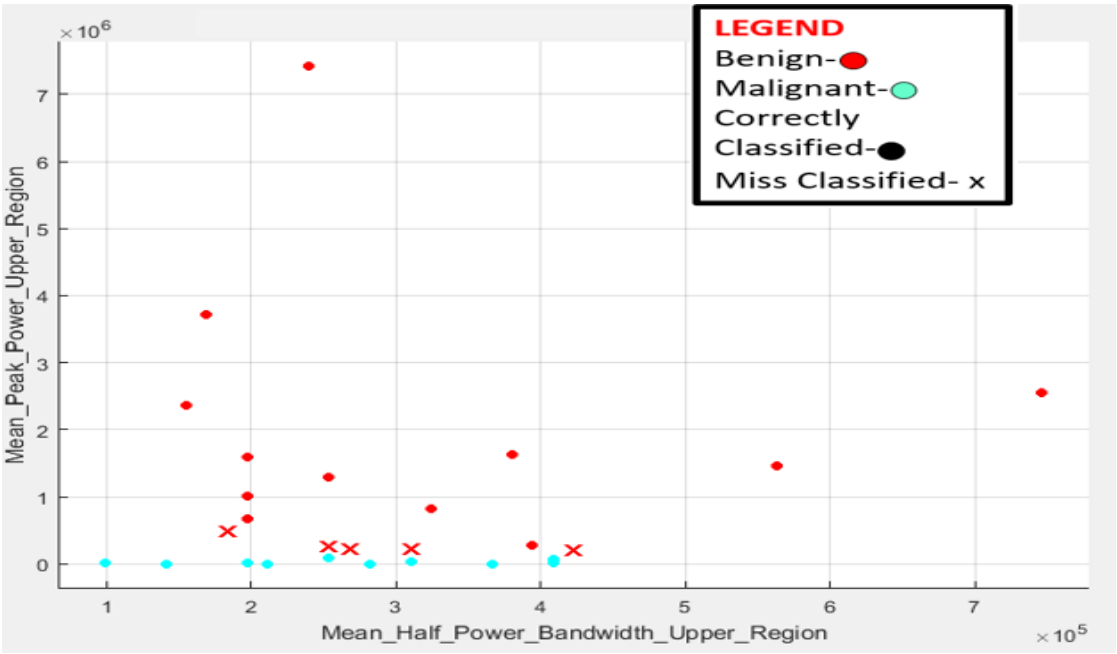


(a)

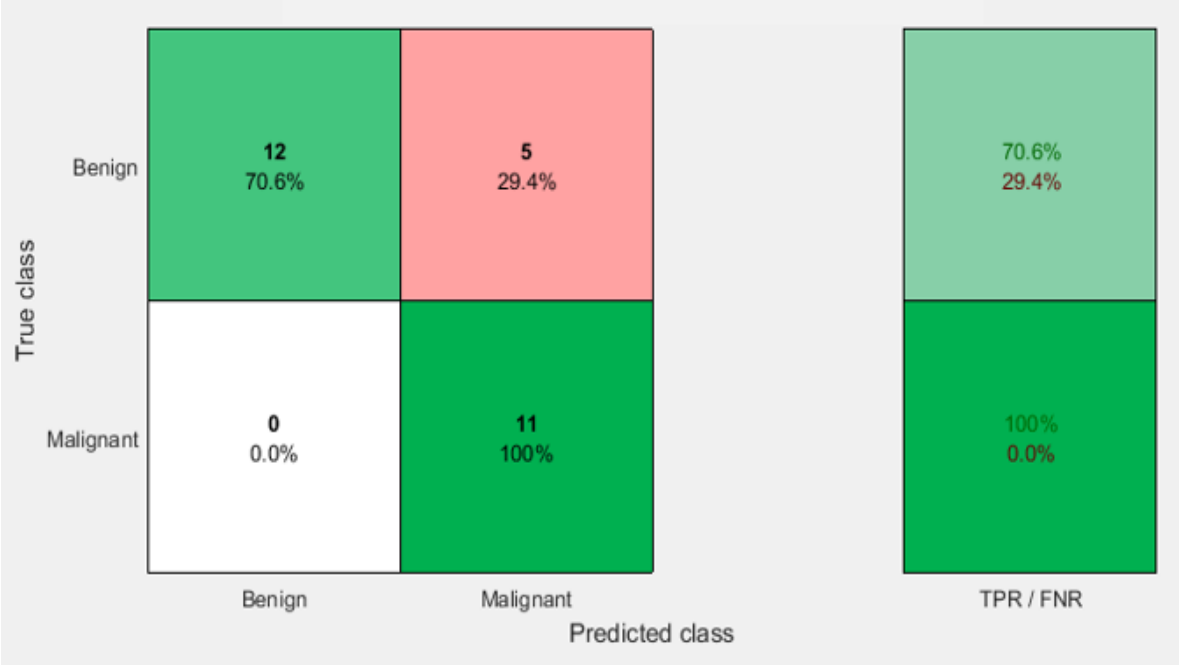


(b)

**Figure 4.28:** (a) Scatter Plot and (b) Confusion Matrix for classification using all parameter values in upper region (70 samples)

| Parameters | Percentage of Accuracy |
|---|---|
| **Peak Power** | 92.9% |
| **Peak Frequency** | 64.3% |
| **Half-power Bandwidth** | 67.9% |
| **Half-power Energy** | 96.4% |

(a)

| Regions | Percentage of Accuracy |
|---|---|
| **Upper Region** | 82.1% |
| **Central Region** | 85.7% |
| **Lower Region** | 71.4% |

(b)

**Table 4.3:** Phase one classification accuracies (70 samples)

Hence, for 30 samples, the two parameters providing the highest classification accuracy are:

(v) Peak power

(vi) Half-power energy

The two ROI providing the highest classification accuracy are:

(v) Upper region

(vi) Central region

**Phase 2: Classification using highest performing parameters and regions**

**Classification using peak power and half-power energy values from all three regions:** This process yielded an accuracy of 85.7%.

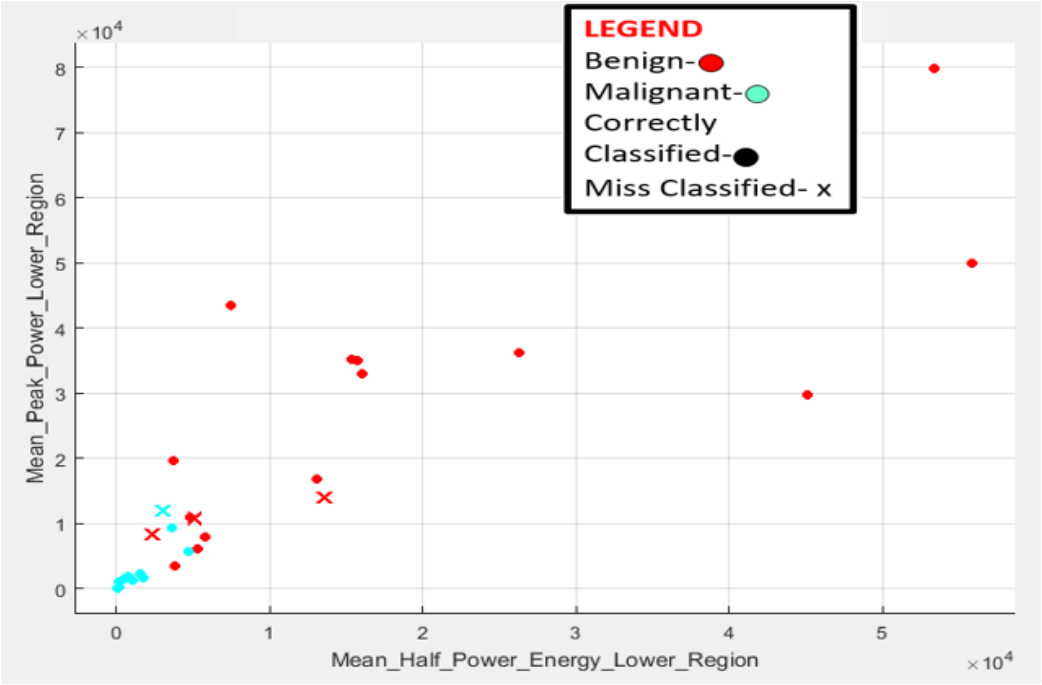


(a)

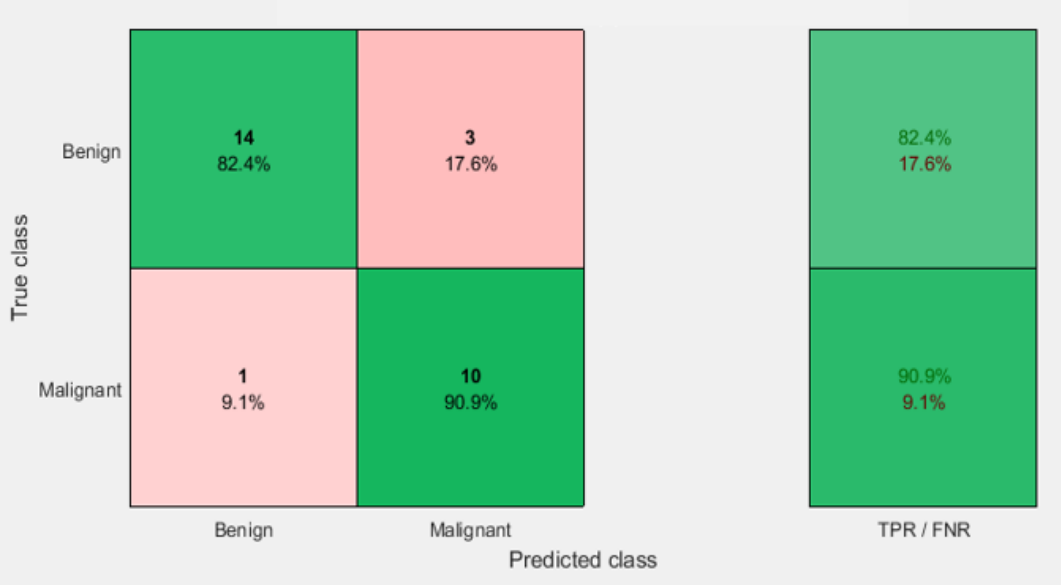


(b)

**Figure 4.29:** (a) Scatter Plot and (b) Confusion Matrix for classification using all peak power and half-power energy values in all three regions (70 samples)

**Classification using peak power and half-power energy values from central region:** This process yielded an accuracy of 85.7%.

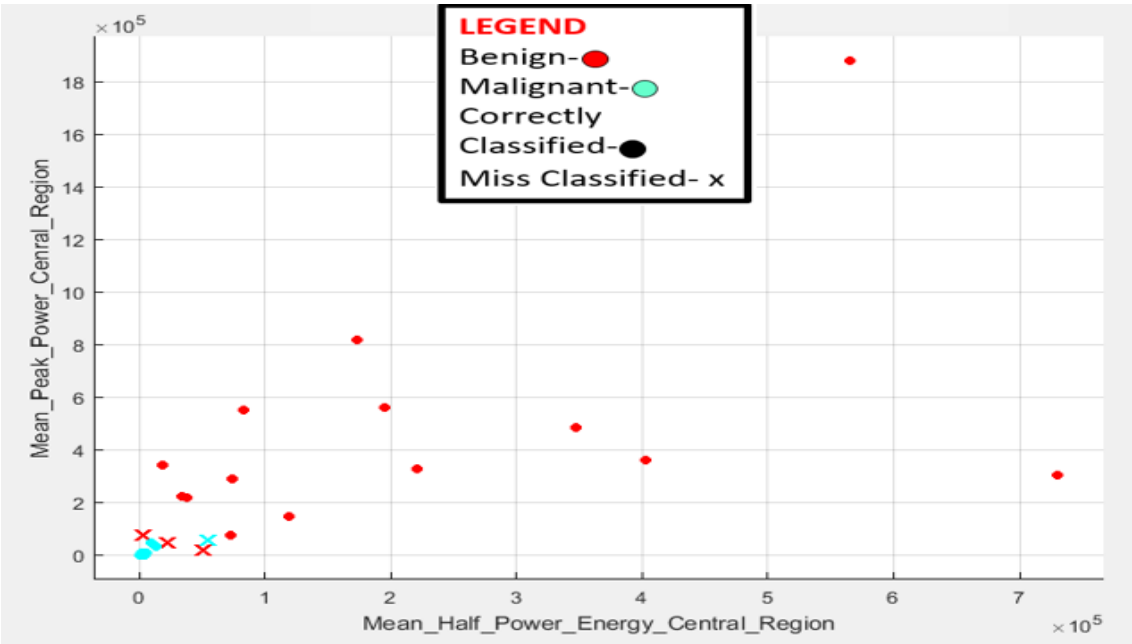


(a)


(b)

**Figure 4.30:** (a) Scatter Plot and (b) Confusion Matrix for classification using all peak power and half-power energy values in central region (70 samples)

**Classification using peak power and half-power energy values from upper region:** This process yielded an accuracy of 100%.

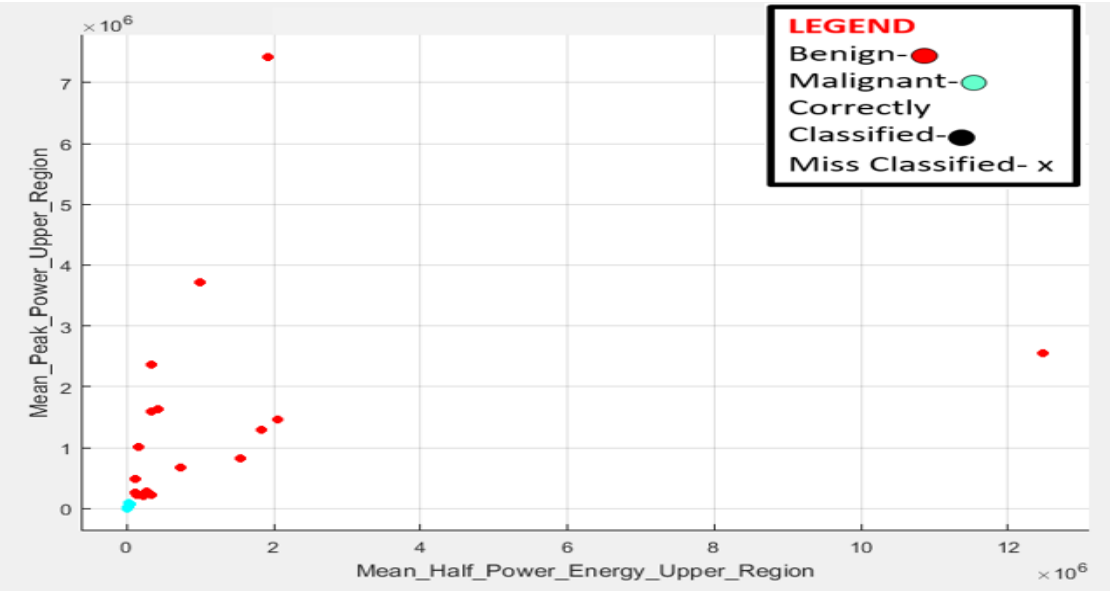


(a)

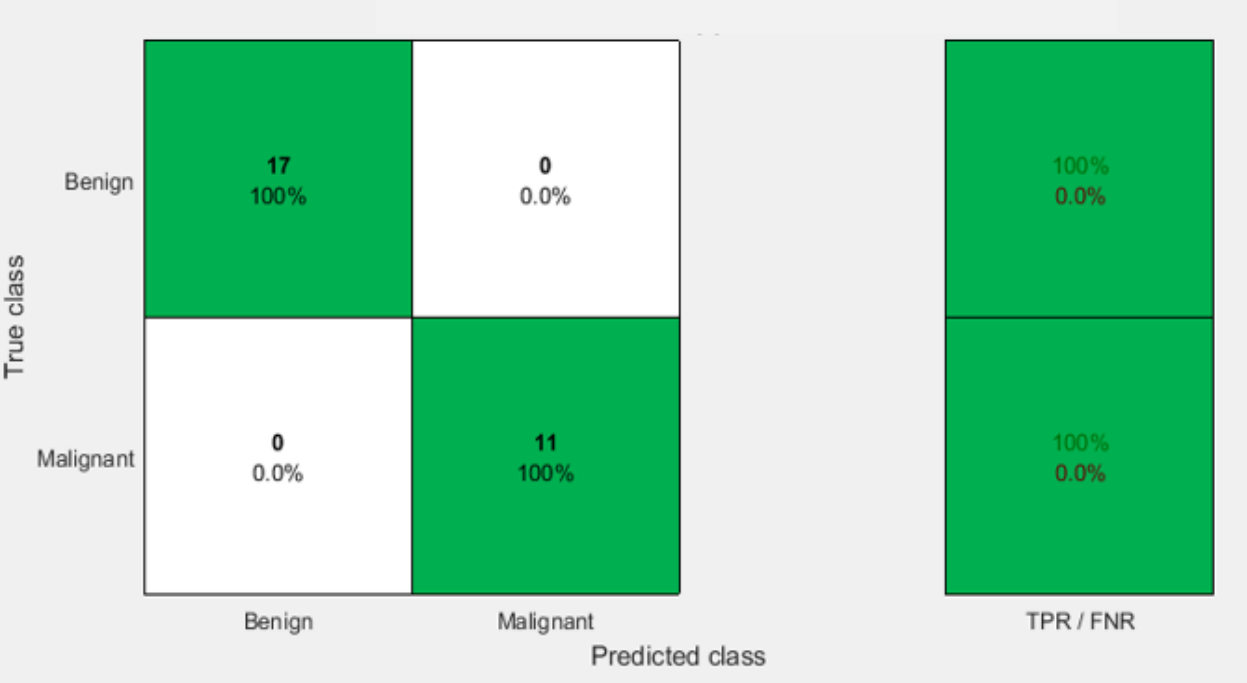


(b)

**Figure 4.31:** (a) Scatter Plot and (b) Confusion Matrix for classification using all peak power and half-power energy values in upper region (70 samples)

The results obtained from the classification procedure are summarized in Table 4.4.

| Number of Samples | Highest Performing Parameter | Highest Performing Region(s) | Highest Classification Accuracy |
|---|---|---|---|
| 30 | Peak Power, Half-power Energy | Upper Region | 92.9% |
| 50 | Peak Power, Half-power Energy | Central and All Three Regions | 96.4%, 96.4% |
| 70 | Peak Power, Half-power Energy | Upper Region | 100% |

**Table 4.4:** Summary of Results

## *4.6 Discussion*

We began our classification approach using four spectral parameters, peak power, peak frequency, half-power bandwidth and half-power energy. After multiple steps of analysis and classification, two highest performing parameters, peak power and half-power energy, were attained, which provided the highest classification accuracy. Our research also showed that the classification accuracy varies for different ROI sizes (based on the varying number of samples taken axially along the A-line) and also for different regions of study. Our findings show that the highest classification accuracy can be obtained in most cases when the analysis is performed by taking the two highest performing parameters from the region axially above the tumor boundary, which we defined as the upper region.

Our study utilized a linear classification approach (Linear SVM) due to the fairly clear separation of values visually observed between benign and malignant tumors, particularly using the peak power and half-power energy values, as indicated by the scatter plots for these parameters. Non-linear classification approaches such as neural networks or non-linear support vector mechanisms may produce different results, as in this case the parameters that did not show a clear separation between cancers and non-cancers, i.e. the peak frequency and half-power bandwidth, might come into play.

For all three different sizes of ROI considered, the parameters of peak power and half-power energy consistently produced high levels of accuracy in classifying between benign and malignant lesions. Thus, these parameters clearly possess a noticeable difference in value between benign and malignant cases, which allows for distinguishing between the two tumor types.

In our analysis, the parameters of peak frequency and half-power bandwidth were not useful in discriminating between benign and malignant lesions. There may be several reasons for this. The use of linear classification approach may be one, and as discussed above, non-linear approaches may yield different results. Another consideration may be the manual selection of points on the lesion boundary, as the points chosen on the tumor boundary did not follow any specific pattern, and were chosen more or less randomly. This may produce discrepancies in parameter values, and a systematic method of choosing the boundary points may produce different results

In terms of the area of the ROI, increasing the area of the ROI was observed to produce higher classification accuracies. An ROI size of 30 samples produced the lowest overall classification accuracy, although it still produced a high overall classification accuracy of 92.9%. An ROI size of 50 samples produced a classification accuracy between that obtained for 30 samples and 70 samples, of 96.4%. Meanwhile, an ROI size of 70 samples produced the highest overall classification accuracy of 100% for the data set utilized. Using areas of ROI above 70 samples might produce similarly high accuracies, although increasing the size too much would likely cause the accuracy levels to drop, as it might mean inclusion of regions consisting of blood vessels and skin into the ROI, which may hamper results. Hence, there may be a theoretical limit for the number of samples which are able to produce high classification accuracies, which may be the target of future research in this domain.

Furthermore, values of the parameter from the upper region produced the best results in terms of classification accuracy for ROI areas of 30 samples as well as 70 samples, whereas for an ROI area of 50 samples, the central region produced the highest classification accuracy. In all three cases, the lower region produced the lowest classification accuracy, pointing to the fact that power spectrum values obtained from the area inside the tumor are not effective in distinguishing between and classifying benign and malignant breast lesions. Hence, for classification of benign and

malignant tumors using the four spectral parameters, the lower region or the region inside the lesion can be avoided while using linear classification module like SVM. In case of ROI having 50 samples, the central region contained 25 samples above the boundary of the lesion, which was sufficient to provide highest classification accuracy using peak power and half-power energy values, as compared to upper and lower region. However, as the upper region was found to provide the highest classification accuracy for both an ROI consisting of 30 samples and an ROI consisting of 70 samples, it appeared more optimal to use upper region as the preferable region while classifying using peak power and half-power energy.

Moreover, as 100% classification accuracy was obtained using peak power and half-power energy from the upper region with an ROI of 70 sample size, it can be concluded that our approach of classifying breast tumors using RF data will be optimum when an ROI of 70 samples will be used, when the sample points are taken axially along the A-line, from the pre-defined upper region and the spectral parameters are peak power and half-power energy. However, the result may vary for different data set or other approaches for classification.

# Chapter 5

# Conclusion

## *5.1 Introduction*

The effectiveness of ultrasound instruments and processes in distinguishing between cancerous and non-cancerous breast tumors has increased significantly, and has even moved to a point where many radiologists recommend periodic follow-ups based on breast ultrasound findings, without performing biopsy. This thesis focused on a classification procedure based on spectral features extracted from different regions in the RF data of the patient, with an ultimate goal to determine whether such an approach might play a role in increasing the specificity associated with diagnostic ultrasound procedures of the breast, and thus reduce the misdiagnoses or unnecessary biopsies associated with breast cancer. The results obtained from this study suggest that such an approach may classify benign and malignant breast lesions with a very high level of accuracy, and thus may be able to play a role in the diagnostic procedure associated with breast cancer.

Our research findings indicate that for classification between benign and malignant breast tumors using parameters extracted from the power spectrum of ultrasound RF echoes, the peak power and half-power energy values obtained are able to distinguish between the tumor types with the highest degree of accuracy, when the values were taken from the region above the boundary of the tumor, and the ROI consisted of 70 samples axially along the A-line. In this case, the selected parameters were able to provide 100% accuracy using the Linear SVM classification procedure, for the selected patient data that we analysed from the dataset used for this research.

## *5.2 Future Scopes of Research*

There are several avenues of research that may be undertaken in the future following this study. We have divided such scopes into short-term, and long-term research prospects.

For research in the near future, a non-linear classification approach such as neural networks may be utilized to observe the differences that may take place regarding classification accuracy using individual parameter values from all three regions, as well as all parameter values in individual regions. This may produce different results than those obtained in this study, as a non-linear

classification approach may increase the accuracy of classification using the parameters of peak frequency and half-power bandwidth, which provided poor accuracy when a linear classification approach was used. Furthermore, as our findings indicate that a higher number of samples in the ROI considered increased the classification accuracy, another scope of future research might be to continue increasing the number of samples in each ROI, to observe if the classification accuracy increases, decreases or remains constant, thus deducing whether 70 samples provides the optimal size of ROI for classification of this nature. Yet another research scope in the near-future would be to follow the procedure outlined in this thesis using some different parameters from the power spectrum, to observe whether other parameters such as peak power and half-power energy, which provide the highest classification accuracy between breast tumor types, exist.

For research in the distant future, an obvious consideration would be to automate the process of selecting the area for analysis, instead of constructing the ROI based on manual selection of boundary points. In an ideal case, the entire upper boundary would be selected automatically, making the process of defining the ROI independent of user interaction. In this case, the visibility of the tumor would not be an issue, and both CV and NCV tumors would be able to be classified using the parameters, as the upper boundary would be automatically selected using appropriate segmentation functions. An automated procedure where the entire upper axial boundary is utilized for classification would be the optimal approach for a study of this type, and the parameter values thus obtained would be regarded as the standard. For further establishing this area of research, the procedures outlined in this thesis could be applied to other breast tumor patient datasets, to observe whether similar results are obtained, or if there are any major differences.

## *5.3 Conclusion*

Demonstrating high percentages of classification accuracy, our algorithm presents a promising aspect of classifying benign and malignant tumors using a quantitative approach based on parameters extracted from the power spectrum. Potential diagnostic advantages could be clearly observed. Improvements and modifications might come into play for varying dataset which remains a scope for future research.

# References


[1] Schneider AP II, Zainer CM, Kubat CK, Mullen NK, Windisch AK, "The breast cancer epidemic: 10 facts", *Linacre Q*, vol 81, issue 3, pp. 244-277, 2014.

[2] Bray F, Ferlay J, Soerjomataram I, Siegel RL, Torre LA, Jemal A, "Global cancer statistics 2018: GLOBOCAN estimates of incidence and mortality worldwide for 36 cancers in 185 countries", *CA Cancer J Clin*, vol. 68, issue 6, pp. 394-424, 2018.

[3] Md. Anisur Rahman Farazy, "Incidence of Breast Cancer in Bangladesh," Health Care, vol. 3, issue 3, pp. 53-54, October, 2015.

[4] American Cancer Society, in Cancer Facts and Figures, 2019.

[5] Siegel RL, Miller KD & Jemal A, "Cancer Statistics, 2019," *CA Cancer J Clin*, vol. 69, issue 1, pp. 7 – 34, 2019.

[6] Tabár L, Vitak B, Chen TH, Yen AM, Cohen A, Tot T, Chiu SY, Chen SL, Fann JC, Rosell J, Fohlin H, Smith RA, Duffy SW, "Swedish two-county trial: impact of mammographic screening on breast cancer mortality during 3 decades", *Radiology*, vol. 260, issue 3, pp. 658–663, 2011.

[7] Duff SW, Tabár L, Chen HH, Holmqvist M, Yen MF, Abdsalah S, Epstein B, Frodis E, Ljungberg E, Hedborg-Melander C, Sundbom A, Tholin M, Wiege M, Akerlund A, Wu HM, Tung TS, Chiu YH, Chiu CP, Huang CC, Smith RA, Rosén M, Stenbeck M, Holmberg L, "The impact of organized mammography service screening on breast carcinoma mortality in seven Swedish counties", *Cancer*, vol. 95, issue 3, pp. 458–469, 2002.

[8] Corsetti V, Houssami N, Ghirardi M, Ferrari A, Speziani M, Bellarosa S, Remida G, Gasparotti C, Galligioni E, Ciatto S, "Evidence of the effect of adjunct ultrasound screening in women with mammography negative dense breasts: interval breast cancers at 1 year follow-up", *Eur. J. Cancer*, vol. 47, pp. 1021–1026, 2011.

[9] Kolb TM, Lichy J, Newhouse JH, "Comparison of the performance of screening mammography, physical examination, and breast US and evaluation of factors that influence them: An analysis of 27,825 patient evaluations", *Radiology*, vol. 225, pp. 165-175, 2002.

[10] Boyd NF, Guo H, Martin LJ, Stone J, Fishell E, Jong RA, Hislop G, Chiarelli A, Minkin S, Yaffe MJ, "Mammographic density and the risk and detection of breast cancer", *N Engl J Med*, vol. 356, pp.227-236, 2007.

[11] Carkaci, S, Santiago, L, Adrada, BE, Whitman GJ, "Screening for breast cancer with sonography", *Semin Roentgenol*, vol. 46, issue 4, pp. 285–291, 2011.

[12] Weigert, J, Steenbergen S, "The Connecticut experiment: the role of ultrasound in the screening of women with dense breasts", *Breast J*, vol. 18, issue 6, pp. 517–522, 2012.

[13] Kolb TM, Lichy J, Newhouse JH, "Comparison of the performance of screening mammography, physical examination, and breast US and evaluation of factors that influence them: An analysis of 27,825 patient evaluations", *Radiology*, vol. 225, pp. 165-175, 2002.

[14] Berg WA, Blume JD, Cormack JB, Mendelson EB, Lehrer D, Böhm-Vélez M, Pisano ED, Jong RA, Evans WP, Morton MJ, Mahoney MC, Larsen LH, Barr RG, Farria DM, Marques HS, Boparai K, "Combined screening with ultrasound and mammography vs mammography alone in women at elevated risk of breast cancer", *JAMA*, vol. 299, issue 18, pp. 2152–2163, 2008.

[15] Stavros AT, Thickman D, Rapp CL, Dennis MA, Parker SH, Sisney GA, "Solid breast nodules: use of sonography to distinguish between benign and malignant lesions", *Radiology*, vol. 196, issue 1, pp. 123-134, 1995.

[16] Oelze ML & Mamou J, "Review of Quantitative Ultrasound: Envelope Statistics and Backscatter Coefficient Imaging and Contributions to Diagnostic Ultrasonic," IEEE Transactions on Ultrasonics, Ferroelectrics and Frequency Control, vol. 63, issue 2, pp. 336-351, February 2016.
[17] J. Mamou & M. L. Oelze, Quantitative Ultrasound in Soft Tissues. New York, NY, USA: Springer, 2013.
[18] Smith, N, & Webb, A (2010). Ultrasound imaging. In Introduction to Medical Imaging: Physics, Engineering and Clinical Applications (Cambridge Texts in Biomedical Engineering, pp. 145-203). Cambridge: Cambridge University Press.
[19] Solomon, SD, Wu, J, Gillam, L, Bulwer, B (2015). Echocardiography. In D. L. Mann, D. P. Zipes, P. Libby, R. O. Bonow, & E. Braunwald (Eds.), Braunwald's Heart Disease: A Textbook of Cardiovascular Medicine (10th ed.) (pp. 179–260). Philadelphia: Elsevier.
[20] D'hooge, J, & Mertens, L L (2016). Ultrasound physics. In W. W. Lai, L. L. Mertens, M. S. Cohen, & T. Geva (Eds.), Echocardiography in Pediatric and Congenital Heart Disease: From Fetus to Adult (2nd ed.) (pp. 2–18). Chichester: John Wiley and Sons.
[21] Armstrong, W. F., & Ryan, T. (Eds.). (2010). Feigenbaum's Echocardiography (7th ed.). Philadelphia: Lippincott Williams & Wilkins.
[22] Cikes M, D'hooge J & Solomon SD (2018). "Physical Principles of Ultrasound and Generation of Images. In Essential Echocardiography, (1st ed.) (pp. 1-15). Elsevier.
[23] Esserman LJ, Thompson IM, Reid B., Nelson P, Ransohoff DF, Welch HG, Hwang S, Berry DA, Kinzler KW, Black WC, Bissell M, Parnes H, Srivasta S, "Addressing overdiagnosis and overtreatment in cancer: a prescription for change," *The Lancet Oncology*, vol. 15, issue 6, pp 234-242, May, 2014.
[24] Welch HG, Black WC, "Overdiagnosis in Cancer," *Journal of the National Cancer Institute*, vol. 102, issue 9, May, 2010.
[25] Mendelson EB, Böhm-Vélez M, Berg WA, et al., ACR BI-RADS® Ultrasound, In: ACR BI-RADS® Atlas, Breast Imaging Reporting and Data System, Reston, VA, American College of Radiology, 2013.
[26] Advanced Technology Laboratories (1994). Summary of Atl-Sponsored Breast Ultrasound Study and Preliminary Findings. ATL publications.
[27] Kolb TM, Lichy J, Newhouse JH, "Occult cancer in women with dense breasts: detection with screening US—diagnostic yield and tumor characteristics", *Radiology*, vol. 207, pp. 191–199, 1998.
[28] Skaane P, Engedal K, "Analysis of sonographic features in the differentiation of fibroadenoma and invasive ductal carcinoma", *AJR*, vol. 170, pp. 109–114, 1998.
[29] Huber S, Danes J, Zuna I, Teubner J, Medl M, Delorme S, "Relevance of sonographic B-mode criteria and computer-aided ultrasonic tissue characterization in differential/diagnosis of solid breast masses", *Ultra sound Med Biol*, vol. 26, issue 8, pp. 1243–1252, 2000.
[30] American College of Radiology Breast Imaging Reporting and Data System (BI-RADS) Atlas (American College of Radiology, Reston, VA, 2003).
[31] D'Astous FT & Foster FS, "Frequency Dependance of Ultrasound Attenuation and Backscatter in Breast Tissue," Ultrasound in Medicine and Biology, vol. 12, issue 10, pp. 795-808, 1986.
[32] Nam K, Zagzebski JA & Hall TJ,"Quantitative Assessment of In Vivo Breast Masses Using Ultrasound Attenuation and Backscatter," Ultrasonic Imaging, vol. 35, issue 2, pp. 146–161, April, 2013.
[33] Lizzi FL, Astor M, Liu T, Deng C, Coleman DJ & Silverman RH, "Ultrasonic Spectrum Analysis for Tissue Assays and Therapy Evaluation," International Journal of Imaging Systems and Technology, vol. 8, issue 1, pp. 3-10, 1997.
[34] Lizzi FL, Astor M, Feleppa EJ, Shao M & Kalisz A, "Statistical Framework for Ultrasonic Spectral Parameter Imaging," Ultrasound in Medicine and Biology, vol. 23, issue 9, pp. 1371-1382, 1997.

[35] Alam SK, Feleppa EJ, Rondeau M, Kalisz A and Garra BS, "Ultrasonic Multi-Feature Analysis Procedure for Computer-Aided Diagnosis of Solid Breast Lesions," Ultrasonic Imaging, vol. 33, issue 1, pp. 17-38, 2011.

[36] Kabir S.M., Bhuiyan M.I.H.: "Classification of Breast Tumor in Contourlet Transform Domain," 2018 10th International Conference on Electrical and Computer Engineering (ICECE), Dhaka, Bangladesh, 2018.

[37] Layek K., Samanta S., Sadhu A., Maity S.P. and Barui A.: Classification of sonoelastography images of prostate cancer using transformation-based feature extraction techniques, Soft Computing Based Medical Image Analysis, Academic press, 2018.

[38] Shankar PM, "A General Statistical Model for Ultrasonic Backscattering from Tissues," IEEE Transactions on Ultrasonics, Ferroelectrics and Frequency Control, vol. 47, issue 3, pp. 727-736, May 2000.

[39] Shankar PM, Dumane VA, Reid JM, Genis V, Forsberg F, Piccoli CW & Goldberg BB, "Classification of Ultrasonic B-Mode Images of Breast Masses Using Nakagami Distribution," IEEE Transactions on Ultrasonics, Ferroelectrics and Frequency Control, vol. 48, issue 2, pp. 569-580, March 2001.

[40] Dutt V & Greenleaf JF, "Ultrasound Echo Envelope Analysis Using a Homodyned K Distribution Signal Model," Ultrasonic Imaging, vol. 16, issue 4, pp. 265-287, October 1994.

[41] Hruska, David P (2009), Improved Techniques for Statistical Analysis of the Envelope of Backscattered Ultrasound Using the Homodyned K Distribution, University of Illinois at Urbana-Champaign, Champaign, IL, USA.

[42] Hruska DP & Oelze ML, "Improved Parameter Estimates Based on the Homodyned K Distribution," IEEE Transactions on Ultrasonics, Ferroelectrics and Frequency Control, vol. 56, issue 11, pp. 2471-2481, November 2009.

[43] Trop I, Destrempes F, Khoury ME, Robidoux A, Gaboury L, Allard L, Chayer B & Cloutier G, "The Added Value of Statistical Modelling of Backscatter Properties in the Management of Breast Lesion at US," Radiology, vol. 275, issue 3, June 2015

[44] Pohlman S., Powell K.A., Obuchowski N.A., Chilcote W.A. and Grundfest-Broniatowski S., "Quantitative classification of breast tumors in digitized mammograms," Medical Physics, vol. 23, issue 8, pp. 1337-1345, August, 1996.